Titre: Title:	Rheological characteristics of hypereutectic Al-Si (A390) in the semi-solid state
Auteur: Author:	Alireza Hekmat Ardakan
Date:	2006
Type:	Mémoire ou thèse / Dissertation or Thesis
Référence: Citation:	Hekmat Ardakan, A. (2006). Rheological characteristics of hypereutectic Al-Si (A390) in the semi-solid state [Mémoire de maîtrise, École Polytechnique de Montréal]. PolyPublie. https://publications.polymtl.ca/7889/

UNIVERSITÉ DE MONTRÉAL

RHEOLOGICAL CHARACTERISTICS OF HYPEREUTECTIC Al-Si (A390) IN THE SEMI-SOLID STATE

ALIREZA HEKMAT ARDAKAN

DÉPARTEMENT DE GÉNIE CHIMIQUE

ÉCOLE POLYTECHNIQUE DE MONTRÉAL

MÉMOIRE PRÉSENTÉ EN VUE DE L'OBTENTION

DU DIPLÔME DE MAÎTRISE ÈS SCIENCES APPLIQUÉES

(GÉNIE MÉTALLURGIQUE)

JUILLET 2006

Your file Votre référence
ISBN: 978-0-494-19308-2
Our file Notre référence
ISBN: 978-0-494-19308-2

UNIVERSITÉ DE MONTRÉAL

ÉCOLE POLYTECHNIQUE DE MONTRÉAL

Ce mémoire intitulé:

RHEOLOGICAL CHARACTERISTICS OF HYPEREUTECTIC Al-Si (A390) IN THE SEMI-SOLID STATE

présenté par: HEKMAT ARDAKAN Alireza
en vue de l'obtention du diplôme de: Maîtrise ès sciences appliquées
a été dûment accepté par le jury d'examen constitué de :

M. PELTON Arthur , Ph.D., président

M. AJERSCH Frank, Ph.D., membre et directeur de recherche

M. VERREMAN Yves, Ph.D., membre

Dedicated to

My wife, my son as well as my parents.

ACKNOWLEDGEMENTS

I would like to acknowledge my professor, Frank Ajersch for his supervision, Professor Artur.D. Pelton, chairman of the thesis committee and Professor Yves Verreman, member of the thesis committee for their valuable comments as well as NSERC (Natural Science and Engineering Research Council of Canada) and REGAL-FQRNT (Fonds Québécois de Recherche sur la Nature et Technologies) for their financial support of this project.

RÉSUMÉ

Les alliages hypereutectiques Al-Si sont employés dans des applications où une résistance élevée à l'usure et à la corrosion, avec une bonne dureté et un bas coefficient de dilatation thermique sont essentiel. Pour maximiser les propriétés de ces alliages, la mise en forme à l'état semi-solide peut être utilisée pour modifier la structure de solidification des cristaux de silicium primaire ainsi que pour réduire la microségrégation et la porosité. Les phénomènes de l'évolution de la morphologie des cristaux de silicium primaire en particules sphériques par cisaillement à l'état semi-solide ne sont pas entièrement compris. L'objectif de ce travail actuel est la détermination des caractéristiques rhéologiques de l'alliage A390 (Al-17%Si-4.5%Cu-0.5%Mg) en utilisant un viscosimètre de type de Couette (Haake RV12) et évaluant l'évolution microstructurale lors de les expériences de refroidissement continu et isotherme à vitesses de cisaillement constantes. L'effet de la vitesse de cisaillement, de la fraction solide (la température) sur l'évolution morphologique des cristaux de silicium ont été étudiés. Le diagramme de phases quaternaire (A390) a été construit en utilisant le logiciel de FACTSAGE développé par le CRCT de l'École Polytechnique de Montréal selon les fonctions thermodynamique.

ABSTRACT

Hypereutectic Al-Si alloys such as A390 (Al17Si4CuMg) exhibit several specific and interesting properties, such as high wear resistance, high strength and hardness, and a low thermal expansion coefficient. As a result, they are used in heavy wear applications. However, their use has always been restricted by several difficulties such as long solidification time, die wear, segregation of large primary silicon particles, and unfavourable shrinkage behaviour. Semi-solid processing allows hypereutectic Al–Si alloys to be shaped into complex near net shape components, with a microstructure of fine and compact Si particles

The objective of the present work is the determination the rheological characteristics of A390 alloy in the semi-solid state using a Couette type (Haake RV12) viscometer. The rheological behaviour was investigated for continuous cooling and during isothermal conditions at 565 ° C and for a range of solid fractions, followed by step change tests. In the continuous cooling test, the alloy is cooled at a rate of -2 ° C/min and sheared at constant rates of 15, 59, 123, 250 and 507 s^{-1} in separate experiments. The effect of shear rate and the solid fraction (temperature) on morphological evolution of the silicon crystals are investigated. A numerical calculation of the phase diagram of A390 alloy is also presented using the FACTSAGE software developed by the CRCT at École Polytechnique de Montreal in order to interpret the solidification path and the compounds and phases that are formed during the solidification period.

CONDENSÉ EN FRANÇAIS

Les alliages hypereutectiques Al-Si sont employés dans des applications où une résistance élevée à l'usure et à la corrosion, avec une bonne dureté et un bas coefficient de dilatation thermique sont essentiel. Pour maximiser les propriétés de ces alliages, la mise en forme à l'état semi-solide peut être utilisée pour modifier la structure de solidification des cristaux de silicium primaire ainsi que pour réduire la microségrégation et la porosité. Les phénomènes de l'évolution de la morphologie des cristaux de silicium primaire en particules sphériques par cisaillement à l'état semi-solide ne sont pas entièrement compris. L'objectif de ce travail actuel est la détermination des caractéristiques rhéologiques de l'alliage A390 (Al-17%Si-4.5%Cu-0.5%Mg) en utilisant un viscosimètre de type de Couette (Haake RV12) et évaluant l'évolution microstructurale lors de les expériences de refroidissement continu et isotherme à vitesses de cisaillement constantes. L'effet de la vitesse de cisaillement, de la fraction solide (la température) sur l'évolution morphologique des cristaux de silicium ont été étudiés. Le diagramme de phases quaternaire (A390) a été construit en utilisant le logiciel de FACTSAGE développé par le CRCT de l'École Polytechnique de Montréal selon les fonctions thermodynamique.

Selon la route de solidification de l'alliage A390 calculé par le logiciel de Factsage, les cristaux de silicium apparaît d'abord à 653 ° C comme phase primaire et continue à précipiter jusqu'à la température eutectique binaire à 566 ° C où le silicium et le α-Al solidifient sous la forme d'une eutectique structure. La fraction solide maximum du

cristal primaire de silicium a été calculée pour être environ 6.1%. Le silicium qui précipite comme phase primaire est d'une morphologie facettée et la phase eutectique est de forme lamellaire. La germination du composé $Cu_2Mg_8Si_6Al_5$ a lieu en général sur la phase θ-Al_2Cu sous forme de structures aciculaires minces ou de forme globulaire [1].

La phase de θ-Al_2Cu précipite sous forme globulaire et eutectique (Al+Al_2Cu) ou comme mélange des deux types selon la vitesse de refroidissement [2]. En état d'équilibre ou aux vitesses de refroidissement très lents, la forme eutectique est prédominent. La phase de Mg_2Si précipite sous forme de grandes particules en forme de caractères chinois [2]. Selon le calcul de Factsage, la réaction eutectique binaire s'effectue à 566 ° C et une grande partie du liquide (88%) transforme en Al (cfc) et Si quand la température est atteinte à 502 ° C. À cette température, la réaction eutectique ternaire s'effectue selon la réaction : (Liq. → Al (cfc) +Si (s)+ Mg_2Si (s)). La solidification continue le long de eutectique ternaire jusqu'à la température de 496 ° C où la solidification devient complète avec la réaction eutectique quaternaire (Liq. → Al-Cu (θ)+ Al (cfc)+ Si (s)+ Mg_2Si (s)).

Il faut noter que le calcul réaliste par Factsage diffère des valeurs expérimentales mesurées. Une des raisons se rapporte au fait que l'enthalpie des composés quaternaires comme $Cu_2Mg_8Si_6Al_5$ n'a pas été tenu compte dans la base de données existante dans le logiciel de Factsage. La réaction eutectique quaternaire observe par Mondolfo [3] et Fan [4] se produit à environ 507 ° C pour cet alliage est (Liq. → Al-Cu (θ) + Al (cfc) + Si(s)+ $Cu_2Mg_8Si_6Al_5$). D'ailleurs, d'ailleurs, le diagramme de phase indique que α-Al solidifie

seulement sous la forme d'une morphologie eutectique binaire aux températures entre 566° C -502° C. Néanmoins, l'observation microstructurale confirme la présence de α-Al sous forme de l'eutectiques et grains individuel dans la matrice pendant la solidification continue. Par conséquent, la région du "Liquide + Si + Al" qui correspond à la région eutectique binaire confirme la solidification de α-Al avec deux morphologies. C'est une caractéristique de solidification dans l'état non-équilibre et ne peut pas être déterminée par diagramme de phase calculé. H.S. Kang et autres. [5] ont observé que la microstructure des alliages hyper-eutectiques Al-Si dépend fortement de la surfusion imposée. Pour l'alliage plus proche de la composition eutectique (Al-13wt %Si), la phase change de l'eutectique à la phase α-Al première en forme dendritique avec eutectique. La raison de ce changement de phase peut attribuer de la vitesse de croissance de la phase de α-Al excédant cela de la phase Al-Si eutectique avec une augmentation de la surfusion imposée. Selon le principe de croissance concurrentielle, c.-à-d. le principe que la microstructure la plus préférée est celle avec la vitesse de croissance la plus élevée à la surfusion donné, des transformations microstructurales peuvent être prévues. En outre, un changement morphologique de α-Al primaire de dendritique à equiaxé a été observé à ce niveau de la surfusion. Ils ont prouvé que les conditions de la nucléation rapide de cristal, de la croissance s'effectuent à la surfusion élevé sont responsables de la transformation de la dendrite à la forme d'equiaxs. En conséquence, Pour deux échantillons de l'alliage hyper-eutectiques Al-Si avec la même composition, plus de α-Al est présent lors de la solidification avec la surfusion élevée de qu'avec faible surfusion. Plusieurs études ont confirmé les mêmes observations entre les

alliages Al-Si hyper-eutectiques et les composites à base d'Aluminium de composition semblable [6].

En ajoutant de 5% du cuivre à Al-Si binaire α-Al stabilise dans l'état semi-solide. Dans la région hyper-eutectique des alliages Al-Si binaires, la zone « Liquide + Si » est la seule zone semi-solide et la solidification deviennent complète avec la réaction eutectique binaire à environ 577 ° C. Pour l'alliage A390, selon le diagramme de phase, la réaction eutectique binaire s'effectue dans la zone « Liquide + Si + Al » dans une gamme de la température entre 566 ° C -502 ° C. Par conséquent, α-Al existe le long de « Liquide + Si » à l'état semi-solide. Généralement, la mise en forme à l'état semi-solide est effectuée dans cette gamme de la température où la fraction solide finale peut être contrôlée en changeant de la fraction solide de α-Al dans cette région. Il faut noter que le traitement thixomoulage doit être effectué à une fraction solide entre 30%-50% parce qu'aux fractions solide plus haut que 50%, le problème du remplissage de matrice se produisent à cause de grande viscosité.

Le comportement rhéologique a été étudié lors du refroidissement continu et en condition isotherme.

Dans le cas des essais de refroidissement continu, l'alliage a été refroidi à une vitesse de - 2 ° C /min et cisaillé aux vitesses de 15, 59, 123, 250 et 507 s^{-1} jusqu'à la température où la limite supérieure du couple du viscosimètre est atteinte. Les résultats expérimentaux montrent que la viscosité des gelées semi-solides de l'alliage agité

pendant le refroidissement continu dépend de la température (fraction solide) et de la vitesse de cisaillement. En diminuant la température dans la zone semi-solide, la viscosité commence à augmenter de façon importante. Cette augmentation est progressive jusqu'à la température eutectique binaire de 566 ° C. La solidification de silicium primaire s'effectue entre 653 ° C - 566 ° C avec la fraction solide maximum seulement de 6.1%, ce qui a révélé une augmentation progressive de la viscosité. À la réaction eutectique binaire (566 C) l'alliage contient une fraction liquide de 93.9% alors que seulement une petite fraction de liquide (3.9%) reste à la température eutectique quaternaire (496 ° C). Dans la zone eutectique binaire en-dessous de 566 ° C, la viscosité augmente rapidement avec augmentation de la fraction solide. Dans tous les essais de refroidissement continu, la température n'atteint pas la température eutectique quaternaire à 496 ° C parce que le couple maximum 4,9 N-cm du viscosimètre est atteint au-dessus de la température eutectique binaire.

Pour une vitesse de cisaillement de 15 s^{-1}, aucune dégradation de la structure n'a été observée. Par contre à 59 s^{-1}, la microstructure était considérablement changée. Environ 50% du silicium primaire a été fragmenté et les débris ont été trouvés à la périphérie des particules primaires. Cependant d'autres particules primaires de silicium restent facettées sans fragmentation. Le silicium eutectique a été partiellement brisé et le silicium aciculaire a également montré une microstructure fragmentée. On a observé que la phase θ-Al_2Cu est entouré par les particules $Cu_2Mg_8Si_6Al_5$ globulaire et peut être associé à l'eutectique qui précipite sur les grandes particules de silicium primaire. Cet effet devient

plus prononcé quand la taille des particules de silicium augmente. Nous pouvons également observer une agglomération d'Al_2Cu globulaire et de silicium eutectique fragmenté dans la matrice. On a également observé que l'aluminium globulaire peut être présent dans plusieurs régions. L'évolution de morphologie de α-Al s'effectue en raison de la force de cisaillement ce qui a révélé une solidification non-dendritique.

A la vitesse de cisaillement de 123 s^{-1}, d'environ 80 % des grandes particules de siliciums primaire avec la morphologie facettée devient fragmentées le long des plans spécifiques tels que plans $\{100\}$et des plans de clivage de$\{110\}$. En outre, les débris se trouvent à la périphérie de la particule originale. Cependant, l'agglomération du silicium fragmenté n'a pas été observée. Les grandes particules primaires de silicium n'ont pas été fragmentées et les fissures ont été observées dans les grandes particules de silicium. Toute la phase aciculaire de $Cu_2Mg_8Si_6Al_5$ a été fragmentée et se trouve généralement à la périphérie des phases Al_2Cu.

A la vitesse de cisaillement de 250 s^{-1}, tout le silicium primaire est fragmenté et la morphologie facettée est entièrement détruite. Les résultats montrent que le couple requis pour la fragmentation du silicium primaire (non métallique) est beaucoup plus grand que celui requis pour la fragmentation du α-Al primaire (métallique). On constate que le mécanisme de fragmentation est très différent des théories de Vogel et al [7] et Doherty et al [8] sur la fragmentation des phases primaires métalliques. Lee et al [9] ont observées que la rupture dans le silicium primaire se produit le long des plans $\{100\}$et des plans de clivage de$\{110\}$.

Enfin, à la vitesse forte de cisaillement de 507 s^{-1}, la majeure partie du silicium primaire se transforme en forme compacte sphéroïdale et se disperse dans la matrice. Ce changement morphologique réduit nettement la viscosité. Les particules dans cette région se composant de silicium eutectique fragmenté, de l'eutectique, de Al_2Cu avec $Cu_2Mg_8Si_6Al_5$ globulaire et aciculaire deviennent aussi plus sphéroïdales en raison de cette vitesse puissante de cisaillement

Pour les essais isothermes, l'alliage est chauffé initialement à la température de 700 ° C et il est refroidi à -2 ° C/min avec un cisaillement de 13 s^{-1} jusqu'à la température de 565 ° C. À cette température, α-Al solidifie dans deux morphologies. L'alliage a été alors cisaillé pendant 20 minutes dans des conditions isothermes et la vitesse de cisaillement a été changée brusquement de 13 s^{-1} à 104 s^{-1}. Cet essai, appelé « Step change », détermine le changement de viscosité avec les changements brusques de la vitesse de cisaillement. Dans une autre expérience de "Step Changes" à 565 ° C, les vitesses de cisaillement ont changé brusque à 52 s^{-1} puis à 104 s^{-1}, 26 s^{-1}, 104 s^{-1} et 13 s^{-1}. Pour cette série d'essais, des petites variations transitoires de viscosité ou le comportement thixotropie (la viscosité change avec temps de cisaillement) ont été détectés pour l'alliage A390. À cette température d'essai isotherme (566 ° C), la fraction solide du silicium primaire est seulement de 6.1% et les changements brusques de la viscosité indiquent un régime transitoire très rapide où un nouvel état d'agglomération des phases solides est rapidement établi à une vitesse de cisaillement constante. À la vitesse de

cisaillement de 104 s^{-1}, la viscosité à l'état d'équilibre est environ 0.20 ± 0.05 Pa.s, pendant qu'elle est environ 12 Pa.s pour le cas de 13 s^{-1}.

On peut voir que les caractéristiques rhéologiques de l'alliage métallique à l'état semi-solide montrent le comportement pseudoplastique qui peut être décrit par équation de loi de puissance (power law equation). A partir des expériences "Step Change", la viscosité apparente à l'état stationnaire a été tracée en fonction de la vitesse de cisaillement ce qui a révélé un comportement pseudoplastique. Ces viscosités stationnaires ont été prises à partir des valeurs du régime quasi-permanent sur la courbe "Step Change" quand la viscosité devient constante avec du temps prolongé de cisaillement à une vitesse de cisaillement constante. L'exposant de loi de puissance à 565 ° C confirme que l'évolution morphologique de la phase primaire de silicium augmente la pseudoplasticité.

SUMMARY

Hypereutectic Al-Si alloys are used in applications where high resistance to wear and corrosion, hardness and a low coefficient of thermal expansion are essential. To maximize the properties of these alloys, semi-solid processing can be utilized to modify the solidification structure of the primary silicon crystals as well as to reduce microsegregation and porosity. The transformation and spheroidization of primary Si crystals by shearing in the semi-solid state are not fully understood. The objective of the present work is the determination the rheological characteristics of A390 (Al-17%Si-4.5%Cu-0.5%Mg) alloy using a Couette type (Haake RV12) viscometer and to evaluate the microstructural evolution during continuous cooling and isothermal shear rate experiments. The effect of shear rate, solid fraction (temperature) and morphological evolution of the silicon crystals are investigated. A study of the thermodynamic properties and the solidification path of A390 was also carried out to analyse the nature of the solid phases that influence the rheological characteristics. This is possible by the numerical modeling of the thermodynamic functions required to construct the quaternary phase diagram of the alloy under study using the FACTSAGE software developed by the CRCT at École Polytechnique de Montreal.

According to solidification path of A390 alloy calculated by the Factsage software, the silicon crystals first appears at 653 ° C (liquidus temperature) as a primary phase and continue to precipitate down to binary eutectic temperature of 566 ° C where silicon and α-Al solidify in form of a eutectic structure. The maximum solid fraction of primary

silicon crystal was calculated to be about 6.1%. The silicon that solidifies as the primary phase has a faceted morphology and the eutectic has coarse plate-like crystals. The $Cu_2Mg_8Si_6Al_5$ phase typically nucleates on θ-Al_2Cu crystal in the form of blocky or thin needle-like structures [1]. The θ-Al_2Cu phase generally precipitates in a blocky θ-Al_2Cu crystal or in the form of a binary eutectic with α-Al (Al+Al_2Cu eutectic). It can also appear as a mixture of both forms depending on the cooling rate [2]. In the equilibrium condition or at very slow cooling rates, the eutectic form is predominant. The Mg_2Si phase precipitates in the form of large Chinese script particles [2]. Based on Factsage calculation, the binary eutectic reaction occurs at 566 ° C and 88% of the liquid changes to binary Al-Si eutectic when the temperature of 502 ° C is reached. At this temperature the ternary eutectic reaction takes place (Liq. → Al (fcc) +Si (s) +Mg_2Si (s)). The ternary eutectic reaction continues down to the temperature of 496 ° C where solidification becomes complete according to the quaternary eutectic reaction (Liq. → Al-Cu (θ) +Al (fcc) +Si (s) +Mg_2Si (s)).

It should be noted that the Factsage calculation differs from measured experimental values in the literature. One of the reasons for this is the fact that the enthalpy of the quaternary compound such as $Cu_2Mg_8Si_6Al_5$ has not been taken into account in the existing data base in Factsage software. According to Mondolfo [3] and Fan [4] the quaternary eutectic reaction was found to occur at about 507 ° C according to the equation (Liq. → Al-Cu (θ) +Al (fcc) +Si (s) +$Cu_2Mg_8Si_6Al_5$). Moreover, the phase diagram indicates that the α-Al solidifies only in form of a binary eutectic morphology at

temperatures between 566 ° C-502 ° C. Nevertheless, the microstructural observation confirms the presence of α-Al in the form of both eutectic and individual grains in the matrix during continuous solidification. Therefore, the region of "Liquid + Si + Al" which corresponds to the binary eutectic region results in the solidification of α-Al with two morphologies. This is a characteristic of non-equilibrium solidification and can not be determined from the calculated phase diagram. H.S. Kang et al. [5] have observed that microstructure of hypereutectic Al-Si alloys depends strongly on undercooling levels. For near eutectic Al-13 wt%Si alloys the phase changes from eutectic to primary α-Al dendrites with eutectic. The reason for this phase change may result from the growth velocity of the α-Al phase exceeding that of the Al-Si eutectic phase with an increasing level of undercooling. Based on the competitive growth principle, i.e. the principle that the most preferred microstructure is that with the highest growth velocity at a given undercooling, microstructural transformations can be expected. In addition, a morphological change of primary α-Al from dendritic to equiaxed grains was observed at this level of undercooling. They showed that the conditions of rapid crystal nucleation, growth, and marked solute trapping effect which occur at high undercooling are responsible for the transformation from dendrite to equiaxed grains. As a result, for two hypereutectic Al-Si samples with same composition, more α-Al is present during solidification at high undercooling than for low undercooling. Several studies have shown the similarity that can occurs between hypereutectic Al-Si alloys and Al-based composites with similar composition [6].

The addition of 5% copper to binary Al-Si stabilizes α-Al in the semi solid state. In the hypereutectic region of binary Al-Si alloys, the "Liquid + Si" is the only semi solid zone and solidification become complete with the binary eutectic reaction at about 577° C. For A390 alloy, according to the phase diagram, the binary eutectic reaction occurs in the "Liquid + Si + Al" in a range of temperature between 566° C-502° C. Therefore, α-Al co-exists with Liquid + Si in the semi solid state. Usually, semi solid processing is carried out in this temperature range where the final solid fraction can be controlled by changing of α-Al solid fraction in this region. It should be noted that the thixoforming process must be carried out at a solid fraction between 30%-50% because at solid fractions higher than 50%, problem of die filling occur due to the very high viscosity.

The rheological behaviour was investigated for continuous cooling and isothermal conditions.

In the case of continuous cooling tests, the alloy was continuously cooled at the rate of -2 ° C/min and sheared at the rates of 15, 59, 123, 250 and 507 s^{-1} down to the temperature when the upper limit of the viscometer torque is reached. The experimental results show that the viscosity of the semi-solid slurry depends on both the temperature (solid fraction) and shear rate. As the temperature is decreased to the semi-solid zone, the viscosity starts to increase in a significant manner. This increase is very gradual up to the binary eutectic temperature of 566 ° C. Primary silicon solidification occurs between 653 ° C-566 ° C with maximum solid fraction of only 6.1%, resulting in gradual increase of viscosity. At the binary eutectic reaction (566 ° C) the alloy contains a liquid

fraction of 93.9% whereas only a small liquid fraction (3.9%) remains at the quaternary eutectic temperature (496° C). In the binary eutectic zone below 566° C, the viscosity increases rapidly as the amount of solid fraction increases. In all continuous cooling tests the temperature does not reach the quaternary eutectic temperature at 496° C because the maximum 4.9 N-cm torque limit of the viscometer is reached before this temperature is attained.

At a shear rate of 15 s^{-1} no degradation of the solidified structure was observed. For a shear rate of 59 s^{-1}, the microstructure was considerably different from the structure at 15s^{-1}. About 50% of the primary silicon was fragmented and the debris was found at the periphery of the primary particles. However, other primary silicon particles remained faceted without fragmentation. The eutectic silicon particles with a plate-like morphology were partially fractured and showed a fragmented (fractured) microstructure. It was observed that the θ-Al_2Cu phase is surrounded by blocky $Cu_2Mg_8Si_6Al_5$ particles which can be associated with the eutectic phase that nucleated on the large primary silicon crystals. As the size of silicon particles increases, this effect becomes more pronounced. We can also observe region of blocky Al_2Cu, eutectic and fragmented eutectic silicon in the matrix. In addition, it was also observed that the globular α-Al phase could be present in several regions. The morphology evolution of the α-Al occurs as a result of shear force resulting in non-dendritic solidification.

At a shear rate of 123 s^{-1} about 80 % of primary silicon usually of a faceted morphology, fragments along specific planes such as $\{100\}$ planes and $\{110\}$ cleavage planes.

Fragmented debris can be found to be at the periphery of the original particles. However, agglomeration of the fragmented silicon was not observed. Large primary silicon particles were not fragmented and only showed cracks. All of the acicular $Cu_2Mg_8Si_6Al_5$ phase was fragmented and generally found at the periphery of the Al_2Cu particles.

At a shear rate of 250 s^{-1}, all of the primary silicon becomes fragmented and the faceted morphology is almost entirely degraded. The results show that the fragmentation of the primary silicon (non-metallic) is much higher when compared to fragmentation of the primary α-Al particles. Furthermore, the fragmentation mechanism is considerably different from that observed by Vogel et al. [7] and Doherty et al. [8] on the fragmentation of the metallic primary phases. A detailed analysis of the etched microstructure of primary silicon was carried out by Lee et al. [9] who revealed that primary silicon particles grow octahedrally and that the fracture takes place along $\{100\}$planes and $\{110\}$cleavage planes.

At a strong shear rate of 507 s^{-1} most of the primary silicon changes to a spheroidal shape which easily disperses in the matrix. This morphological change reduces the viscosity dramatically. In addition, at this shear rate, the region consisting of the particles such as fragmented silicon eutectic, eutectic, blocky Al_2Cu and broken acicular $Cu_2Mg_8Si_6Al_5$ has been observed to be spheroidal due to this powerful shear rate

In the case of isothermal tests, the alloy was first heated to a temperature of 700 ° C and then continually cooled at -2 ° C/min and sheared at 13 s^{-1} to the temperature of 565 ° C.

At this temperature, the α-Al solidifies in two morphologies. The alloy was then sheared for 20 minutes under isothermal conditions at new constant shear rates. This test, called "step change", determines the viscosity change with abrupt changes of shear rate. In another "step change" test at the same temperature of 565 ° C, the shear rates were abruptly changed in a sequence of 52-, 104-, 26-, 104- and $13s^{-1}$. For these experiments, small transient viscosity (or thixotropic) regions were detected for the A390 alloy. At this isothermal test temperature, the solid fraction of primary Si is only 6.1% and abrupt changes in the viscosity indicate that the transient period (thixotropic) is very short where a new agglomeration state of the solid phases is rapidly established at a given shear rate. At shear rate of 104 s^{-1} the steady state viscosity is about 0.20 ± 0.05 Pa.s while it is only 11.60 ± 0.40 Pa.s for the case of 13 s^{-1}.

It was observed that the rheological characteristics of metal alloys in the semi-solid state exhibit pseudoplastic behaviour which can be described by power law equation. Based on the "Step Change" experiments, the apparent steady state viscosity was plotted as a function of the shear rate, resulting in pseudoplastic behaviour. These steady state viscosities were taken from the points on the 'Step Change' curve (viscosity versus time for each shear rate) when the viscosity becomes constant with prolonged shear time at a constant shear rate. The power law index (n) at 565 ° C confirms that the morphological evolution of Si primary phase increases the pseudoplasticity.

TABLE OF CONTENTS

LIST OF TABLES

PAGE

LIST OF FIGURES

PAGE

LIST OF APPENDIXES

PAGE

CHAPTER 1

INTRODUCTION

As the trend of automakers towards weight reduction continues, the need to replace the iron and steel components with lighter materials has led to the increased use of aluminum and magnesium castings in automobiles.

The automakers are now focusing on components with more demanding functional performance specifications. To produce these lightweight components, the automakers are using manufacturing processes that can produce near-net shape, thin wall aluminum or magnesium components, combining excellent mechanical and functional performance with low total manufactured costs.

Semi-Solid Metal (SSM) processing has been shown to meet these requirements. The original experiment leading to the discovery of rheocasting was performed in 1972 by Spencer et al. [10]. They used Sn–15Pb alloy as a model system to evaluate the viscosity of the partially solidified alloy using a Couette viscometer. They discovered that when the dendritic structure is sheared, the partially solidified alloy has a greatly reduced viscosity and exhibits thixotropic behaviour.

The commercial SSM process is a relatively new technology of metal forming. Different from the conventional metal forming technologies which use either solid metals (solid state processing) or liquid metals (casting) as starting materials, SSM processing deals

with semisolid slurries, in which non dendritic solid particles of the alloy are dispersed in a liquid matrix. Therefore, it offers several potential advantages such as energy saving for forming, reduction of microsegregation and porosity, especially for near net shape manufacturing of components.

Semisolid metal slurries exhibit distinctive rheological characteristics: the steady state behaviour is pseudoplastic (shear-thinning) which can be described by the power law equation (see section 2.3.1.2.1, power law fluids), where the flow is characterized by a decrease in viscosity as shear is increased. However, the transformation of the semi-solid microstructure with time is a transient state phenomenon leading to a change of the viscosity, characteristic of a thixotropic behaviour. All the currently available technologies for SSM processing have been developed on the basis of these unique rheological properties, which originate from the transformation of microstructures of the solid phase particules.

Semi-solid processing in generally is carried out using two typical methods of forming: rheocasting and thixocasting. Rheocasting involves the application of shear during solidification to produce non-dendritic semisolid slurry that can be transferred directly into a mould or die to produce a component. Thixoforming is a near net shape where the feedstock (billet) with a non-dendritic structure is used as a starting material. This microstructure can be obtained by a rheocasting process using mechanical or Magneto-Hydrodynamical (MHD) stirring during solidification or by other methods, such as, the Strain Induced Melt Activated processes (SIMA) (for achieving non-dendritic structures)

or by a Spray forming process. The feedstock is heated up to the semi-solid temperature and injected into a metal die. Thixoforming has advantages compared to other processes because the material is injected at lower temperatures, allowing for laminar material flow rather than the highly turbulent flow of conventional die casting processes. Accordingly, the thixoforming process reduces the defects associated with die-casting and results in components with excellent mechanical properties and functional performance with low total manufactured costs.

Hypereutectic Al-Si alloys such as A390 (Al-17%Si-4.5%Cu-0.5%Mg) are used in the automotive industry and other applications where good wear resistance is necessary. Significant improvements in properties can be obtained with increases in Si content but high temperatures are required for melting high Si content alloys. Consequently, a coarse network of primary silicon particles leads to adverse ductility and toughness when conventional casting techniques are used. However, the commercial potential for their outstanding resistance to wear and corrosion, higher hardness, low coefficient of thermal expansion and density, dimension stability and good cast performance is well recognized.

The addition of 5% Cu to the binary Al-Si was found to be necessary in order to stabilize the α-Al phase in the semi-solid state, making the Al-Si more readily thixoformable. Furthermore, the particle size could be further reduced to < 20 μm when 2% magnesium was added to the alloy [11]. This addition also inhibited the formation of a continuous

silicon network in the material. However, as mentioned before, the application of these alloys is restricted as a result of reduced ductility and toughness.

The forming of hypereutectic alloys by the semi-solid route needs to overcome these difficulties. The casting temperature and heat content are very much reduced in thixoforming these alloys, producing a microstructure of homogeneously distributed primary silicon particles. Also, the solidification shrinkage of semisolid materials is significantly reduced when compared with casting of the liquid alloy.

The rheological characteristics of SSM slurries can be determined by carrying out 4 types of experiments:

(1) Continuous cooling verifies the viscosity change during continuous cooling at fixed cooling rate and at a constant shear rate.

(2) Isothermal shearing determines the shear rate dependence of steady state viscosity, or shear thinning behaviour (Pseudoplasticity) by varying the shear rate.

(3) Step change tests which describes the time dependence of viscosity as the shear rate is instantaneously changed for one value to another. This defines the thixotropic character of the alloy.

(4) Another type of experiment need to evaluate the thixotropic nature of the alloy is the continuous change of shear rate to a maximum value. The hysteresis loops obtained are indicative of the thixotropic properties.

The main objective of this research is the better understanding of the mechanisms involved during semi-solid processing of hypereutectic Al-Si alloys.

Chapter 2 consists of the literature review, describing the structure and properties of unstirred (dendritic) and stirred (non dendritic) alloys in the semi-solid state and the mechanisms associated with non-dendritic solidification. In addition, the rheology of the suspension of rigid particles and rheological model of the suspensions exhibiting Newtonian and non-Newtonian behaviour are presented.

The general solidification characteristics of the A390 are also presented in this chapter. Initially, the advantages and disadvantages of using cast A390 are listed. Subsequently the fragmentation mechanism of the primary silicon by external force and collision between particles and the Si coarsening of hypereutectic alloy in the semi-solid state are presented.

Chapter 3 describes the methodology of the experiments carried out in this work. The thermodynamic analysis of the system is first presented followed by description of the experimental procedure for the continuous cooling and isotherm tests.

Chapter 4 is divided into three sections. The first section presents the results of thermodynamic evaluation of the alloy system including a numerical simulation of the phase diagram of the A390 alloy. The matrix of A390 corresponds to a quaternary system Al-Si-Cu-Mg in the Al corner of the diagram. At first, the experimental phase diagrams relevant to this study are presented and compared with the models that are

determined by the mathematical representation of the thermodynamic functions (Gibbs' free energy) required to compute the phase diagrams. Calculations of the phase diagrams were carried out by the Factsage software developed by the group CRCT of *Ecole Polytechnique de Montréal.* The effect of Cu and Mg additions to the quaternary system were also presented.

The second section of chapter 4 presents the experimental results of the measurements of the apparent viscosity in the semi-solid state for the continuous cooling and isothermal tests carried out by means of a Couette (Haake RV12) viscometer. In the continuous cooling tests, the effect of variable shear rate on the modification of the microstructure was studied at fixed cooling rate. In the isothermal tests, the thixotropic region was analysed using a "Step Change" test, which was used to evaluate the pseudoplastic behaviour. The rheological characteristics of A390 and A357 (hypoeutectic Al-Si) were also compared. In the last part of chapter 4, the metallographic interpretation of A390 is briefly explained.

Chapter 5 presents the conclusions and recommendations based on the experiments carried out in chapter 4.

The specific objectives of this work are:

1) To investigate the mechanisms involved during semi-solid processing and rheological model of suspensions and to identify the general solidification characteristics of A390.

2) To evaluate the thermodynamics and phase relationships of A390 alloy using the FACTSAGE software.

3) To carry out viscosity measurements (rheological characteristics) of semi-solid A390 using two types of experiments: continuous cooling, isothermal.

4) To compare the rheological behaviour of the semi solid slurry in hypo- and hyper-eutectic Al- Si alloys in the continuous cooling condition.

CHAPTER 2

LITERATURE REVIEW

Structure and properties of alloys stirred in the semi-solid state

This chapter presents the principal characteristics of alloys stirred in the semi-solid state. Initially, we begin by describing the structure which develops during conventional solidification (without stirring) that will allow us, in the next stage, to compare the behavior of this structure with that of alloys stirred in semi-solid state.

2.1 Conventional (non stirred) solidification

2.1.1 Dendritic solidification

The growth condition and particularly the degree of undercooling are two important parameters that define the structure, which develops during conventional solidification of pure metal and alloys.

The undercooling of pure metals is achieved by means of thermal treatment. In alloys, undercooling can be produced indirectly by change of temperature and composition (constitutional undercooling). In this case, undercooling occurs as a result of crystal growth in a negative temperature gradient in the liquid.

In this case, the tip of the dendrite is in an area where undercooling is more significant than on the remainder of the dendrite interface and it will tend to grow even more quickly in the liquid and consequently, columnar or equiaxed dendrite solidification will develop [12].

During constitutional undercooling, the rejection of solute (solute redistribution) from the growing interface produces a solute diffusion layer in the liquid. This solute concentration gradient corresponds to a change in the liquidus temperature. Thus, the liquid ahead of a growing interface can become constitutionally supercooled, and the possibility arises of a critical degree of undercooling (ΔT_{crit}) that is required for nucleation to occur in this liquid ahead of the interface (Fig 2.1) [13].

This condition [14] occurs for the case

$$\frac{G_L}{R} < mC_0D\left(\frac{1-K_0}{K_0}\right) \tag{2.1}$$

Where G_L is the temperature gradient in the liquid, R is the solidification rate, C_0 is the alloy composition, D is diffusion coefficient, K_0 is distribution coefficient and m is the liquidus slope.

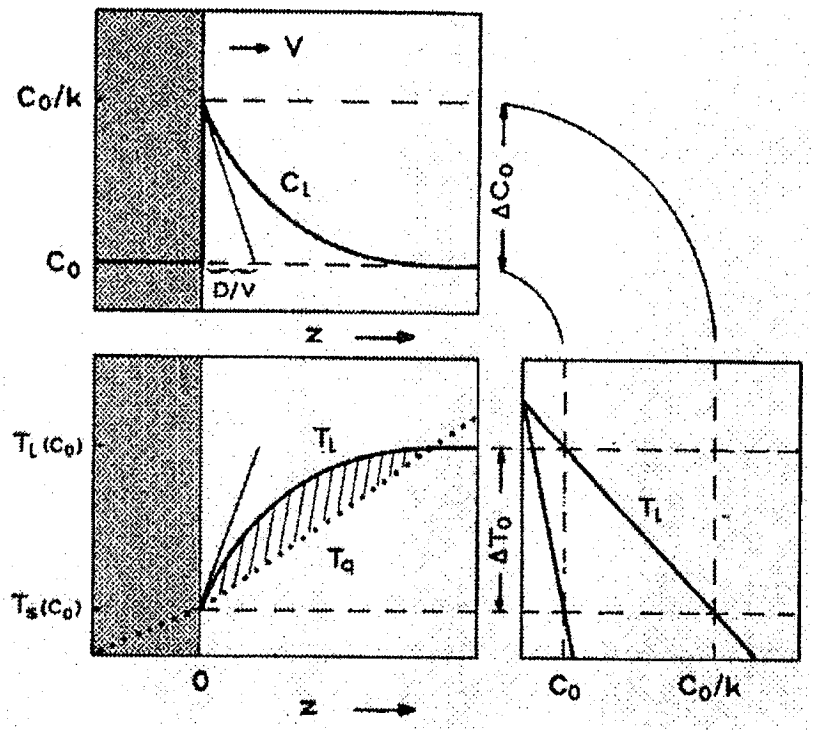

Figure 2.1: Constitutional undercooling [13].

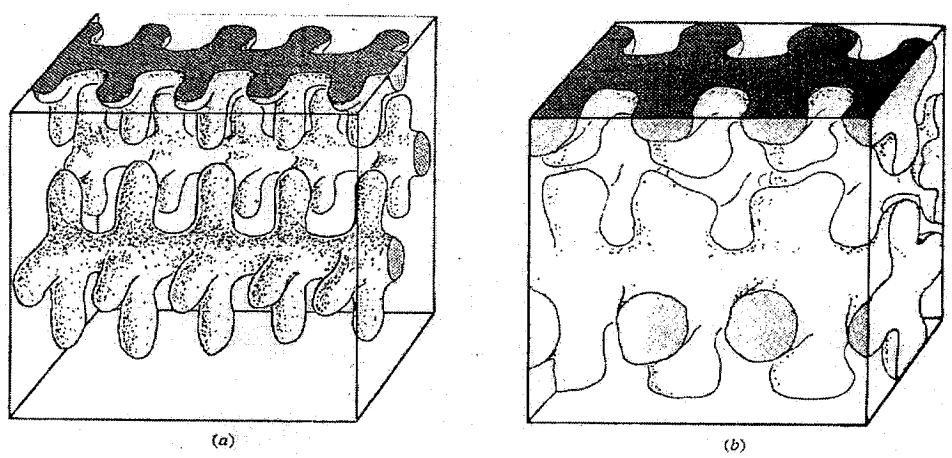

Figure 2.2: Schematic illustration of dendrite growth. Dendrite structure showed (a) early in solidification and (b) at about 50 pct solid. [14]

2.1.2 Dendrite morphology

In both equiaxed and columnar structures, the dendrites evolve during solidification as a result of ripening (coarsening). During coarsening, the dendrite volume increases and the number of particles decrease due to the decrease in total interfacial energy which causes remelting (dissolving) of dendrite arms of smaller radius. This process is described as Ostwald- ripening defined by equation 2.2 for spherical particles of diameter. Fig.2.2 shows this schematically for a dendritic structure [14]. The parameter usually chosen to measure this change is the secondary dendrite arm spacing, d.

In accordance with expected ripening kinetics, it is found that final dendrite arm spacing bears an approximately cube-root relationship to the local solidification time [15] due to the Ostwald-ripening equation:

$$d^3 - d_0^3 = k_0 t \tag{2.2}$$

Where t is the time, k_0 is the rate constant, d and $d_\circ$ are the variable and the initial particle diameter, respectively [16]. Larger particles grow at the expense of smaller ones so as to reduce the surface energy of the system. In the case of purely diffusion-driven Ostwald ripening, k_0 has the form:

$$k_0 = \frac{8TD\Gamma}{9m(C_S - C_L)} \tag{2.3}$$

Where T is the temperature, Γ is the characteristic length, m is the liquidus slope, C_S is the solid composition and C_L is the liquid composition. In section 2.8, Si coarsening in the semi-solid state will be discussed in terms of this relation.

2.1.3 Dendrite coalescence

The growth of secondary branches of dendrites causes dendrite coalescence [17]. This phenomenon is similar to the ripening phenomena but there is an important difference between these two phenomena that relates to the shape of the dendrite surface. Generally, the ripening phenomenon is predominant for solid fraction up to 0.5; beyond this value the coalescence is predominant.

2.1.4 Deformation behaviour of dendritic structures

During solidification, the grains first nucleate in the melt and are free to move. At some critical local fraction solid, the grains form a network. At this stage "mass feeding" ceases and "interdendritic feeding" starts (Dendrites start to form a resistant skeleton) [14]. The fraction solid at which the dendrites form a cohesive network results in increased strength and depends on dendrite size and morphology. A number of studies of different alloys show it to be in the range of about 0.1 to 0.2 and occasionally higher (Fig. 2.3). In well grain-refined alloys, strength did not begin to develop until a solid fraction of 0.40 is reached.

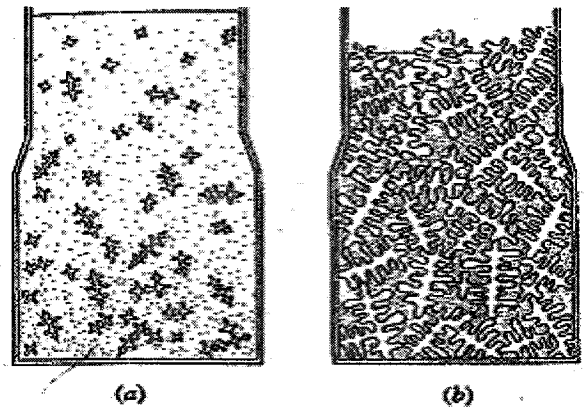

Figure 2.3: Feeding of freezing alloy, a) mass feeding stage and b) interdendritic feeding stage [14]

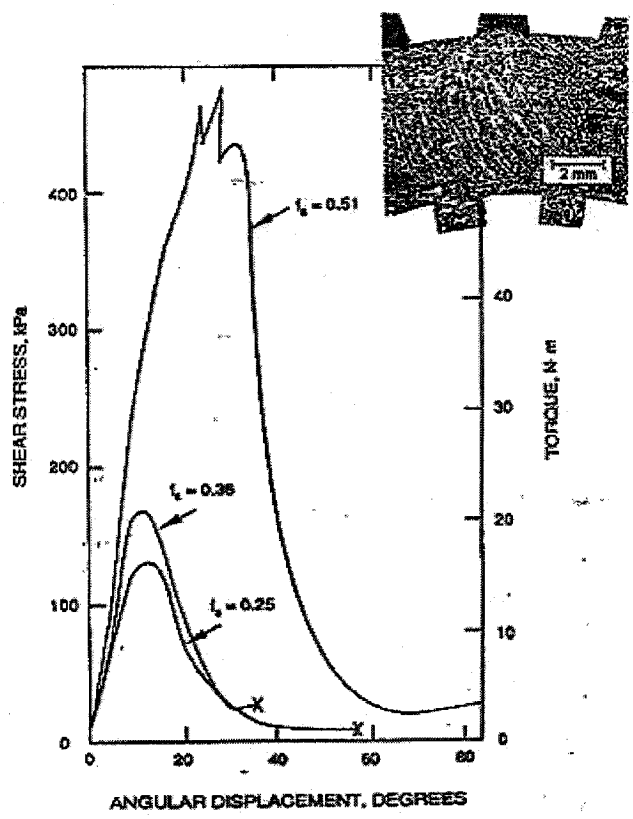

Figure 2.4: Isothermal shear test results of semi-solid Sn-15%Pb alloy [14]

Typical isothermal stress-strain curves for semi-solid Sn-Pb alloy [18] are shown in (Fig. 2.4). The test apparatus of this study consisted of flow between two grooved rotating cylinders. At the given strain rate, stress increases with increase angular displacement to a maximum, after which it falls to a low value. The maximum stress increases with increasing solid fraction. Deformation at solid fractions up to about 0.9 occurs primarily by grain-boundary sliding, with some dendrite distortion, as shown by the microstructure at the upper right micrograph of Fig. 2.4. The increase of stress with strain is probably because strain increases the number of contacts (the "welds") betweens particles. At sufficiently high strain, continuous fissures open, so stress falls to a low level. The fissures become filled with the liquid except at very high solid fraction and segregation can occur.

2.2 Non-dendritic Solidification

During dendritic solidification, a number of processes take place simultaneously in the semi-solid region. These include crystallization, solute redistribution, ripening, interdendritic fluid flow, and the solid movement. The dendrite structure which forms, is greatly affected by convection during the early stages of solidification. With vigorous convection and slow cooling, the grains become spheroidal. Semi-solid alloys with this microstructure possess rheological properties, which are quite different from those of dendritic alloys. They behave thixotropically and the apparent viscosity can vary over a wide range of shear rate depending on processing conditions.

Vigorous convection is achieved by using external forces such as mechanical or electromagnetic stirring. Generally, the alloy is sheared in the liquid state and the alloy is then slowly cooled into the solidification range while it is being sheared [14]. The shear stress increases only very slowly as temperature is decreased below the liquidus and is orders of magnitude smaller than alloys that are cooled to the given temperature for the non-sheared case. The grain structure obtained in these early experiments was non-dendritic and the material was found to consist of a liquid like slurry, with an apparent viscosity lower than for the dendritic case.

2.2.1 Processes for achieving non-dendritic structures

Fig. 2.5.a schematically illustrates the simple "batch rheocaster," in which a crucible of molten liquid is mechanically stirred while being cooled. A second type of process known as the "continuous rheocaster" illustrated in Fig. 2.5.b has the following characteristics:

(1) Higher shear rate is readily achievable.

(2) The stirring is well below the surface of the metal, thus minimizing air entrapment.

(3) Cooling rate can be high so as to achieve a fine structure.

The third type of process (Fig. 2.5.c) is vigorous electromagnetic stirring used in continuous casting. This process is of considerable technological importance today, since it permits production of large tonnage using a variant of a well-established technology and it is applicable to high-temperature melting such as steel. It avoids any

problem of wear or erosion since it does not require any agitator and results in better mixing because it acts effectively on the whole of the semi-solid slurry contrary to the case of mechanical mixing with agitator.

Another completely different approach used to obtain non-dendritic structure has been termed "strain-induced melt activation" (SIMA). In this case, an alloy billet or bar (usually of relatively small cross section) is cold worked to a critical level so that, on reheating into the liquid-solid zone, the desired spheroidal structure is obtained [18]. By this method, the semi-solid slurries of Al-Si, Al-Cu, and Cu-Zn have been produced successfully.

Previously, the only processes in significant commercial use were electromagnetic stirring of continuous cast ingots ("magneto-hydrodynamic (MHD) process") and the SIMA process. Recently, the "slurry on demand" processes such as NRC (New Rheo-Casting) and SEED (Swirled Enthalpy Equilibration Device) have been developed for new applications of semi-solid forming process.

2.2.2 Physical mechanism associated with non-dendritic solidification

As solidification begins, vigorous agitation results in the formation of new grains from initial dendrite fragments as shown in Fig. 2.6.a [14]. The early growth of each dendrite fragment then continues dendritically as shown schematically in (Fig. 2.6.b). With continuing shear and time during solidification, the dendrite morphology changes to the

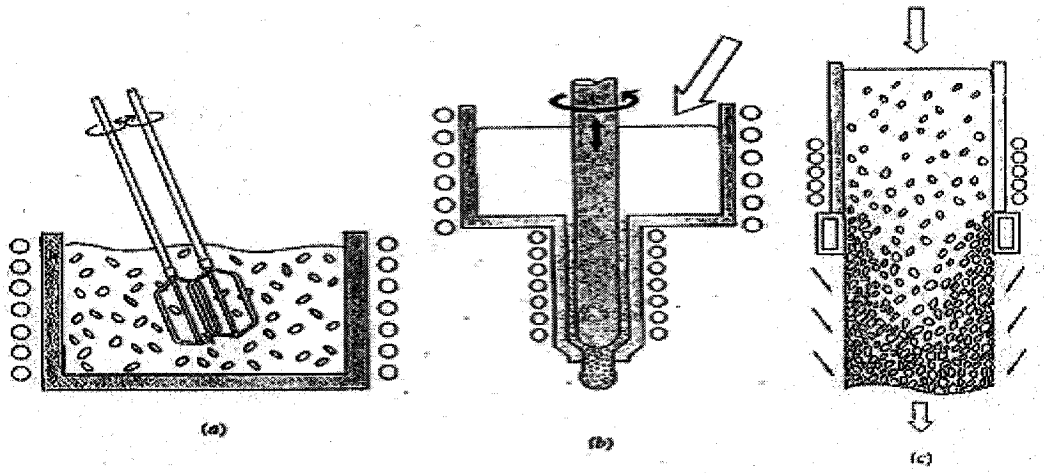

Figure 2.5: Schematic diagram of method of producing of non-dendritc structure a) bath b) continuous and c) electromagnetic stirring with continuous casting [14].

form of a "rosette" (Fig. 2.6.c), as a result of ripening, shear and abrasion with other grain ripening proceeds during further cooling (Fig. 2.6.d) and with sufficiently slow cooling and high shear, the particles become spheroidal (or in some case, ellipsoidal), often with a small amount of entrapped liquid, as shown in (Fig. 2.6.e).

The extent to which the morphology evolves from that of (Fig 2.6.a) to that of (Fig. 2.6.e) increases with increasing shear rate and with decreasing cooling rate.

Spencer et al. [10] observed the spherical morphology of primary Al crystal under high shear rates and suggested that the morphological change from dendritic to spherical grains occurs through the initial deformation of individual dendrites followed by the total collapse of the dendritic structure.

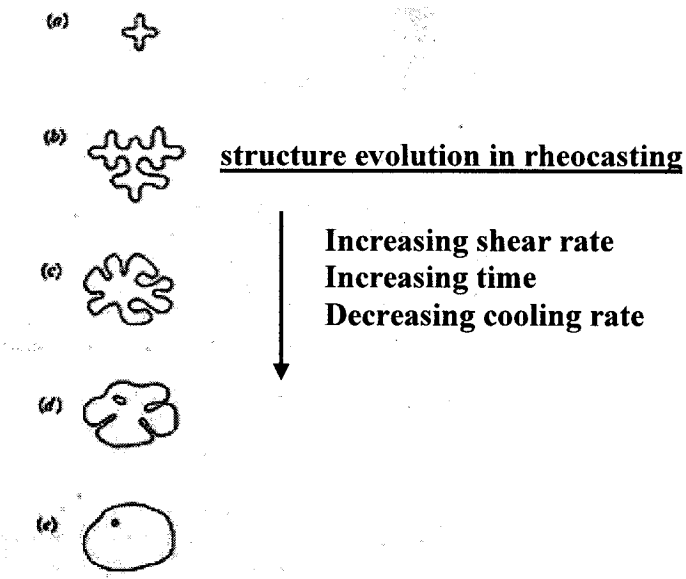

Figure 2.6: Globularisation mechanism a) initial dendrite fragment b) dendrite growth c) rosette d) ripened rosette and e) spheriod [14]

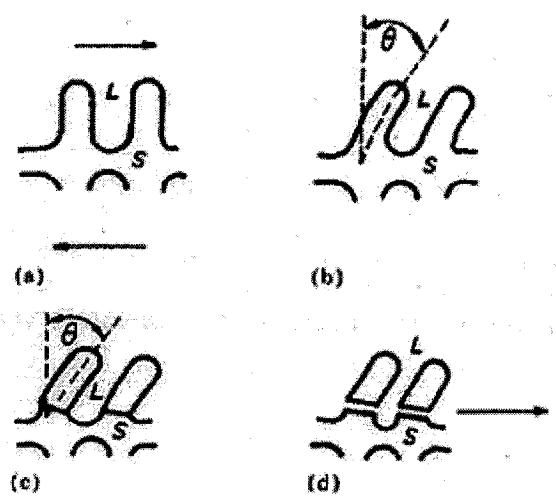

Figure 2.7: Dendrite fragmentation mechanism [7]

Vogel et al. [7], and Dohetry et al. [8], on the other hand, proposed that the fragmentation of metallic dendrites could occur by dendrite arm bending during stirring, creating boundaries within the dendrite and complete wetting by the liquid phase leading to eventual break up of dendrites. (Fig.2.7)

Lee et al. [9] showed that the break down of the dendrites and their coarsening is caused by shear rupture at a high fraction of solid phase (f_s >0.5) and by the Gibbs-Thompson effect during isothermal stirring. The Gibbs-Thomson effect relates surface curvature to chemical potential. It leads to the fact that small particles exhibit a higher surface energy since the surface is larger in comparison to the volume. In fact, the driving force for coarsening the fragmented dendrites can be attributed to this effect. However, it remains to be determined as to which mechanism is dominant for the formation of spherical non-dendritic particles.

2.3 Rheology of Suspensions

Suspended solids are divided into high-gravity and low-gravity solids (HGS and LGS). LGS are sometimes further subdivided into active and inactive solids. A mixture of suspended solids and liquids is called slurries. In the case of alloys, the suspension is called a semi solid metal slurry.

Rheology is, generally, the study of how matter deforms and flows, including its elasticity, plasticity and viscosity based on external forces such as stirring. In the next section, the rheology of suspensions will be described.

2.3.1 Rheology of suspension of rigid particles

Viscosity is a property of fluids and slurries that indicates their resistance to flow, defined as the ratio of shear stress to shear rate. Viscosity can be expressed mathematically as follows:

$$\mu = \frac{\tau}{\dot{\gamma}} \tag{2.4}$$

Where τ is shear stress, $\dot{\gamma}$ is shear rate and μ is viscosity. Shear rate is the rate of change of velocity at which one layer of fluid passes over an adjacent layer with a dimension of reciprocal second (s^{-1}). The apparent viscosity is the overall viscosity of a suspension of particles in a fluid measured at a given shear rate at a fixed temperature and solid fraction. In order for a viscosity measurement to be meaningful, the shear rate must be stated or defined.

2.3.1.1 Newtonian fluids

A fluid that has a constant viscosity at all shear rates at a constant temperature and pressure, and which can be described by a one-parameter rheological model is called a Newtonian fluid.

$$\tau = \mu(\dot{\gamma}) \tag{2.5}$$

Where τ is the shear stress, $\dot{\gamma}$ is the shear rate and μ is the viscosity. This means that a plot of shear stress versus shear rate at a given temperature gives a straight line with a constant slope that is independent of the shear rate. We call this slope the viscosity of the fluid (Fig. 2.8). Table 2.1 shows the viscosity of some common metals at the melting point temperature [19]

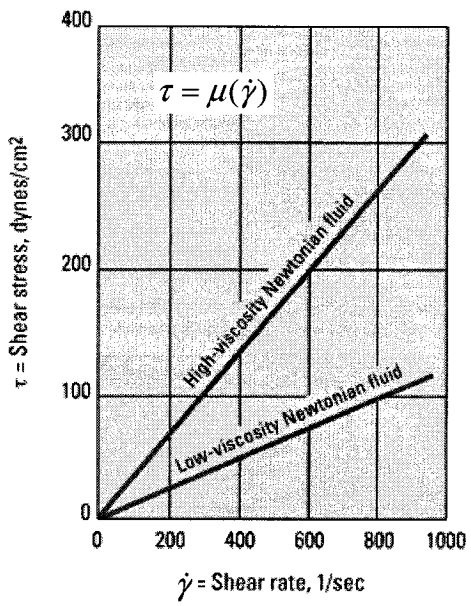

Figure 2.8: Newtonian fluid. Whether of low or high viscosity, Newtonian fluids have constant viscosity at all shear rate.

Table 2.1: The viscosity of some common metals at the melting point temperature [19]

Element	Melting Point $T_m(^0C)$	μ (T_m) mPa.s	ρ (T_m) $kg.m^{-3}$
Al	660	1.38	2380
Cu	1083	4.38	8000
Fe	1535	6.93	7030
Mg	650	1.25	1590
Mn	1244	5	5760
Si	1414	0.8	2530
Zn	419	3.5	6580
Ag	960	4.27	9300
Cr	1905	5.7	6290
Ni	1455	4.9	7900
Sn	231	1.87	6980
Ti	1725	2.2	4130

2.3.1.2 Non-Newtonian fluids

A fluid with a viscosity that varies with shear rate is generally called non-Newtonian (Fig. 2.9). In this case, the slope of the shear stress versus shear rate curve will not be constant as we change the shear rate (Fig. 2.10).

Some fluids such as metals in the semi-solid state, blood, paint and certain plastics are called shear-thinning fluids. The relevant characteristic of these fluids is a decrease in apparent viscosity with increasing shear rate. Fluids that exhibit this property are referred to as "pseudoplastic" (Fig. 2.11). For the opposite case, where the viscosity increases as the fluid is subjected to a higher shear rate, the fluid is called shear-thickening or dilatant. These fluids have found application in some all wheel drive systems where a torque converter filled with dilatant fluid provides power transfer between the front and rear wheels.

Many shear-thinning fluids will exhibit Newtonian behavior at extreme shear rates, both at low and high values. When log apparent viscosity is plotted against log shear rate, the behavior can be represented by Fig. 2.12.

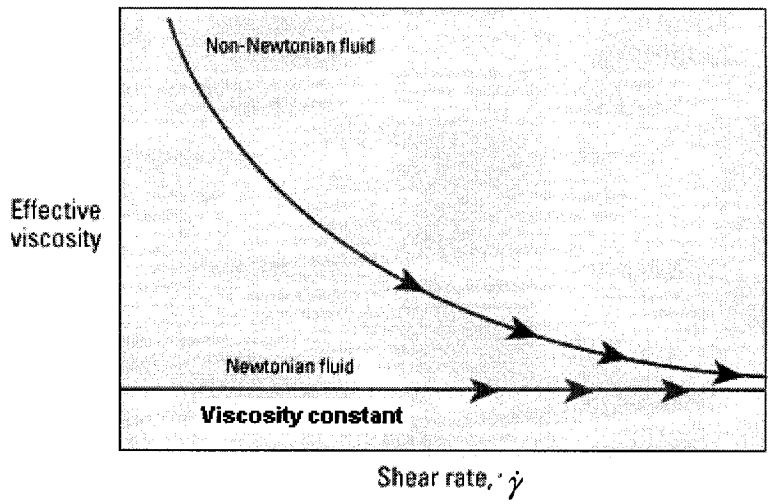

Figure 2.9: Non-Newtonian fluid. The viscosity of Non-Newtonian fluids varies with shear rate

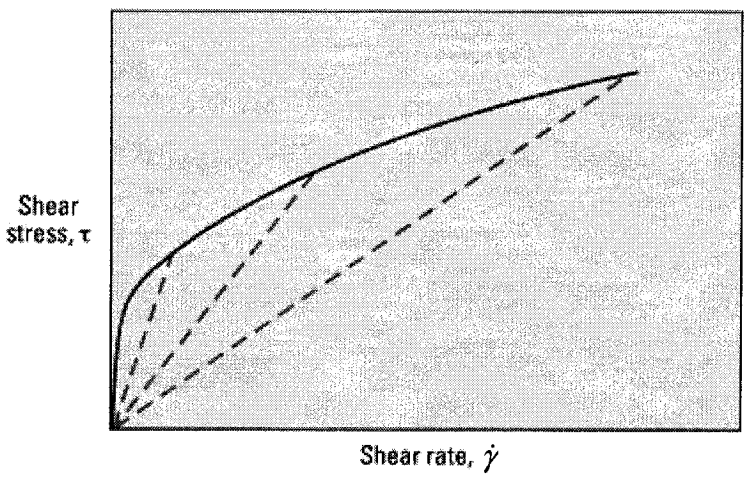

Figure 2.10: Non-Newtonian fluids do not exhibit a linear relationship between shear stress and shear strain rate, as shown in this rheogram. A certain threshold must be applied to initiate flow

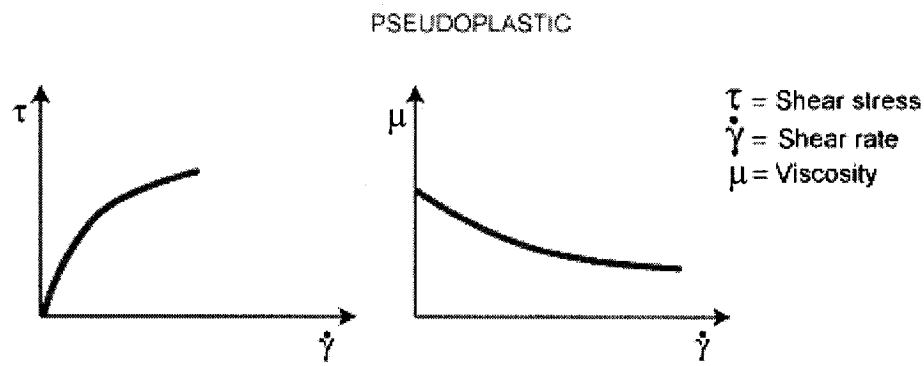

Figure 2.11: Pseudoplastic behavior

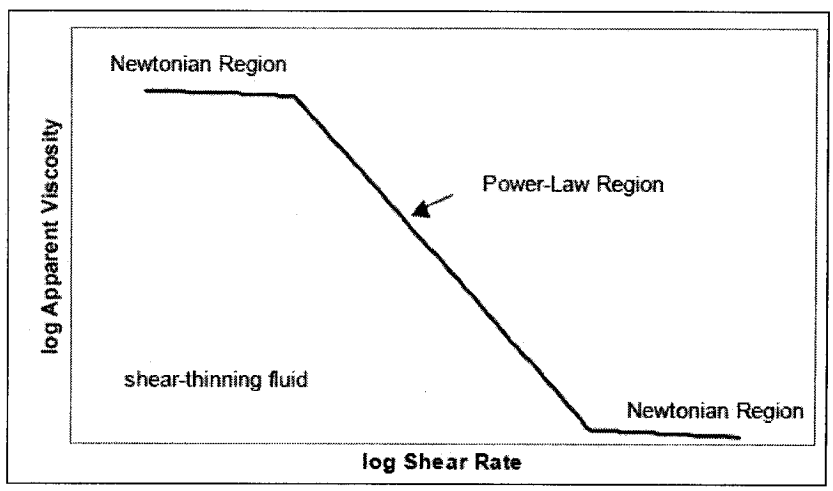

Figure 2.12: Many shear-thinning fluids will exhibit Newtonian behaviour at extreme shear rates.

2.3.1.2.1 Power-law fluids

Fluids described by the two-parameter rheological behaviour, known as power-law fluids, can be described mathematically as follows:

$$\tau = k(\dot{\gamma})^n \tag{2.6}$$

Where τ is the shear stress, $\dot{\gamma}$ is the shear rate and k is the consistency. In this region, we can calculate the viscosity using equation 2.6, where $\mu = \frac{\tau}{\dot{\gamma}}$ such that:

$$\mu = k\dot{\gamma}^{n-1} \tag{2.7}$$

and where k is the consistency of the fluid which depends on solid fraction and n is called the power-law index or degree of pseudoplasticity. Typically, for shear thinning fluid (metal semi solid), n lies between 1/2 and 1/3 ($0< n <1$), even though other values are possible as shown in Table 2.2.

It should be mentioned if $n \prec 0$ the equation describes the viscosity in the isostructural state. This result is apparently in contradiction with pseudoplastic behavior. In fact, a value of n-1 smaller than -1 corresponds to a decrease of shear stress when shear rate is increased. McLelland [20] attributed this to an effect of structure and proposed a model for explaining isostructural change.

Table 2.2: Value of n for various type of fluid

n	Type of fluid
<1	Pseudoplastic (most common)
1	Newtonian fluid
>1	Dilatants
<0	Isostructural

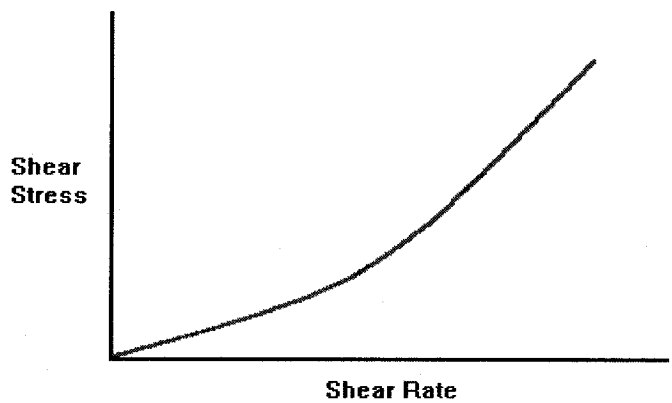

Figure 2.13: Dilatant fluids

2.3.1.2.2 Dilatant Fluids (shear-thickening fluids)

These fluids too obey the power-law relationship for the case where n >1. As a result, the curve for a dilatant fluid looks the same as a pseudoplastic fluid, except that it is concave upwards. Because the apparent shear stress increases with increasing shear rate, such fluids are also known as shear thickening (Fig. 2.13).

2.3.1.2.3 Bingham plastic fluids

A two-parameter rheological model is widely used in industry to describe flow characteristics of many types of flows [21]. Another important type of non-Newtonian fluid is a viscoplastic or "yield stress" fluid. This is a fluid, which will not flow when only a small shear stress is applied. The shear stress must exceed a critical value known as the yield stress τ_0 for the fluid to flow. For example, when you open a tube of toothpaste, it would be good if the paste does not flow at the slightest amount of shear stress. We need to apply an adequate force before the toothpaste will start to flow. So, viscoplastic fluids behave like solids when the applied shear stress is less than the yield stress. Once it exceeds the yield stress, the viscoplastic fluid will flow just like a fluid. Bingham plastics are a special class of viscoplastic fluids that exhibit a linear behaviour of shear stress against shear rate. It can be described mathematically as follows:

$$\tau = \tau_0 + \mu(\dot{\gamma}) \tag{2.8}$$

Where τ is the shear stress, $\dot{\gamma}$ is the shear rate, μ is viscosity (constant) and τ_0 is the yield strength. Fluids obeying this model exhibit a linear shear-stress, shear-rate behaviour after an initial shear-stress threshold have been reached (Fig. 2.14).

2.3.1.2.4 Herschel-Bulkley fluids

A Herschel-Bulkley fluid can be described mathematically by a three-parameter rheological model as follows:

$$\tau = \tau_0 + k(\dot{\gamma})^n \tag{2.9}$$

This fluid behaviour is like Bingham fluid but does not exhibit a linear behaviour after an initial shear-stress threshold has been reached [21]. The Herschel-Bulkley equation is preferred to a power law or Bingham relationship because it results in more accurate models of rheological behaviour when adequate experimental data are available (Fig. 2.15).

2.3.1.3 Thixotropy and Rheopexy.

Some fluids display a change in viscosity with time under conditions of constant shear rate. There are two categories to consider:

1) Thixotropy (transient state viscosity): is the property of some non-Newtonian pseudoplastic fluids that show a time-dependent change in viscosity.

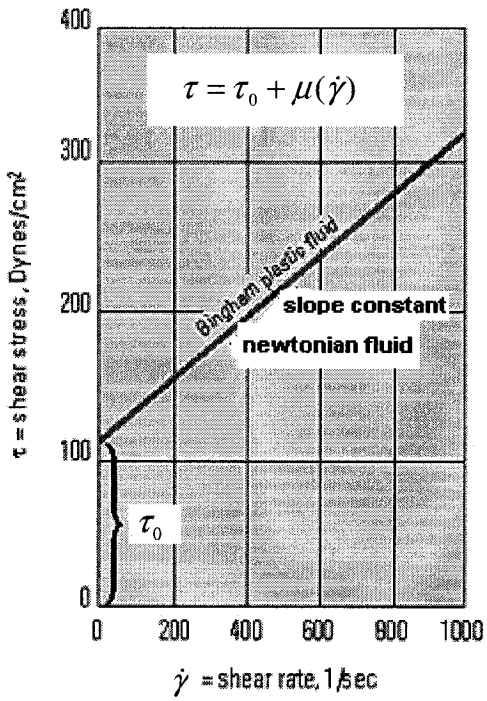

Figure 2.14: Bingham plastic model [21]

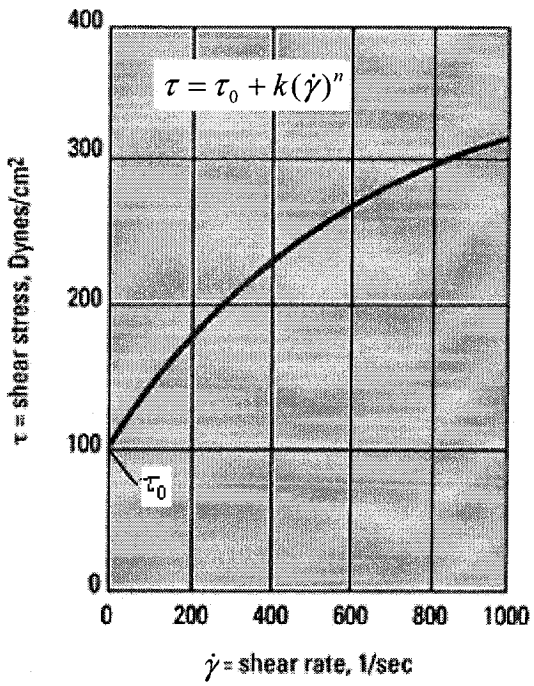

Figure 2.15: Herschel-Bulkley fluid [21]

Thixotropy is generally associated with pseudoplastic fluids. The viscosity of these materials, such as semi solid metal alloys will decrease with time under a constant applied shear stress until a steady state viscosity is reached (Fig. 2.16.a). However, when the stress is removed, the viscosity will tend to return to its original condition (Fig. 2.17).

2) Rheopexy: This is essentially the opposite of thixotropic behaviour, in that the fluid's viscosity increases with time as it is sheared at a constant rate (Fig. 2.16.b). Both thixotropy and rheopexy may occur in combination with any of the previously discussed flow behaviours, or only at certain shear rates. The time element is extremely variable under conditions of constant shear. Some fluids will reach their final viscosity value in a few seconds, while others may take up to several days.

The evaluation of thixotropic behavior can be tested using shear rate "step change" or "hysteresis loop" experiments (Fig. 2.17). This method makes it possible to evaluate the transient state viscosity (thixotropic) and steady state viscosity when the viscosity no longer varies with prolonged shear time at a constant shear rate. In figure 2.17 at the time t_1, the shear rate is abruptly changed from $\dot{\gamma}_2$ to $\dot{\gamma}_1$. Point (a) indicates steady state viscosity for shear rate $\dot{\gamma}_2$ whereas point (b) is starting point of thixotropic behavior for shear rate $\dot{\gamma}_1$. It is now generally accepted that the steady state viscosity at a given shear rate depends on the degree of agglomeration between solid particles, which, in turn, is the result of a dynamic equilibrium between the agglomeration and de-agglomeration processes [4]. The time to reach steady state defines of the thixotropic behavior where

the time dependence of transient state viscosity and is measured by step change experiments. It has been shown that re-agglomeration occurs after a shear rate decrease, whereas a degradation of agglomerates takes place when the shear rate is increased. The "hysteresis loop" experiments (Fig. 2.18) are an indication of the degree of thixotropy of the fluid. In this experiment, the sample of Sn-15%Pb is initially sheared at 100 s^{-1} with solid fraction of 45%. The shear is then stopped and the sample held at different rest times (t_r = 30s, 150s, 1000s). Thereafter, the shear rate is increased for a period of 2 seconds (t_u = 2s) for the different rest time samples, up to the maximum shear rate of 500 s^{-1} followed by a shear rate decrease to zero for the same interval (t_d = 2s). With increasing rest time the degree of agglomeration increases and results in different shear stresses at given shear rate for different rest time samples. This means that for different agglomeration conditions, de-agglomeration increases with increasing the shear rate each t_u = 2s. On the other hand, when shear rate decrease (t_d = 2s) between 500 s^{-1} to zero, the shear stresses are the same at given shear rate for different rest time samples. This means that the amount of agglomeration which occurs with decreasing shear rate, does not affect the shear stress for different rest time samples (insufficient time). In fact, the de-agglomeration kinetics is much faster than the agglomeration kinetics.

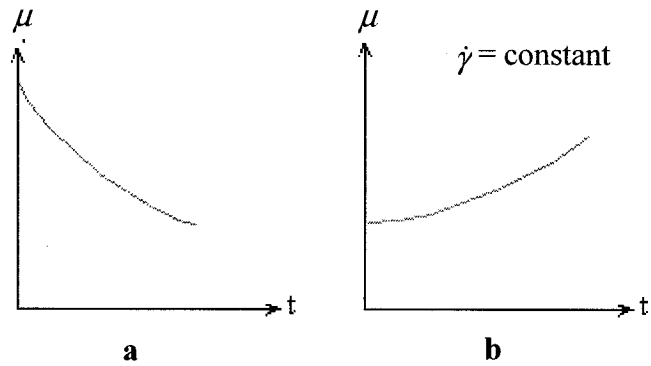

Figure 2.16: a) Thixotropy and b) Rheopexy

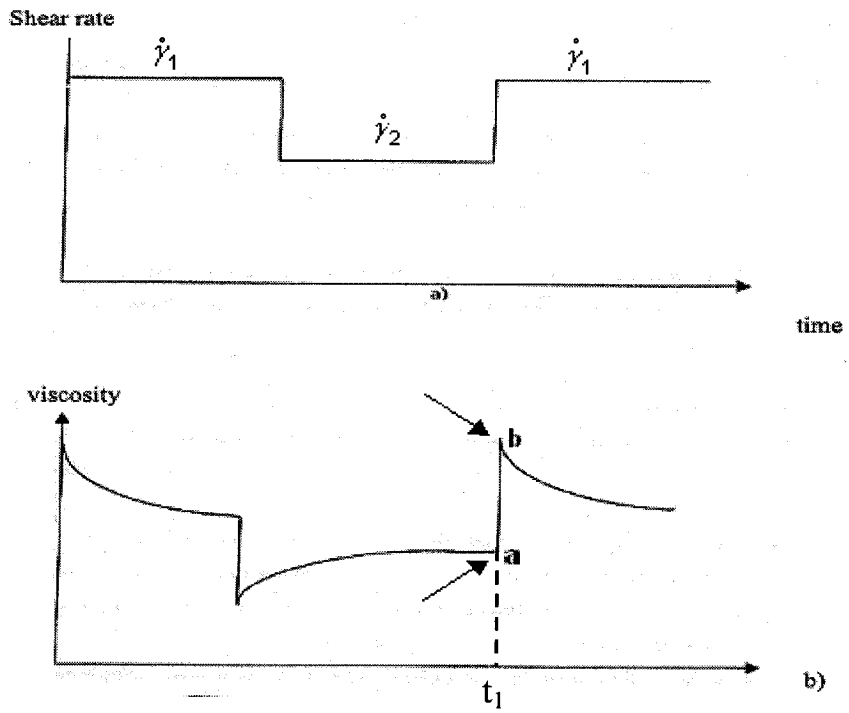

Figure 2.17: Behavior of thixotropic fluid during Step Change test a) shear rate profile and b) evolution of viscosity.

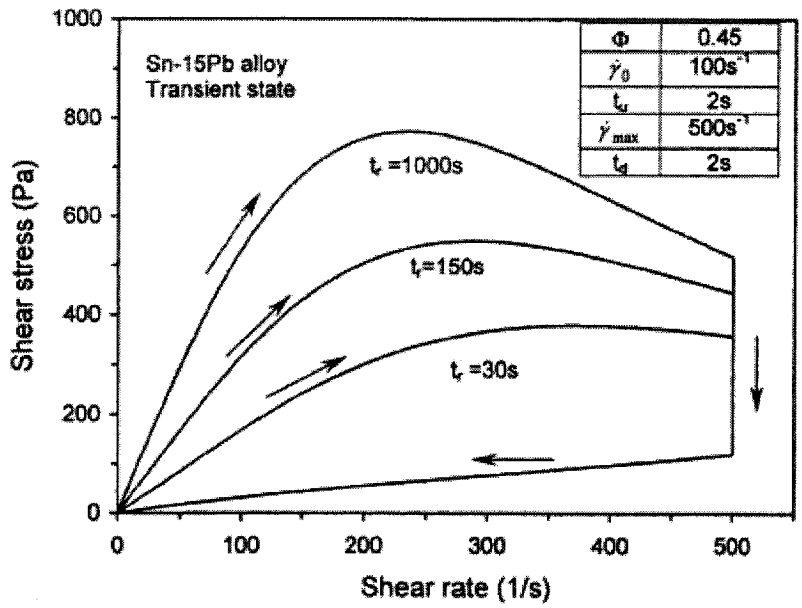

Figure 2.18: Calculated hysteresis loops for Sn–15Pb alloy showing effect of resting time t_r on degree of thixotropy. t_u and t_d are respectively used for ramping-up and ramping-down of shear rate [4].

2.4 Characteristics of A390 alloy

A390 (Al-17%Si-4.5%Cu-0.5%Mg) is a hypereutectic Al-Si alloy inoculated generally with copper, magnesium and phosphorus.

Fig. 2.19 shows a SEM micrograph of a solidified binary Al-17%Si alloy and the faceted morphology of primary silicon particles [22] (Fig. 2.19.a). Most of the primary silicon crystals exhibit the basic characteristics of octahedral growth resulting in faceted crystal with {111} planes [23]. Cross-sections of octahedral crystals can appear as hexagonal, trapezoidal and octahedral shapes. Fig. 2.19.b shows a microstructure of as-cast A390 while Fig. 2.19.c shows a microstructure of a thixoformed alloy.

The addition of 5% Cu to the binary Al-Si is necessary in order to stabilize the α-Al phase in the semi-solid state, making the Al-Si more readily thixoformable [11]. In the hypereutectic region of the binary Al-Si alloys, the semi solid zone consists of only "Liquid + Si" and the solidification becomes complete with the binary eutectic reaction at 577 ° C. According to the phase diagram, the A390 alloy, the binary eutectic reaction occurs in a range of temperature between 566 ° C-502 ° C in the "Liquid + Si + Al" region where α-Al co-exists with Liquid + Si in the semi solid state. Usually the semi solid process is carried out in this temperature range where the final solid fraction can be controlled by the α-Al solid fraction in this region. Generally, the thixoforming process is carried out at solid fraction between 30%-50% because values higher than 50%, die filling problems can occur due to the high viscosity. For solid fraction smaller than 30%, die filling becomes turbulent which results in reduce mechanical properties. For A390 alloy this range of solid fraction is located in the "Liquid + Si + Al" zone. Microstructural observation confirms the presence of α-Al in forms of both eutectic and individual grains in the matrix [5]. In fact, in the region of "Liquid + Si + Al" the α-Al solidifies with two morphologies. This is a characteristic of non-equilibrium solidification and can not be justified from the calculated phase diagram.

H.S. Kang et al. [5] have observed that microstructure of hypereutectic Al-Si alloys depend strongly on undercooling levels. For near eutectic Al-13wt%Si binary alloy the phase changes from eutectic to primary α-Al dendrite with eutectic due to different undercooling levels. The reason for this phase change may be caused by the growth rate

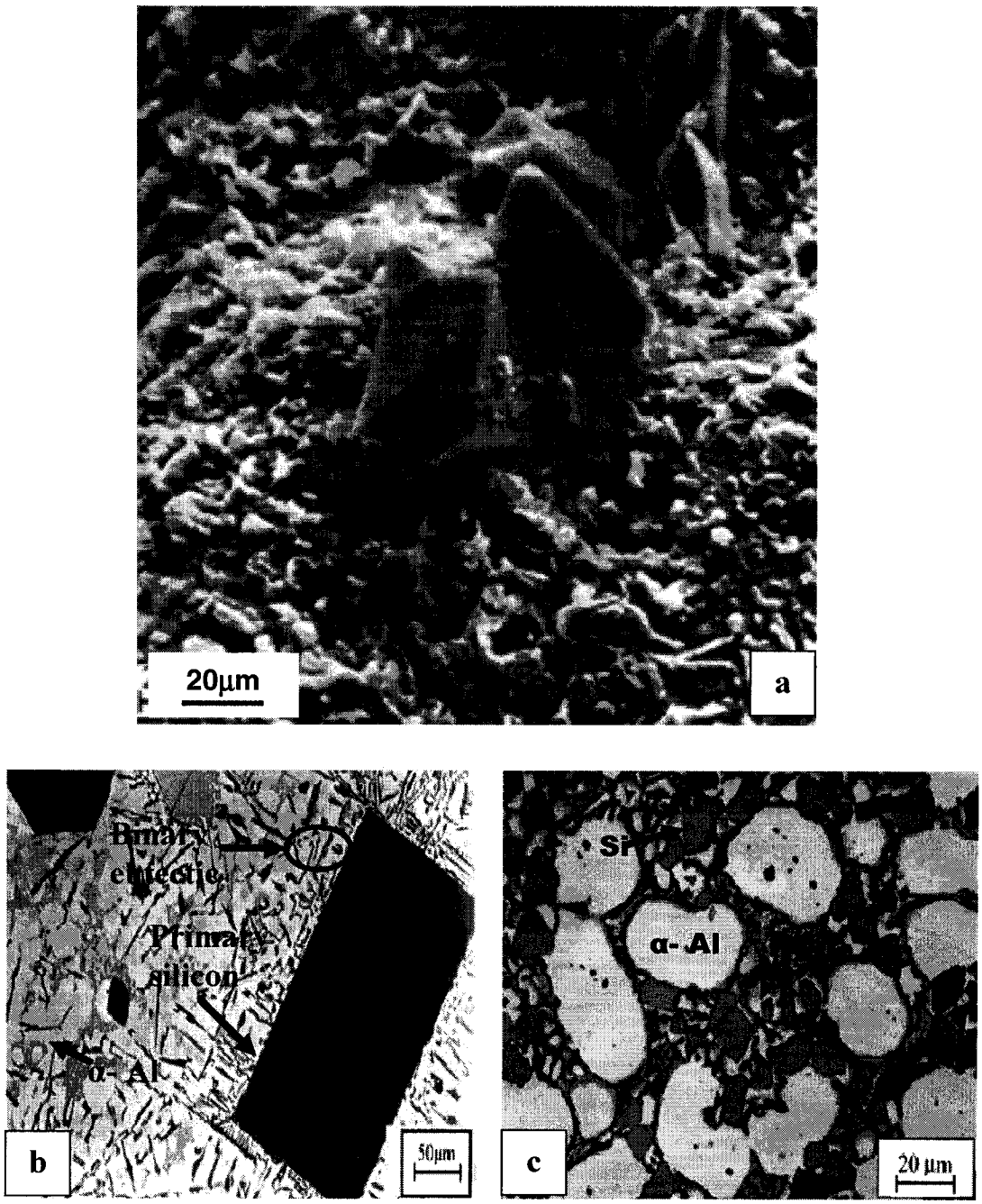

Figure 2.19: a) SEM micrograph of Al-17%Si with faceted morphology of primary silicon [22], b) As-cast microstructure of A390 and c) Microstructure of thixoformed billet of A390 shows networks containing eutectic phases of α-Al and Si, along with other phases such as Mg_2Si, Al_2Cu, and $Al_5Mg_8Cu_2Si_6$

of the α-Al phase which exceeds that of the Al-Si eutectic phase with increased undercooling. Based on the competitive growth principle, i.e. the principle that the most preferred microstructure is that possessing the highest growth velocity at a given undercooling, microstructural transformations can be expected. In addition, a morphological change of primary α-Al from dendritic to equiaxed grains was observed at this level of undercooling. They showed that the conditions of rapid crystal nucleation, growth, and significant solute trapping at high undercooling condition are responsible for the transformations from dendritic to equiaxed phases. The results show that for two hypereutectic Al-Si samples with same composition, more α-Al is present during solidification at high undercooling than with low undercooling. Several studies have confirmed the substantial similarity between hypereutectic Al-Si alloys and Al-based composites with a similar composition [6].

It should be noted in Fig. 2.19.c that there is a "network" containing α-Al and Si, along with other phases such as Mg_2Si, Al_2Cu, and $Al_5Mg_8Cu_2Si_6$ marked by arrow in the Al-matrix of the thixoformed sample. This network is not present in the as-cast sample.

Ward et al. [11] have demonstrated a marked difference between the microstructure of thixoformed binary Al-Si and A390 which contains copper and magnesium. In a binary Al-20%Si, the microstructure is found to consist of regions containing α-Al spheroids, eutectic and silicon, alongside other areas containing only eutectic and silicon phases. In thixoformed Al-36%Si and Al-50%Si, only eutectic and silicon phases are present. This indicates that in the hypereutectic region of the binary system, where the α-Al is

thermodynamically unstable, it is difficult to obtain a controlled uniform liquid fraction in the thixoformed billet. As the silicon content increases the α-Al spheroids often completely dissolve. The poor result of thixoforming the binary alloys is illustrated by the fact that the Young's modulus of Al-20%Si was greater than that of Al-36%Si (81 and 73 Gpa, respectively) [11]. Gross porosities were observed for the binary Al-Si alloy. This was attributed to a large liquid content (owning to the lack of α-Al phase and a small solid fraction of silicon), resulting in turbulent flow and air entrapment. As described before, control of the liquid content on heating the alloy into semi-solid state is achieved by the addition of 5wt% copper.

The 2% Mg addition appears to weaken the Si network considerably, and enhances the flow properties of the semi-solid material on shearing [11]. H.V. Atkinson et al. [24] have observed that for alloy with more than 27% silicon, the silicon forms a three dimensional network, with enough strength to hinder flow in the semi-solid state, but that the presence of Mg inhibits this formation. When Al-30%Si-5%Cu and Al-30%Si-5%Cu-2%Mg alloys were rapidly compressed in the semi-solid state after holding at various times and temperatures, the initial resistance to flow decreased for Mg containing alloys where no networks are observed and a much smaller peak loads were measured.

2.5 Microstructure of undercooled hypereutectic Al–Si alloys

For hypereutectic Al–Si alloys with different Si levels, H.S. Kang et al. [5] have observed various microstructural transitions for different levels of undercooling. For near-eutectic Al–13 wt%Si binary alloys, a phase change from eutectic to primary α-Al dendrite plus eutectic and a morphological change from α-Al dendrite to equiaxed Al grains were observed with increasing undercooling levels as shown in Fig. 2.20. The phase change from eutectic to primary α-Al dendrite with eutectic is observed for undercooling of 14 K. For the higher undercooling level of 24 K, morphological changes of primary α-Al from dendritic to equiaxed were observed.

To analyze the phase changes in Al–13 wt%Si, the growth velocity of each phase at different undercoolings is calculated theoretically using the dendrite and eutectic growth model which have been developed by J. Lipton et al. [25] and K. Jackson et al. [26].

The results of the calculations on the growth velocity of each phase at different undercoolings are represented in Fig. 2.21. Based on the competitive growth principle, i.e. the principle that the most preferred microstructure is that possessing the highest growth velocity at a given undercooling, microstructural transitions can be expected. Based on theoretical calculations, the level of critical undercooling was estimated quantitatively to be 19 K. This means that below this amount of the critical undercooling ($\Delta T^* = 19K$), the growth velocity of the eutectic phase is higher than that of the α-Al phase and the most preferred microstructure is eutectic. For undercooling of about 14 K,

the phase change from eutectic to primary α-Al dendrite plus eutectic was observed experimentally and corresponds to the theoretically calculated results. A morphological change from dendritic to equiaxed grains of primary α-Al phases with fibrous eutectic was also observed at the higher undercooling level. It is thought that the conditions of rapid crystal nucleation, growth and marked solute trapping effect under high undercooling are responsible for this morphological transition [27].

Preliminary experiments and phase diagram calculation were carried out by Z.Fan et al. [28] to determine the equilibrium phase diagram of the Al-Mg_2Si pseudobinary section shown in Fig. 2.22. At the pseudoeutectic composition of Al-13.9 wt % Mg_2Si, a pseudoeutectic reaction takes place between the temperatures of 583.5 and 594 ° C. In terms of properties and solidification behaviour, great similarities exist between Mg_2Si and Si. This similarity is shown [29] in Table 2.3. For hypereutectic Al-15 wt%Mg_2Si alloy the pseudoeutectic reaction begins when the temperature of the surplus liquid reaches the upper line of the ternary phase field in the diagram. Grains of α-Al form in the ternary field together with Al+Mg_2Si pseudoeutectic [28] as shown in Fig. 2.23.

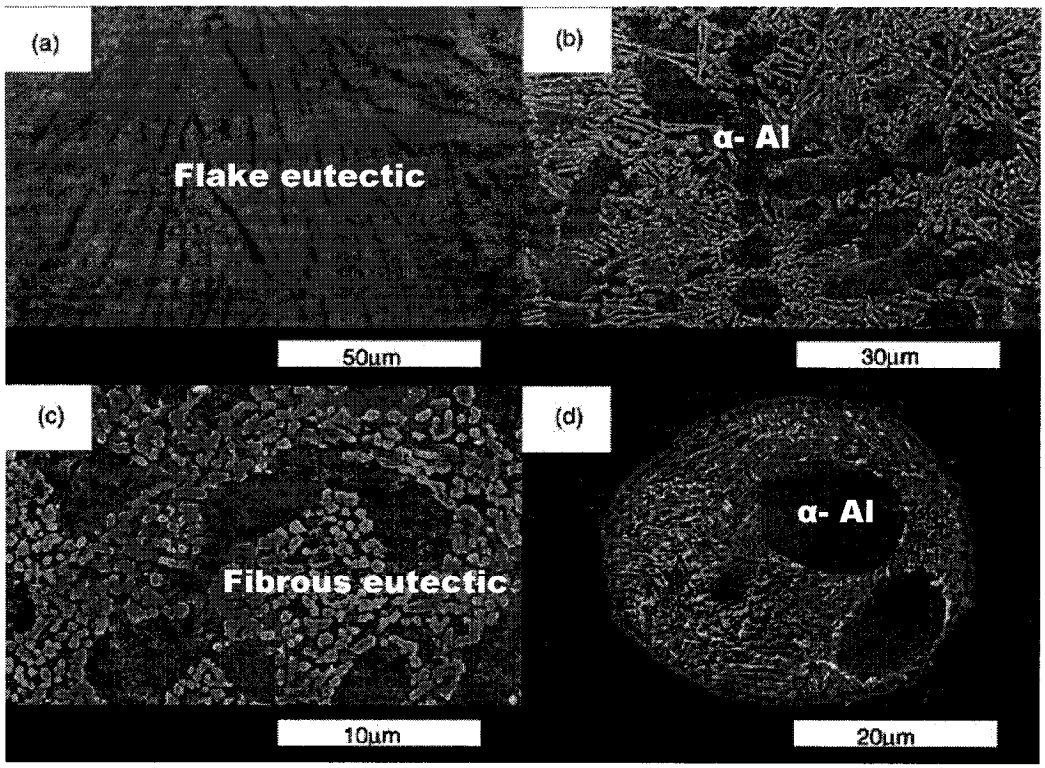

Figure 2.20: The effect of an undercooling on microstructures of Al–13 wt%Si (SEM image). (a) Bulk, (b) ΔT=14K, (c) ΔT = 19K and (d) ΔT=24K [5].

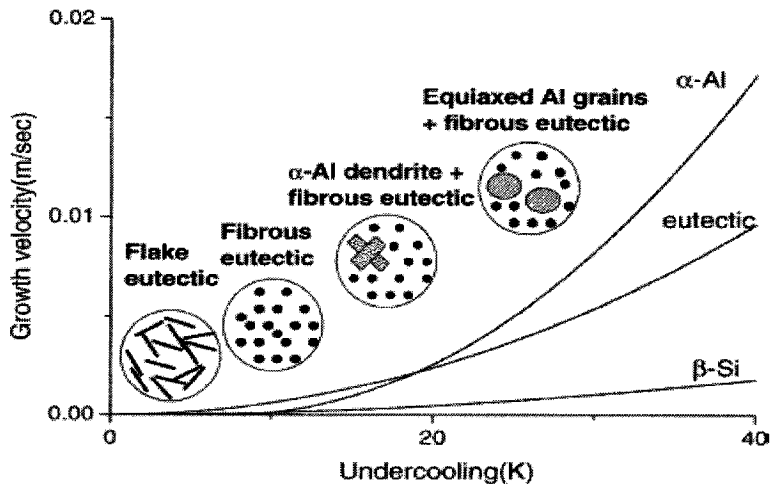

Fig. 2.21: Crystal growth velocities in undercooled Al–13 wt%Si alloy and the experimentally observed microstructures [5].

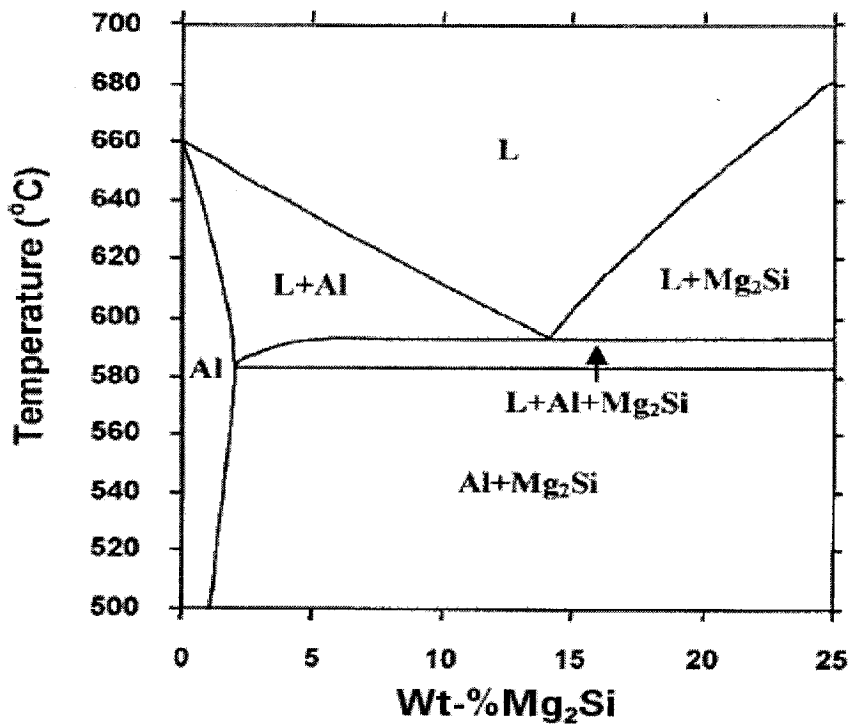

Fig. 2.22: Calculated equilibrium phase diagram of the Al-Mg_2Si phase diagram, pseudoeutectic point at Al-13.9 wt % Mg_2Si, temperatures range of ternary region at this composition between 583.5 and 594 ° C [28].

Table 2.3: Physical and mechanical properties of Mg2Si and Si [29]

Phases	Crystal structure	Lattice parameter (nm)	Density ($g\ cm^{-3}$)	C.T.E[a] ($10^{-6}\ k^{-1}$)	Elastic modulus (Gpa)	Melting point (° C)
Mg_2Si	Cubic	0.635	1.99	7.5	120	1085
Si	Cubic	0.542	2.33	3.06	112	1411

[a] Coefficient of thermal expansion

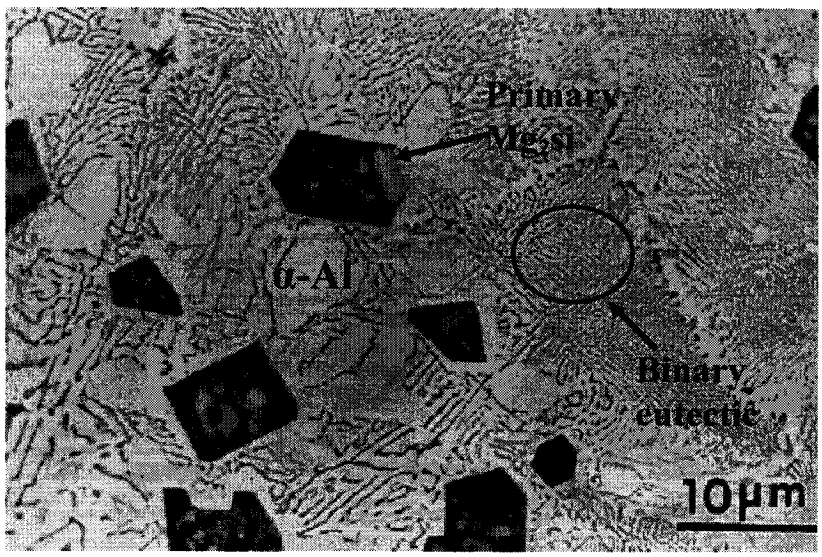

Fig. 2.23: Microstructure of hypereutectic Al-15 wt%Mg_2Si alloy with grains of α-Al in hypereutectic region [30]

2.6 Advantages and disadvantages of A390 alloy

The advantages of A390 alloy are:

- High resistance to wear.
- High resistance to corrosion.
- High hardness and strength.
- Low thermal expansion coefficient.
- Low weight and good castability.

As a result, it is very attractive to the automotive industry in heavy wear applications at elevated medium temperatures.

The disadvantages of A390 alloy are:

- Large solidification interval (150°C).
- Coarse network of primary silicon with a high volume fraction of binary eutectic phase (about 88%).
- Low ductility and toughness.
- Significant Si segregation.
- High degree of shrinkage.

Semi-solid metal (SSM) processing can overcome most of these disadvantages, in order to obtain:

- Fine primary Si particles.
- Homogeneously distributed primary silicon.
- Low casting temperature and energy saving.
- Reduction of segregation and shrinkage and porosity.
- High toughness

2.7 The fragmentation mechanism of the primary silicon under shear force

Structural changes of the primary crystals have been well documented for hypoeutectic (less than 12.2% Si) Al alloys (section 2.2.2) where the vigorous stirring of slurry during rheocasting can exert enough force to deform and eventually break up the dendrites of primary Al.

Subsequent growth of fragmented Al crystals is also possible when the rheocasting temperature is close to the melting point of Al. On the other hand, the agglomeration and spheroidization of primary Si crystals of hypereutectic Al-Si alloys are not fully understood as primary Si crystals are much harder and have a melting point of 1414 ° C, much higher than the typical rheocasting temperature of around 600 ° C. [9]

Several mechanisms have been proposed to explain the morphological changes of primary crystals during rheocasting. One of the important parameters to be considered is solute redistribution in the melt and in the primary crystal. The stirring of the melt in the rheocast process will eliminate the constitutional undercooling (see Fig. 2.1) of the melt near the primary crystal interface and solute redistribution will take place according to the equilibrium solute concentration determined by the phase diagram. [9]

The experimental work of Lee et al. [9] showed that isothermal shearing of the Al-15.5 wt % Si alloy at slightly above the eutectic temperature is believed to promote diffusion of Al into the primary Si crystal, producing a highly supersaturated solid solution of Si, and possibly introducing the interstitial Al into the Si crystal.

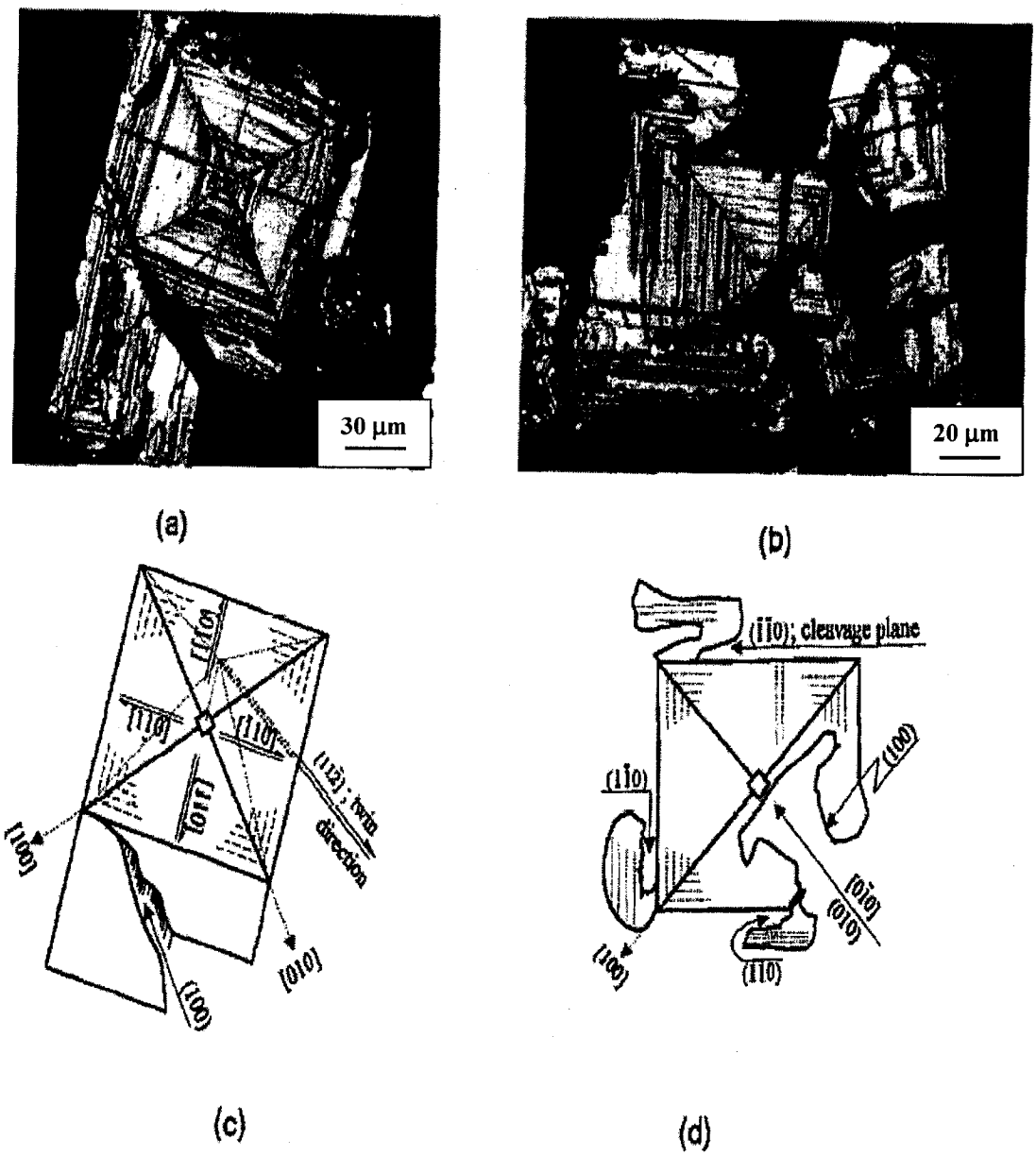

Figure 2.24: Micrograph of the ruptured Si crystals subjected to the shearing force a) and b) optical bright-field image, c) and d) schematic description of the crystallographic orientation of four operational $\{111\}$ twinning systems which crack propagation on $\{100\}$ planes and crack propagation on $\{100\}$ and $\{110\}$ cleavage planes. [9]

Crystallographic and morphological analyses were carried out to study the fragmentation / agglomeration behaviour of Si crystals in hypereutectic stir cast alloy by analyzing the etch pattern of individual Si crystals. Fractured primary Si single crystals preserve the well-developed faceted are frequently observed as shown in Fig. 2.24.

Careful analysis of the etch patterns reveals that the fracture took place along $\{100\}$ planes and $\{110\}$ cleavage planes. This provides the crucial evidence for the fragmentation process occurring during the shearing of semi-solid slurry.

As a result, the fragmentation process can be considered to be caused by the mutual collision of large irregular shaped Si crystals suspended in the rapidly moving viscous liquid medium, similar to the attrition process of ceramic particles. As the attrition proceeds, the shape of silicon crystal will become more compact and spherical. The small fragmented Si particles will also tend to agglomerate due to the surface tension of the liquid phase.

The higher density of twin planes [30] in the silicon crystals in the stirred microstructure compared to the unstirred microstructure may also be interpreted as a direct consequence of the deformation accompanying this fragmentation process.

2.8 Si coarsening of hypereutectic alloy in the semi-solid state

It has been observed that the solid Si phase in the liquid matrix coarsens quite rapidly, which may affect the final microstructures and mechanical properties significantly. During coarsening, the size of the solid phase increases and the number of particles decreases, because the driving force for the process is the decrease in total interfacial energy [31]. The typical behavior for spherical particles was described by the theory developed by Lifshitz, Slyozov and Wagner (LSW theory) based on Ostwald's theory (section 2.1.2), in which the relationship [32] between the mean particle size (R) and initial radius (R_0) with holding time is given by:

$$R^3 - R_0^3 = K_{LSW}\, t = \frac{8}{9}\frac{D\sigma\Omega C_\infty}{K_\beta T(C_\beta - C_\infty)} \qquad (2.10)$$

K_{LSW} is the coarsening rate constant, D is the diffusivity of solute in the matrix, σ is the surface energy, Ω is the atomic volume, K_β is Boltzman's constant, and C_β and C_∞ are the equilibrium concentrations of solute in the coarsening phase and in the matrix, respectively. The exponent of the variation of the particle radius indicates that the coarsening phenomenon is controlled by volume diffusion.

The limitations of the LSW theory are that the relation is only valid for spherical particles, with a small volume fraction of the coarsening phase which is static in the liquid matrix.

Other studies [33] have shown that the measured coarsening rate constant was a function of the solid volume fraction, which exceeded the theoretically calculated values by factors ranging from approximately 2–5. Hence, Eq. (2.10) can be rewritten as follows:

$$R^3 - R_0^{\ 3} = K(\phi)t = f(\phi)K_{LSW}t \tag{2.11}$$

Where $K(\phi)$ denotes the rate constant equal to the product of K_{LSW} and $f(\phi)$, $f(\phi)$ is a function of the solid volume fraction, ϕ. According to the simulations of Voorhees and co-worker [33], when the volume fraction of the coarsening phases, ϕ, was in the range from 0.05 to 0.5, f(ϕ) could be expressed by $\alpha^3 \,/\, 1-\phi^{1/3}$, where α was a numerical factor which varied from 1 to 0.5.

Experimental work was carried out by C.H. Chiang, and Y.A Chi [31] on the Si coarsening of spray-formed Al-25%Si, Al-35%Si and Al-45%Si alloys at different temperatures (solid fractions) and holding time in the semi-solid state. Fig. 2.25 shows the relations between solid fraction and temperature calculated by the Thermo-calc software [31]. It was found that during coarsening in the semisolid state, the convection of the liquid phase leads to significant differences in the size distribution and spatial distribution of the Si particles in different areas at low solid fractions, but shows almost no difference at high solid fractions. They have shown that at the same temperature, as indicated by dashed grouping in Fig. 2.27, the value of K_{LSW} for Al-35 and A-45 is nearly the same, which was different from the value of K, increasing with increasing Si content as shown in Fig. 2.26. As the rate constant, K, is equal to the product of K_{LSW}

and $f(\phi)$, the increase of K was therefore attributed to the increase of $f(\phi)$ with solid fraction. For the case of the same alloy at various temperatures, as shown by the solid lines, the K_{LSW} now increased with decrease of solid fraction, as shown in Fig. 2.27, However, the $f(\phi)$ decreases with a decrease in solid fraction. As the rate constant K is equal to the product of K_{LSW} and $f(\phi)$, it was found to increase with decrease in solid fraction, as shown in Fig. 2.26 and indicates that the contribution of K_{LSW} to K was larger than the value of $f(\phi)$. This large contribution of K_{LSW} was attributed to the continued effect of large changes of equilibrium concentration of matrix and coarsening phases, and the diffusivity at various temperatures.

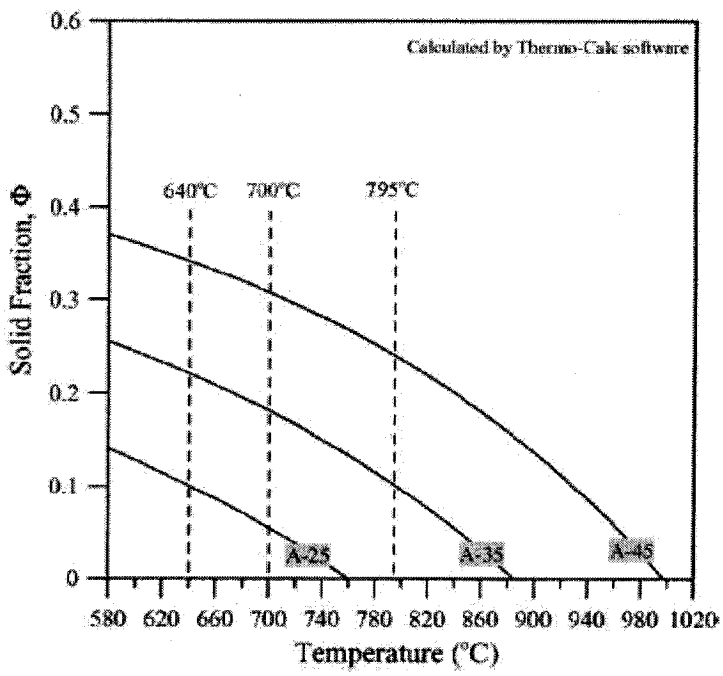

Figure 2.25: Solid fraction vs. temperatures for A-25Si, A-35Si and A-45Si binary alloys. [31]

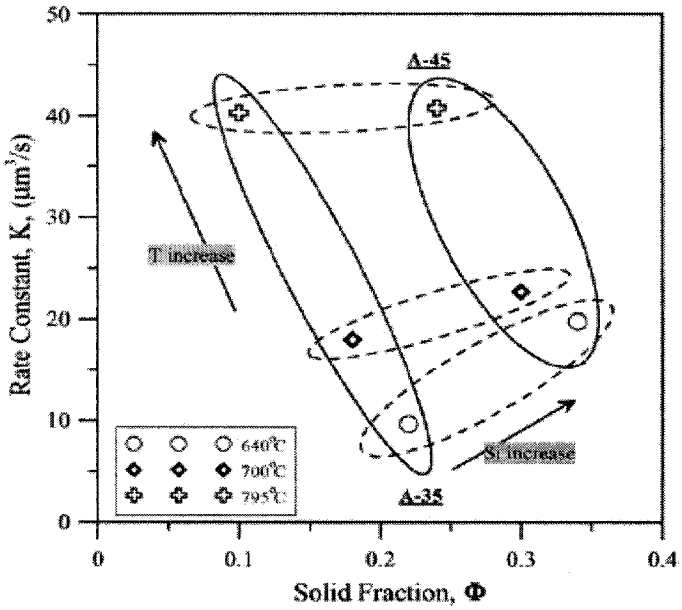

Figure 2.26: Rate constants variation with solid fractions for A-35Si and A-45Si alloys at various temperatures.[31]

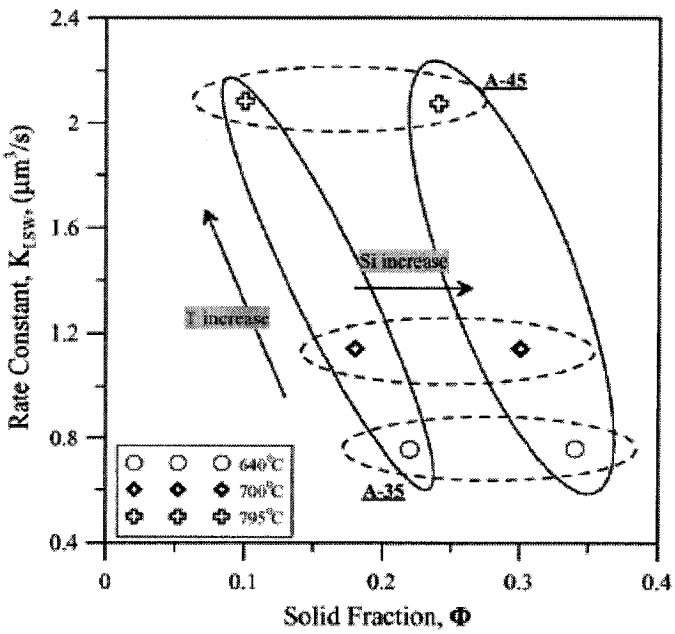

Figure 2.27: K_{LSW} variation with solid fraction for A-35Si and A-45Si alloys at various temperatures [31].

CHAPTER 3

METHODOLOGY

3.1 The FACTSAGE software

A study of the thermodynamic properties and the solidification path of the A390 was necessary in order to analyse the rheological characteristics. This was made possible by means of the numerical modeling of the thermodynamic functions required to construct the quaternary phase diagram of the alloy under study using the Factsage software developed by the CRCT at *Ecole Polytechnique de Montréal*. Initially, the experimental phase diagrams relevant to this study developed by other researchers are presented and compared with the models that are determined by the mathematical representation of the thermodynamic functions (Gibbs' free energy) necessary for the construction of the phase diagrams using the Factsage software. The effects of the addition such as Cu and Mg on the quaternary phase diagram are also presented.

3.2 Measurement of the rheological characteristics

A measurement of the apparent viscosity in the semi-solid state was carried out by means of a Haake RV12 viscometer. A schematic diagram of the apparatus used in this study [34] is shown in Fig. 3.1, 3.2.

It is made up primarily a motor with a speed controller, which makes it possible to vary the rotational speed from 0.01 to 512 rpm. The speed may be maintained constant or varied with the speed controller. This is coupled to the torque sensor, which makes it possible to measure a torque from 0 to 4.9 N.cm using a torsion spring whose maximum angle of torsion is 0.5^0 when it is subjected to the maximum torque. The angle of torsion is directly proportional to torque and transformed by a magnetic sensor.

The alloy material to be tested was placed in a graphite crucible and is heated in a resistance furnace with precise temperature control zones. The furnace temperature is measured at three locations: in the middle of the central zone of furnace where the heating element are located at the bottom of upper zone of furnace and at the top of the lower zone of the furnace, as shown in Fig. 3.1.

The temperature of the melt was measured using by two thermocouples placed in the crucible wall very near the bottom and near the surface of the bath (Fig. 3.2). The height of the crucible and support was fixed, so that the sample is positioned in the central zone of furnace where the temperature variation is less than 1^0C. During the test, the semi-solid alloy as well as the graphite crucible were protected against oxidation by a

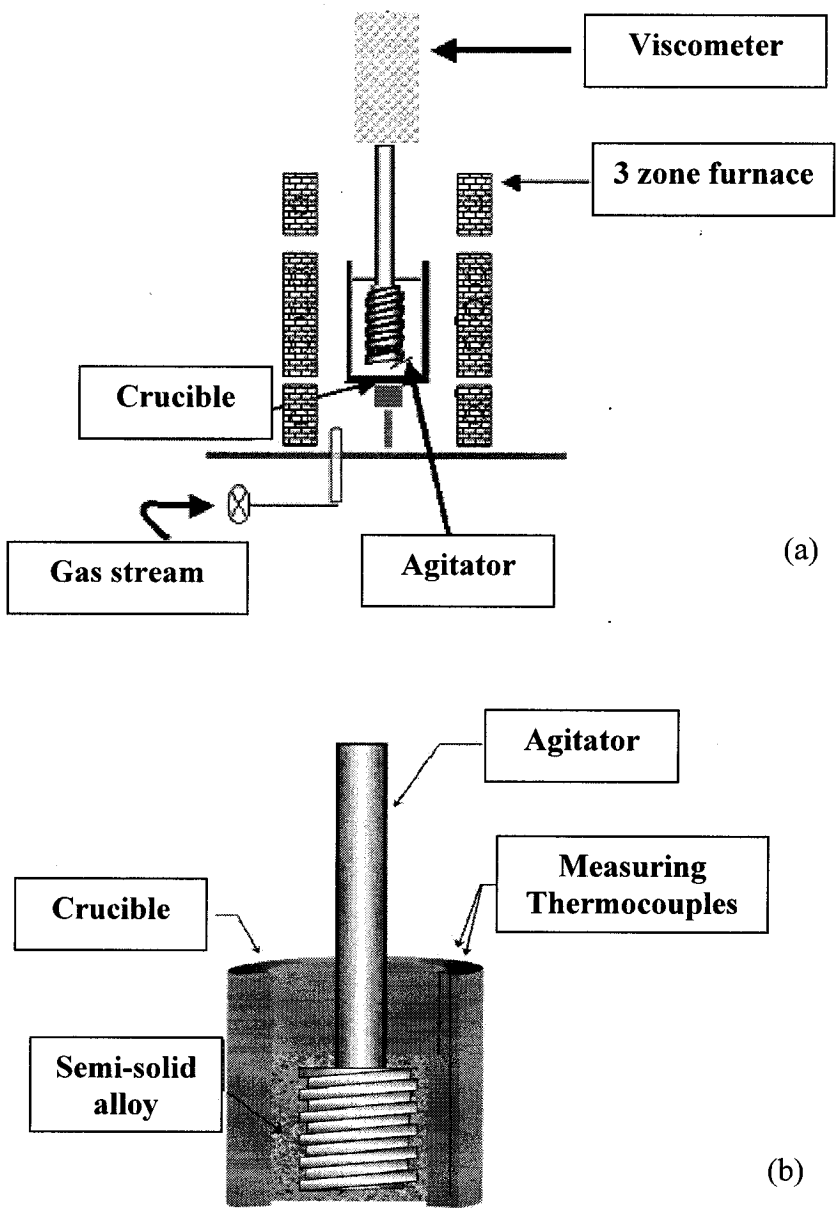

Figure 3.1: (a) Schematic diagram of experimental set up (b) detail of crucible and agitator [34]

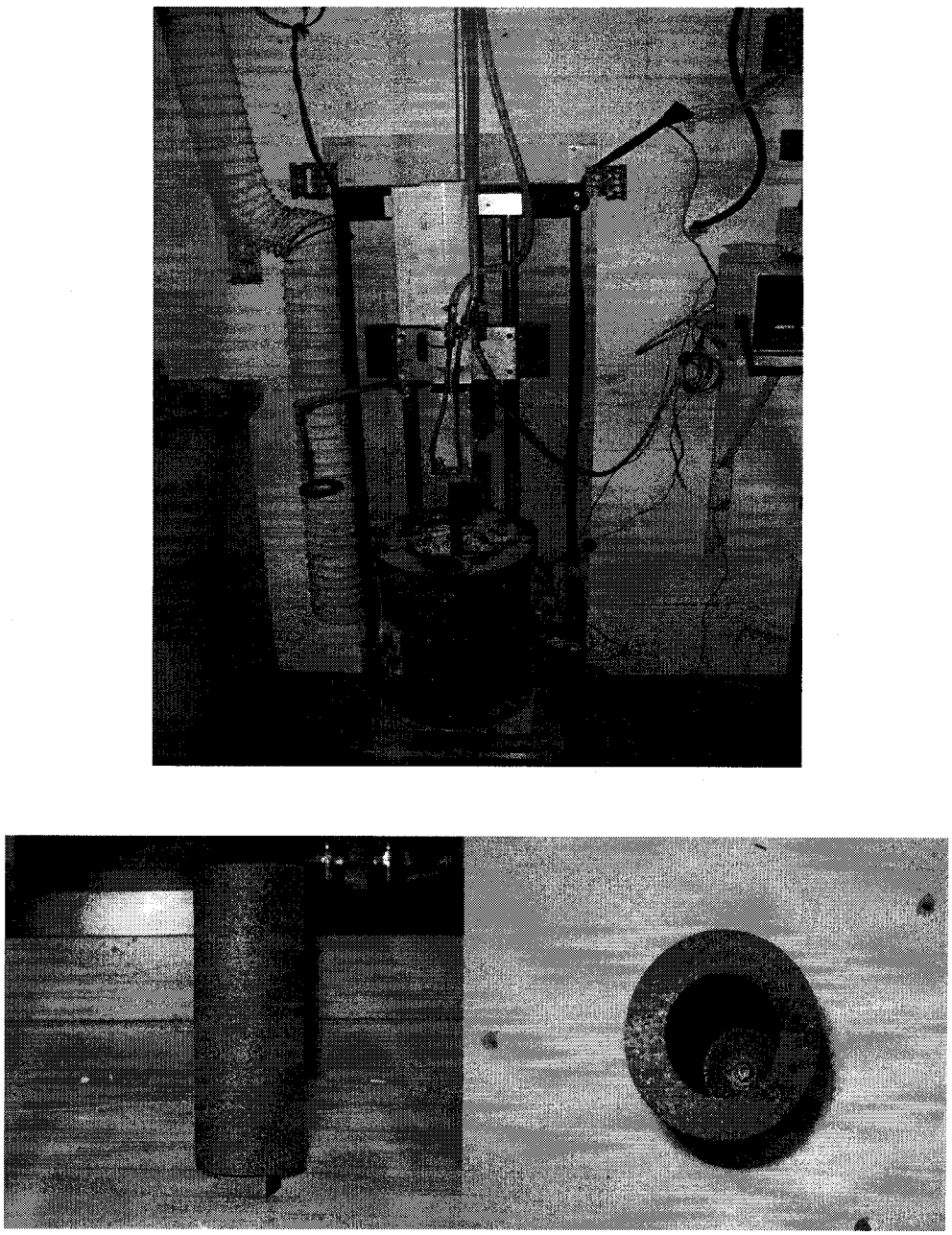

Figure 3.2: Photograph of viscometer and crucible.

flow of argon gas introduced into the bottom of furnace. The rotational speed, the torsion couple as well as the temperature were recorded using data acquisition software.

3.2.1 Calculation of viscosity based on Haake RV12 (Couette) viscometer

The Couette viscometer (coaxial rotational cylinder) consists of two concentric cylinders which move at a relative angular velocity, Ω. The radius of the inner cylinder is R_i (or cylindrical agitator radius) and the outer cylinder (or crucible radius) is R_o (αR_i). The length of the cylinders contacting the fluid is L. For the limiting case, the Couette viscometer can be approximated as two parallel plates. The velocity of the fluid near the moving cylinder (plate) is the rotational velocity of the adjoining plate under the no-slip assumption. The velocity of the fluid near the static plate is 0 for the same assumption. The shear force F(r) exerted at radius r is connected to the couple C and shear stress $\tau(r)$ by the relation:

$$C = r\,F(r) = 2\pi r^2 L\,\tau(r) \tag{3.1}$$

Then:

$$\tau(r) = \frac{C/L}{2\pi r^2} \tag{3.2}$$

The linear velocity is related to angular velocity by the relation u = rw and the rate of shear is then given by:

$$\dot{\gamma}(r) = r\frac{dw}{dr} = f\left[\frac{C/L}{2\pi r^2}\right] \tag{3.3}$$

This relation can be rearranged in the following way:

$$w = \int_{R_i}^{\alpha R_i} f\left[\frac{C/L}{2\pi r^2}\right]\frac{dr}{r} \tag{3.4}$$

If assume a no-slip condition i.e. perfect adherence with the walls, the boundary conditions are:

$$r = R_i \qquad u = R_i\Omega$$

$$r = R_o = \alpha R_i \qquad u = 0$$

For a Newtonian fluid i.e. the viscosity is given by $\eta = \frac{\sigma}{\dot{\gamma}}$ and we can show that the apparent rate of at the surface of the agitator is given:

$$\dot{\gamma}(R_i) = \frac{2\alpha^2}{\alpha^2 - 1}\Omega \tag{3.5}$$

In practice, we use the average rate of shear, because the rate of shear varies across the gap of viscometer. The average rate of shear is given by the relation:

$$\dot{\gamma}_{average} = \frac{2R_iR_O}{R_O^2 - R_i^2}\Omega = \frac{4\pi R_iR_O}{60\left(R_O^2 - R_i^2\right)}N \tag{3.6}$$

Where N is the rotational speed (rpm).

The calculation of viscosity by Haake RV12 apparatus is carried out by using a calibration method. The calibration consists of correlating the couple measured by the viscometer for the viscosity of material under study. This is made possible using the dimensionless power number, P_0, and Reynolds number defined as follows:

$$P_0 = \frac{C}{\rho \Omega^2 r_a^5} \tag{3.7}$$

Where C, ρ, Ω and r_a are torque, density, rotational speed (angular speed)and stirring radius, respectively as determined from the calibration. [34]

The Reynold number can be calculated as:

$$\mathrm{Re} = \left(\frac{P_0}{K}\right)^{\frac{1}{a}} \tag{3.8}$$

Where K and a are constants that depend on stirring geometry. In this study K = 842.3 and a = -0.995.

Thus, the viscosity is calculated by:

$$\mu = \frac{\rho \Omega r_a r_c}{\mathrm{Re}} \tag{3.9}$$

Where r_c is the crucible radius.

3.2.2 Experimental procedures

The rheological behaviour was investigated during continuous cooling and isothermal "step change" experiments. For the continuous cooling experiments, the alloy is first heated to the temperature of 700 ° C and then held at the given temperature and sheared at maximum rotation velocity of 512 rpm,($\dot{\gamma}$ = 471s^{-1}) for a period of 10 minutes in order to achieve a homogeneous composition. After this period, the alloy is continuously cooled at a rate of -2 ° C/min and sheared at constant rates of 15, 59, 123, 250 and 507 s^{-1} in separate experiments. The test was stopped when the upper limit of the viscometer torque is reached.

For the isothermal tests, the alloy was also heated to a temperature near 700 ° C and then continually cooled at -2 ° C/min and sheared at 13 s^{-1} to a temperature of 565 ° C which is very close to the binary eutectic temperature. The alloy was then sheared for 20 minutes under isothermal conditions while the shear rate was abruptly changed to a new value. The other isothermal experiments (step change) at 565 ° C, the shear rates were changed in a sequence of 52-, 104-, 26-, 104- and 13 s^{-1}. Table 3.1 presents all the type of tests carried out in this study.

Table 3.1: Summary of tests carried out in this study

Experiments	Cooling rate (°C/min)	Shear rate (s^{-1})					Experimental temperature (°C)	Solid fraction (%)
		$\dot{\gamma}_1$	$\dot{\gamma}_2$	$\dot{\gamma}_3$	$\dot{\gamma}_4$	$\dot{\gamma}_5$		
Continuous Cooling	-2	15	59	123	250	507	Variable	Variable
Isothermal	-	13	104	-	-	-	565	6.1
		52	104	26	104	13	565	6.1

3.3 Metallography of A390

Samples of the alloy used for metallography were obtained by cutting sections of the solidified alloy and mounting in 1-¼ inch diameter moulds using Bakelite powder. Generally, polishing is performed in successive steps using silicon carbide abrasive papers of 180, 220, 320, 400 and 600 grit. The starting grit size depends on the condition of the surface. If the specimens had been cut with band saw, 180- or 220-grit paper was first used. Further polishing using wet 220, 320, 400 and 600 grit silicon carbide papers with an applied force of 20-25 pounds for three to four minutes was used for the initial stage.

Final stage polishing was performed using a suspension of 600-grit alumina powder with distilled water (50 gr/500 ml H2O) on a standard rotating wheel. Diamond abrasives of 15, 3 and 0.05 micron were used for fine polishing. Wheel speeds of 300-400 rpm were typical. A commonly used etching reagent for aluminium and aluminium alloys is Keller's etchant (95 ml water, 1.5 ml hydrochloric acid, 1 ml hydrofluoric acid and 2.5 ml nitric acid) and was found to be unsatisfactory for use on the 390 alloy. The desirable etchant recommended for hypereutectic aluminium-silicon alloys was found to be R.L.Anderson's reagent (AINQ2) [22], (Fig. 4.14). This etchant is composed of 90 ml water, 4 ml hydrofluoric, 4 ml sulphuric acid and 2-gram chromic acid. Etching is done by immersion for 10 seconds.

CHAPTER 4

RESULTS AND DISDUSSION

4.1 Thermodynamic evaluation (Factsage software)

Before investigating the rheological characteristics of A390, it was necessary to determine the solidification path of the alloy and to identify the compounds and phases that are formed during the solidification period based on a calculated phase diagram. The composition of A390 corresponds to a quaternary system of Al-Si-Cu-Mg in the Al-rich corner. We will begin by presenting the experimental diagrams relevant to our study that will give us a base for comparing with the model.

4.1.1 Ternary phase diagrams of Al-Si-Mg and Al-Si-Cu in the Al rich corner.

4.1.1.1 The Al-Si-Mg system

The experimental phase diagram of the ternary Al-Si-Mg system is well established. The eutectic reactions and their transformation temperature [35] were given in Table 4.1. A binary Al-Si with an isopleth of 1% Mg was also calculated by H. Phillips [36] and is shown in Fig. 4.1. During solidification, Si solidifies first until a binary eutectic is first reached. This is followed by a binary Al-Si eutectic solidification and finally by a ternary eutectic at 555 ° C according to reaction (1) in Table 4.1. Other eutectic reactions

occur, depending on the Mg and Si content in the alloy. Reaction (3) in the Table 4.1 occurs only in the low Si and rich Mg region. It is important to note that aluminium and Mg_2Si form a quasi binary system. Mg_2Si (melting point =1102° C) has a simple cubic structure, while the cube centers are alternately empty (holes) and occupied by silicon atoms. These precipitates develop on {100} aluminium planes. The solubility of Mg_2Si in α-Al decreases as the temperature is lowered. [37].

4.1.1.2 The ternary Al-Si-Cu

The projection of the liquidus surface in the aluminium corner is shown in Fig. 4.2. The ternary eutectic occurs at 525° C (below the ternary eutectic of the Al-Si-Mg system: 555° C) and is described by reaction [3] as shown in Table 4.2.

For alloys containing less than 2 percent copper and 1.5 percent silicon, the alloy consists of a solid solution of copper and silicon in aluminium. For alloys containing more than 2 percent copper (up to 10 percent) and from 1.5 to 10 percent silicon, the alloy consists of a solid solution of copper and silicon in aluminium together with the binary Al-Si eutectic as well as the ternary Al-Si-θ-Al_2Cu eutectic. For alloys containing from 2 to 10 percent copper and more than 10.5 percent silicon (interest zone), primary silicon, binary Al-Si eutectic as well as ternary Al-Si-θ-Al_2Cu eutectic phases are present. The θ-Al_2Cu generally forms on the {100} planes of aluminium [37].

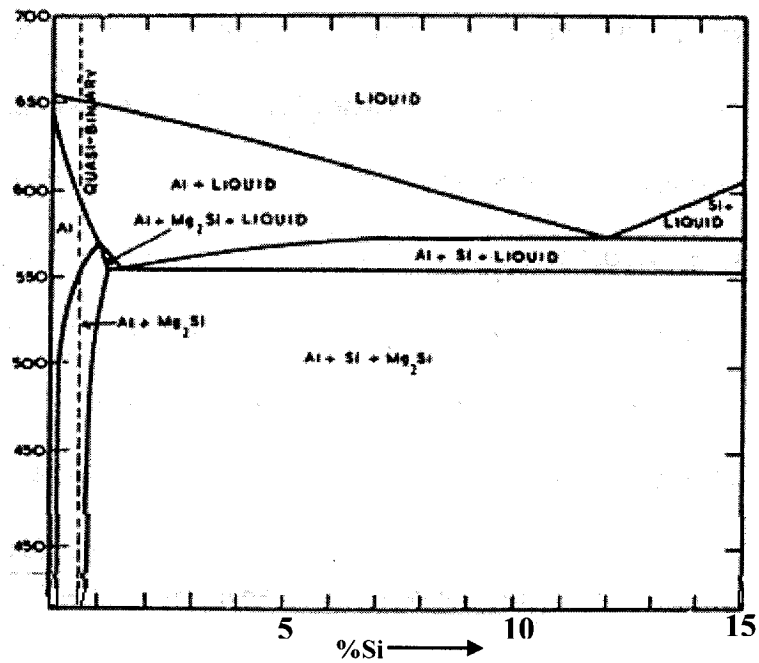

Figure 4.1: Pseudo binary Al-Si phase diagram with 1% Mg. [36]

Table 4.1: Eutectic reactions in Al-Si-Mg and liquid composition of eutectic. [3]

System	Reaction	%Mg(L)	%Si(L)	Temperature
1-Al-Si-Mg	Liq. $\rightarrow$ $Al + Mg_2Si + Si$	5.0	13.0	555
2-Al-Si-Mg	Liq. $\rightarrow$ $Al + Mg_2Si$ (quasibinary)	8.1	7.8	585
3-Al-Si –Mg	Liq. $\rightarrow$ $Al+Mg_2Si+Mg_2Al_3(\beta)$	32.2	0.4	448

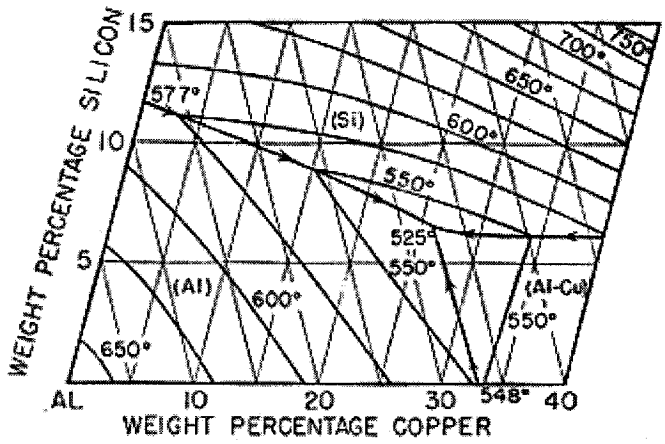

Figure 4.2: Projection of liquidus surface in aluminum corner. [36]

Table 4.2: Ternary eutectic reaction in Al-Si-Cu and liquid composition of eutectic. [3]

System	Reaction	%Cu(L)	%Si(L)	Temperature
1-Al-Si-Cu	Liq. $\rightarrow Al + Al_2Cu + Si$	26.7	5.2	525

4.1.2 The Quaternary Al-Si-Cu-Mg

Different intermetallic phases can appear [3] for the quaternary system depending on the alloy composition according to the reactions shown in Table 4.3.

Generally $CuAl_2$, Mg_2Si, $Cu_2Mg_8Si_6Al_5$ are the most common phases observed in the microstructure of A390 alloy [38, 39, 40]

Table 4.3: Phases present in Al-Si-Cu-Mg. [3]

Reaction		%Mg(L)	%Si(L)	%Cu(L)	T
eutectic	Liq. $\rightarrow Al + Mg_5Al_8 + Mg_2Si + CuMg_4Al_6$	33.0	0.3	1.5	446
peritectic	Liq.+ $CuMgAl_2 \rightarrow Al + Mg_2Si + CuMg_4Al_6$	25.5	0.3	10.0	467
eutectic	Liq. $\rightarrow Al + Mg_2Si + CuMgAl_2$	10.5	0.3	23.0	516
eutectic	Liq. $\rightarrow Al + CuAl_2 + Mg_2Si + CuMgAl_2$	$\approx$6.5	$\approx$0.3	30-33	500
eutectic	Liq. $\rightarrow Al + CuAl_2 + Mg_2Si$ (quasiternary)	31.5	3.9	31.5	515
peritectic	Liq.+ $Mg_2Si \rightarrow Al + CuAl_2 + Cu_2Mg_8Si_6Al_5$	2.2	6.0	28.0	512
eutectic (solidus)	Liq. $\rightarrow Al + CuAl_2 + Cu_2Mg_8Si_6Al_5$ +Si	2.2	6.0	28.0	507
peritectic	Liq.+ Mg_2Si +Si $\rightarrow$ Al + $Cu_2Mg_8Si_6Al_5$	3.3	9.6	13.8	529

4.1.3 Modeling Results

The objective of this section is to calculate the phase diagrams using the Factsage software (version 5.4.1) developed by the group CRCT of *Ecole Polytechnique de Montréal.* In the aluminium rich corner, the thermodynamic data of the Al liquid phases, Al (fcc) and Si with a diamond structure, as well as the intermetallic phases such as Mg_2Si and θ-Al_2Cu, were used to model the phase diagrams of Al-Si-Mg, Al-Si-Cu and Al-Si-Cu-Mg according to the Fslite (Factsage light metal alloy database) database. The FactSage FSlite light alloy database has been derived from the database that resulted from the European COST Action 507 (*COST 507, Thermochemical database for light metal alloys*) [44]. However, it has been much improved by corrections of the original data and by many additions in terms of binary and higher order subsystems. Some amendments and some updates were incorporated in this upgraded light alloy database to calculate the binary, ternary and quaternary diagrams. The database is generally valid for the temperature range of approximately 200°C to 1800°C and all ranges of composition. For some alloys with high melting point metals, the data was still found to be reliable. In the calculations, the liquid phase was described using a simple substitutional solution approach based on the Redlich-Kister-Muggianu polynomial expression. Most solid solution phases were described using sub-lattice models which include interstitials and vacancies where appropriate.

4.1.3.1 The ternary Al-Si-Mg system

The experimental Al-Si binary with 1% Mg was shown previously in Fig. 4.1. The numerical simulation is in good agreement with experimental work and is shown in Fig. 4.3. According to the Factsage calculation, for Al-17%Si-1%Mg alloy, the transition temperatures are: 639.05 °C (liquidus), 572.59 °C (Binary eutectic) and 557.43 °C for the ternary eutectic reaction (Liq. $\rightarrow$ $Al + Mg_2Si + Si$).

4.1.3.2 The ternary Al-Si-Cu system

There is no isopleth diagram for Al-Si-4.5%Cu system in the literature to compare with numerical simulation as it was carried out for Al-Si-1%Mg, but the ternary eutectic reaction (Liq. $\rightarrow$ Al + θ-Al_2Cu + Si) is the same for all Cu contents. As we can see in Fig. 4.4, for a composition of Al-Si-4.5%Cu, solidification starts with Si precipitation and down to the binary eutectic temperature. Thereafter solidification continues down to the ternary eutectic temperature of 508 °C for the isopleth at 4.5%Cu where complete solidification occurs based on above-mentioned ternary reaction.

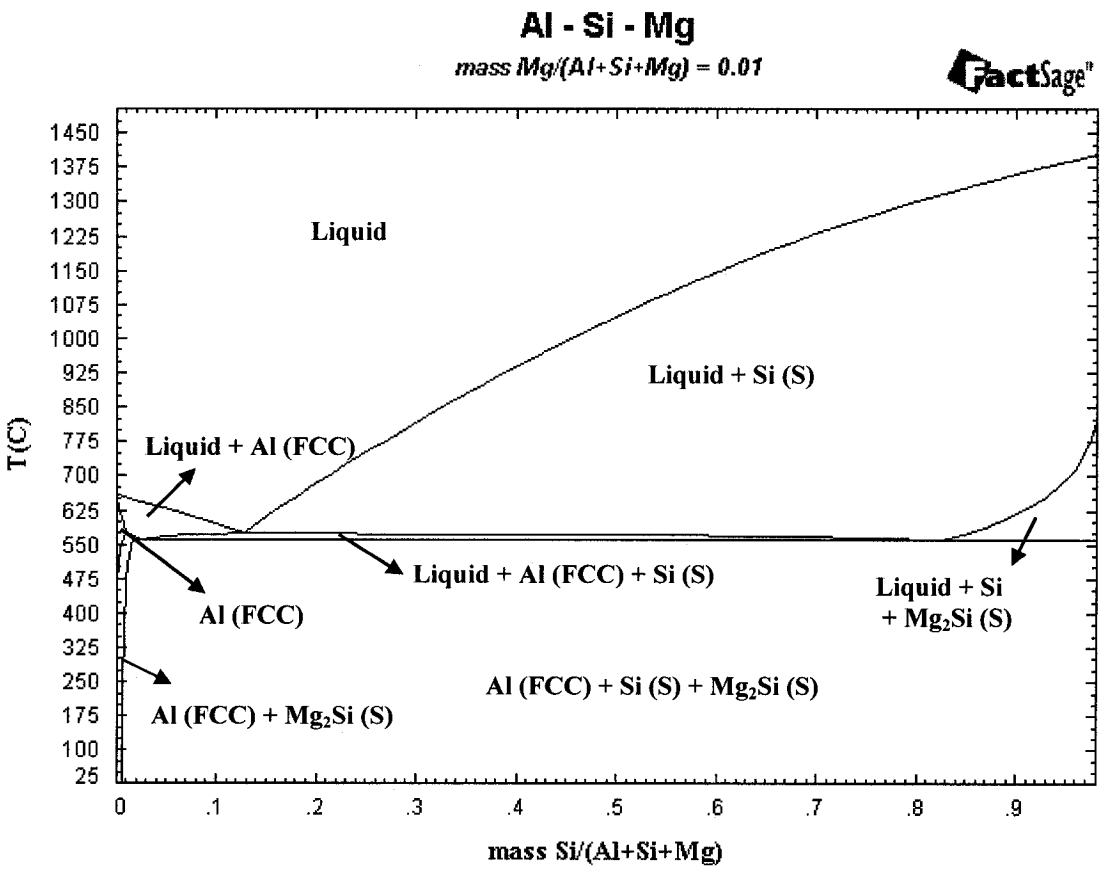

Figure 4.3: A vertical cut at 1%Mg in Al-Si-Mg

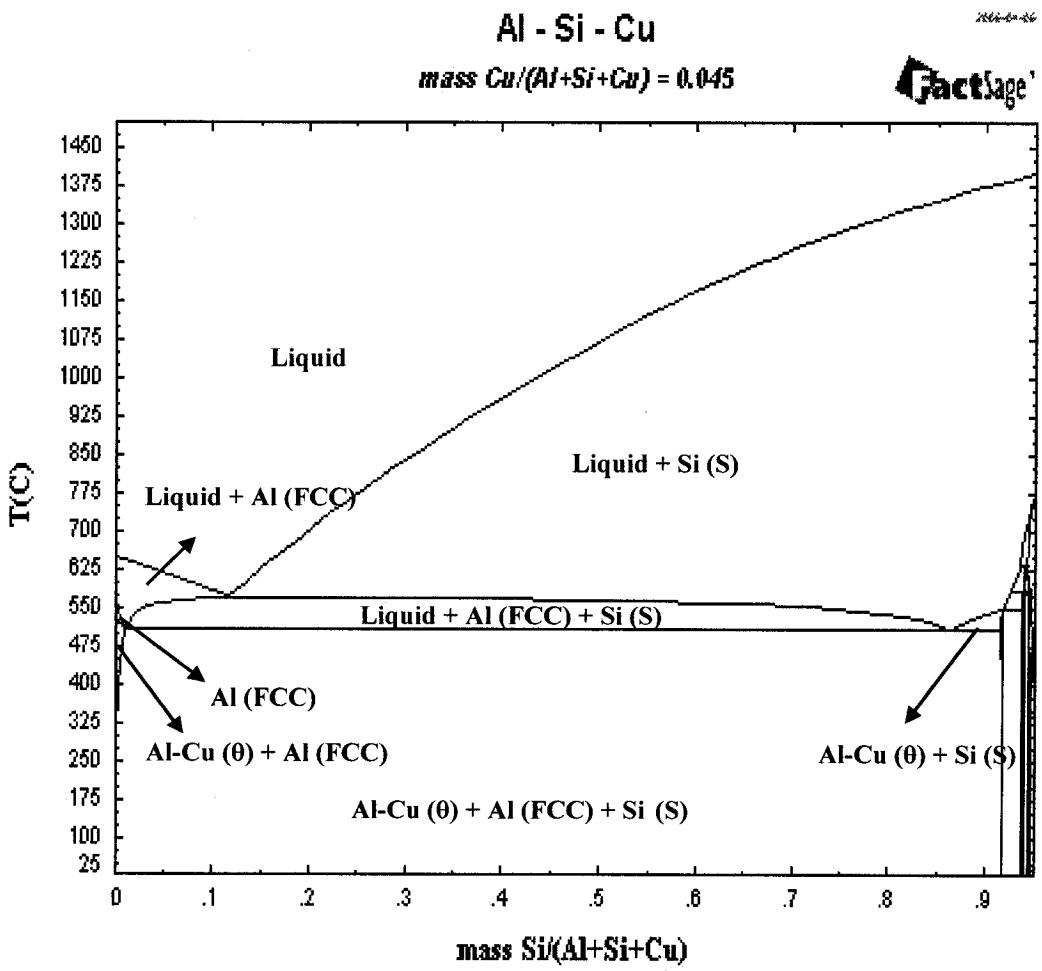

Figure 4.4: A vertical cut at 4.5%Cu in ternary Al-Si-Cu

4.1.3.3 The quaternary Al-Si-Cu-Mg

Sections of the quaternary phase diagram of Al-Si-4.5Cu-0.5Mg are shown In Fig. 4.5 and Fig. 4.6. The vertical line shows the composition of A390. The solidification path shows that the silicon starts to precipitate in the liquid phase at 653 ° C and continues down to the temperature of 566 ° C. At this point primary precipitation is complete (6.1% liquid is changed to primary silicon) and binary eutectic starts to solidify to Al (fcc) and Si. The binary eutectic reaction will continue down to 502 ° C where 88% of the liquid phase is solidified. The ternary eutectic reaction:

$$\text{Liq.} \rightarrow \text{Al (fcc)} + \text{Si (s)} + \text{Mg}_2\text{Si (s)} \qquad (4.1)$$

continues down to the temperature of 496 ° C where solidification becomes complete with the quaternary eutectic reaction:

$$\text{Liq.} \rightarrow \text{Al-Cu } (\theta) + \text{Al (fcc)} + \text{Si (s)} + \text{Mg}_2\text{Si (s)} \qquad (4.2)$$

The solid fraction remaining at each stage of the solidification is shown in Table 4.4, including the solid and liquid phase compositions.

It should be noted that the Factsage calculation differs from measured experimental values. One of the reasons for this is the fact that the thermal properties of the quaternary compounds such as $Cu_2Mg_8Si_6Al_5$ have not been entered in the Fslite database. The quaternary eutectic reaction was found to occur at about 507 ° C [3, 4]:

$$\text{Liq.} \rightarrow \text{Al-Cu } (\theta) + \text{Al (fcc)} + \text{Si (c)} + \text{Cu}_2\text{Mg}_8\text{Si}_6\text{Al}_5 \qquad (4.3)$$

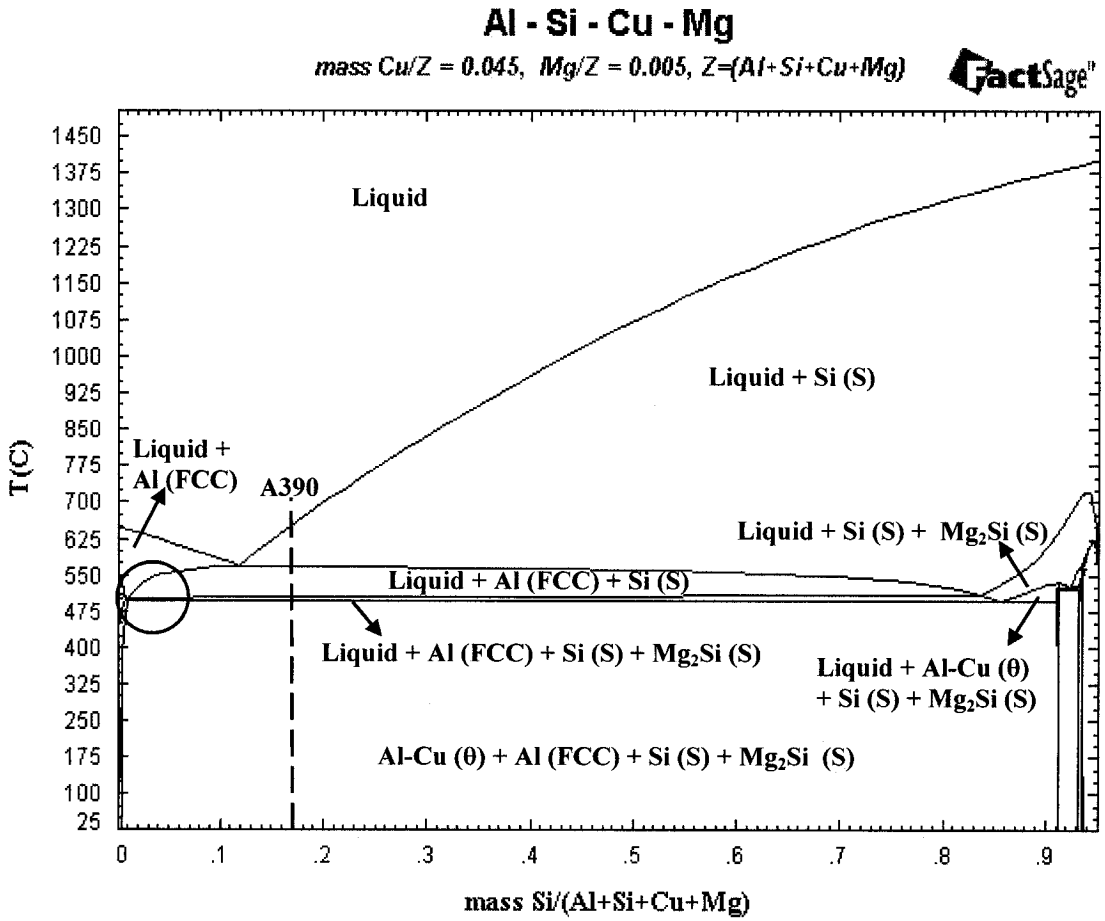

Figure 4.5: The Al- Si- Cu- Mg phase diagram for the Isopleth of 4.5%Cu and 0.5%Mg calculated by Factsage. The Vertical Line Represents the Si Content of A390.

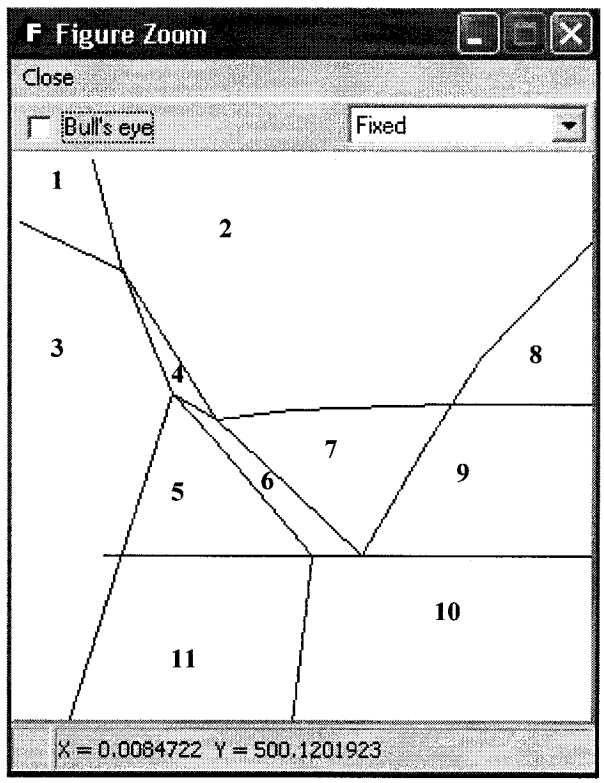

1- Al (S)

2- Liquid + Al (S)

3- Al (S) + Al-Cu (θ)

4- Liquid + Al (S) + Al-Cu (θ)

5- Al (S) + Al-Cu (θ) + Mg_2Si (S)

6- Liquid + Al (S) + Al-Cu (θ) + Mg_2Si (S)

7- Liquid + Al (S) + Mg_2Si (S)

8- Liquid + Al (S) + Si (S)

9- Liquid + Al (S) + Si (S) + Mg_2Si (S)

10- Al (S) + Al-Cu (θ) + Mg_2Si (S) + Si (S)

11- Al (S) + Al-Cu (θ) + Mg_2Si (S)

Figure 4.6: Circled zone in Figure 4.5

This quaternary reaction identifies $Cu_2Mg_8Si_6Al_5$ as a reaction product instead of Mg_2Si.

It should be noted that the solidified α-Al has two morphologies in the undercooled (non-equilibrium) condition and the microstructural observation confirms the presence of grains α-Al in the matrix as was previously explained in sections 2.4 and 2.5. Many studies have confirmed the close similarity between hypereutectic Al-Si alloys and Al-based composites with similar composition [6] where α-Al grains were observed due to undercooling for the case of hypereutectic alloys.

Table 4.4: The liquid and solid fraction as well as corresponding compositions for each transition reaction for A390 alloy.

A390	liquid Fraction (%)	Liquid composition (%wt)				Solid Fraction (%)	Solid composition (%wt)			
Temperature (°C)		Al	Si	Cu	Mg		Al	Si	θ*	Mg_2Si
653,1	100	78	17	4.5	0.5	0	-	-	-	-
566,2	93,9	83,0	11,6	4,9	0,5	6,1	-	100	-	-
502,4	5,9	62,8	7,5	27,1	2,6	94,1	83,2	16,8	-	-
496,9+δT	3,9	61,5	7,2	28,9	2,4	96,1	83,1	16,7	-	0,2
496,9-δT	0	-	-	-	-	100	81,4	16,2	2,1	0,3

* θ = Al-Cu (θ) or $CuAl_2$

4.1.3.4 Effect of Cu content

The isopleths of the quaternary Al-Si-Cu-Mg diagram with 4.5%Cu and 0.5%Mg is shown in Fig. 4.5. The variation of Cu changes the Si content in the liquid at the formation of the binary and ternary eutectic as well as the corresponding temperature at which they occur but there is no effect on quaternary eutectic formation as shown in Table 4.5 and Fig 4.7. With increasing Cu content (n=4.5%, 7%, 10%, 15%, 20%) at 17%Si, the binary eutectic temperature as well as the silicon content in liquid both decrease. In the ternary eutectic region for 7%Cu and higher, the reaction becomes (liquid→ Al(S) + Si + θ-$CuAl_2$), whereas for the Cu content lower than 7%, Mg_2Si appears in the temperature interval of the ternary region and the formation of the theta phase (θ-$CuAl_2$) become almost negligible. For 7%Cu the temperature interval of the ternary region becomes very small (about 3 ° C, Table 4.5) which can not be observed in the phase diagram. With increasing Cu content the temperature interval of the ternary region becomes larger, so that for 20% Cu this value is 8 ° C (between 504 and 496 ° C) and the silicon content in liquid increase to 4.5%. Variation of Cu has no significant effect on quaternary eutectic.

Table 4.5: Effect of Cu variation on silicon content in liquid of binary, ternary and quaternary eutectic and corresponding temperature for Al-17%.Si-n%Cu-0.5%Mg (n=4.5,7,10,15,20) alloys.

	Start of binary reaction		Start of ternary reaction		Quaternary reaction	
%Cu	T (°C)	%Si *	T (°C)	%Si*	T (°C)	%Si*
4.5 **	566	11.7	502	1.0	496	0.91
7	561	11.1	499 ***	1.5	496	1.0
10	554	10.6	501	2.2	496	1.0
15	542	9.6	503	3.3	496	1.1
20	529	8.6	504	4.5	496	1.1

*** Silicon content in liquid at the first precipitation of binary, ternary and quaternary eutectic**
**** A390 composition**
***** With increasing the copper content from 7%, ternary eutectic changes to**
Liquid→ Al(s) + Si + θ-$CuAl_2$

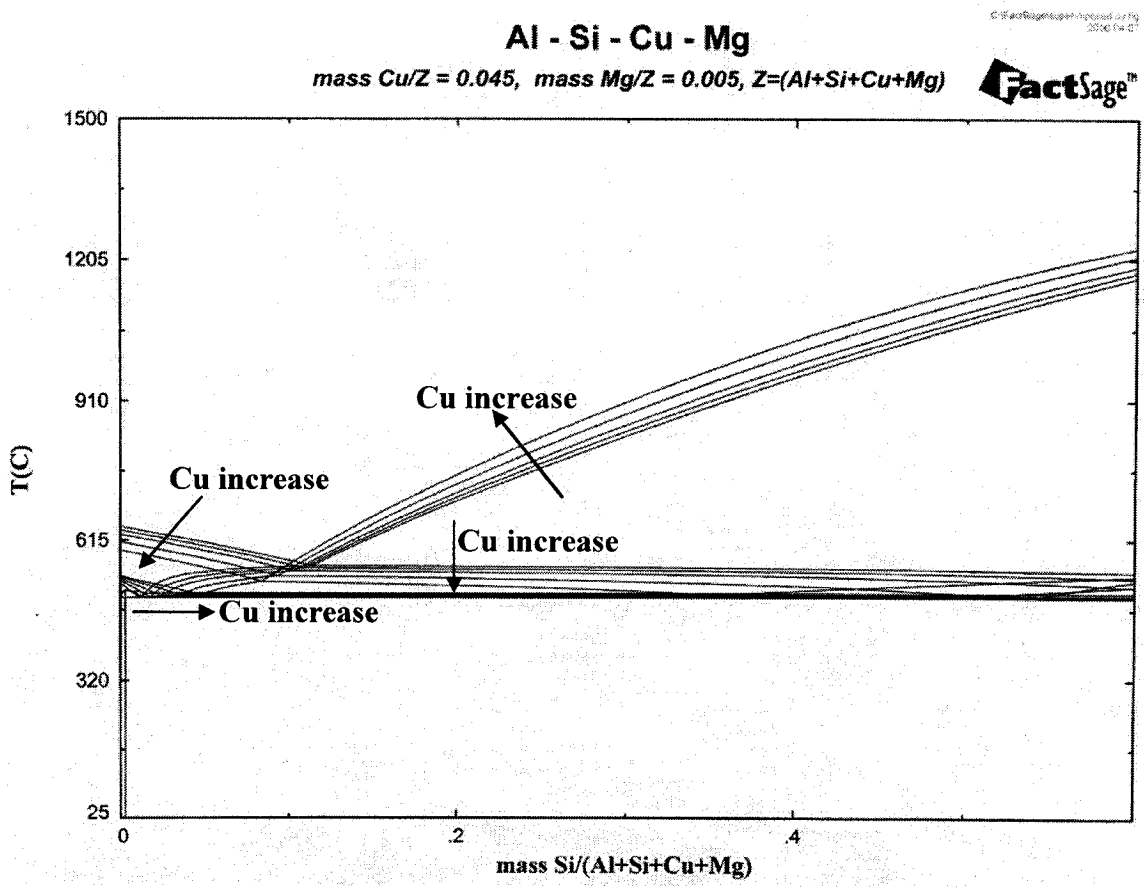

Figure 4.7: Effect of copper variation on the phase diagram of Al-Si-nCu-0.5%Mg (n=4.5%, 7%, 10%, 15%, 20%).

4.1.3.5 Effect of Mg content

The effect of Mg was calculated for values of 0.5%, 1%, 3%, 5% and 10% for the Al-17%Si-4.5%Cu-n%Mg system and shows a unique characteristic. This is clearly shown in Table 4.6 for increasing Mg contents where the binary eutectic temperature increases more slowly than the ternary eutectic temperature. This is principally due to the fact that the melting point of Mg_2Si is about 1102 ° C [37]. Figure 4.8 shows binary Mg-Si alloy and intermetallic Mg_2Si with melting point of 1085 ° C. the temperature ranges for the binary and ternary reaction are indicated in Table 4.6:

For 1% Mg, the effect is nearly same as 0.5%Mg (390 alloy) except for ternary eutectic temperature.

For 3% Mg, binary and ternary transition temperatures are very close (555 ° C and 546 ° C respectively) and the Si content in the liquid at the first precipitation of the ternary eutectic increases to 9.65%, Fig. 4.9.

As shown in Fig. 4.10, at 5%Mg, for hypereutectic alloy, a new region (Liquid + Si + Mg_2Si) appears with precipitation of Si and Mg_2Si in the liquid phase before the ternary eutectic reaction occurs. Thereafter, the ternary eutectic reaction takes place and the solidification becomes complete with the quaternary eutectic reaction at 496 ° C.

Table 4.6: Effect of Mg variation on silicon content in liquid of binary, ternary and quaternary eutectic and related temperature for Al-Si-4.5%Cu-n%Mg systems at 17%Si.

	Start of binary reaction		Start of ternary reaction		Quaternary reaction	
%Mg	T (°C)	%Si [1]	T (°C)	%Si[1]	T (°C)	%Si[1]
0.5[2]	566	11.70	502	7.49	496	7.09
1	564	11.75	526	9.65	496	7.09
3	555	12.20	546	12.08	496	7.09
5	565[3]	13.76	549	12.51	496	7.09
10	588	15.65	549	12.43	496	7.09

1- Silicon content in liquid at the first precipitation of the binary, ternary and quaternary eutectic.
2- A390 composition.
3- At Mg content higher than 4.2% the Binary eutectic reaction changes to (Liquid → Si (S) + Mg2Si (S)) instead of (Liquid → Al (S) + Si (S)).

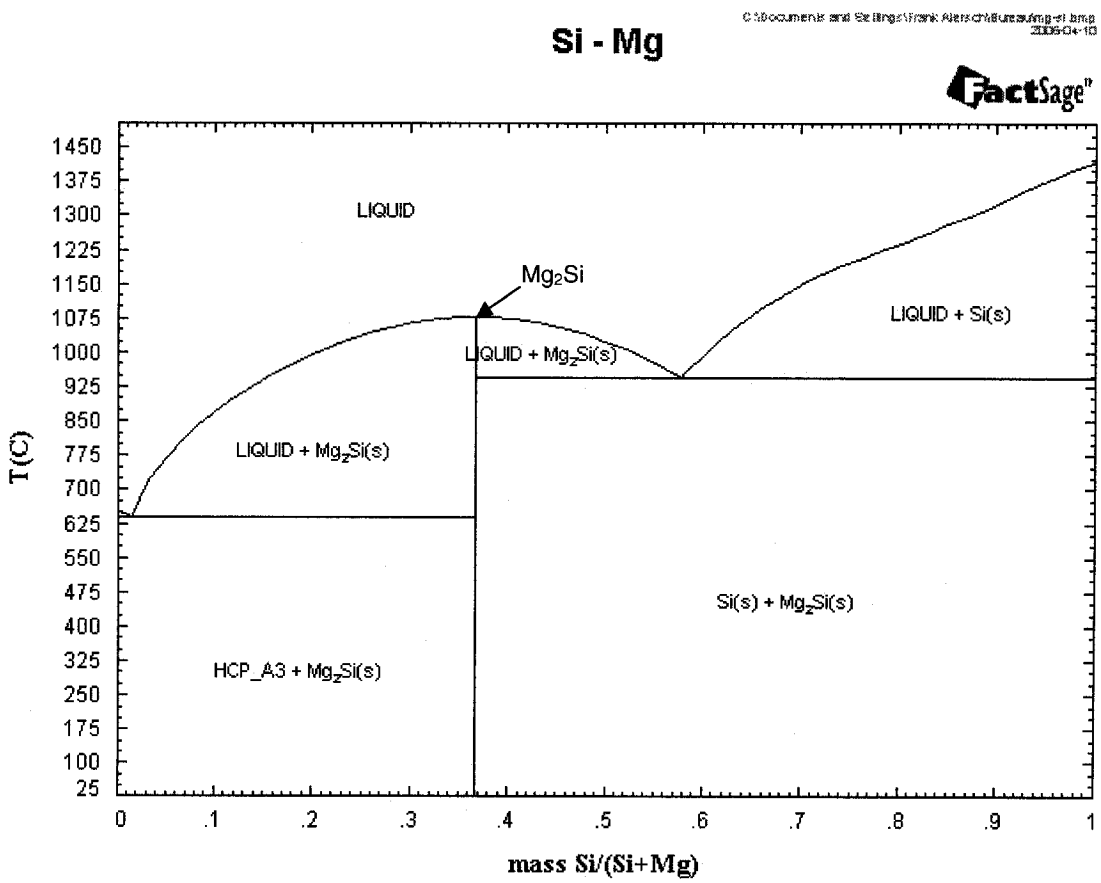

Figure 4.8: Binary Si-Mg phase diagram

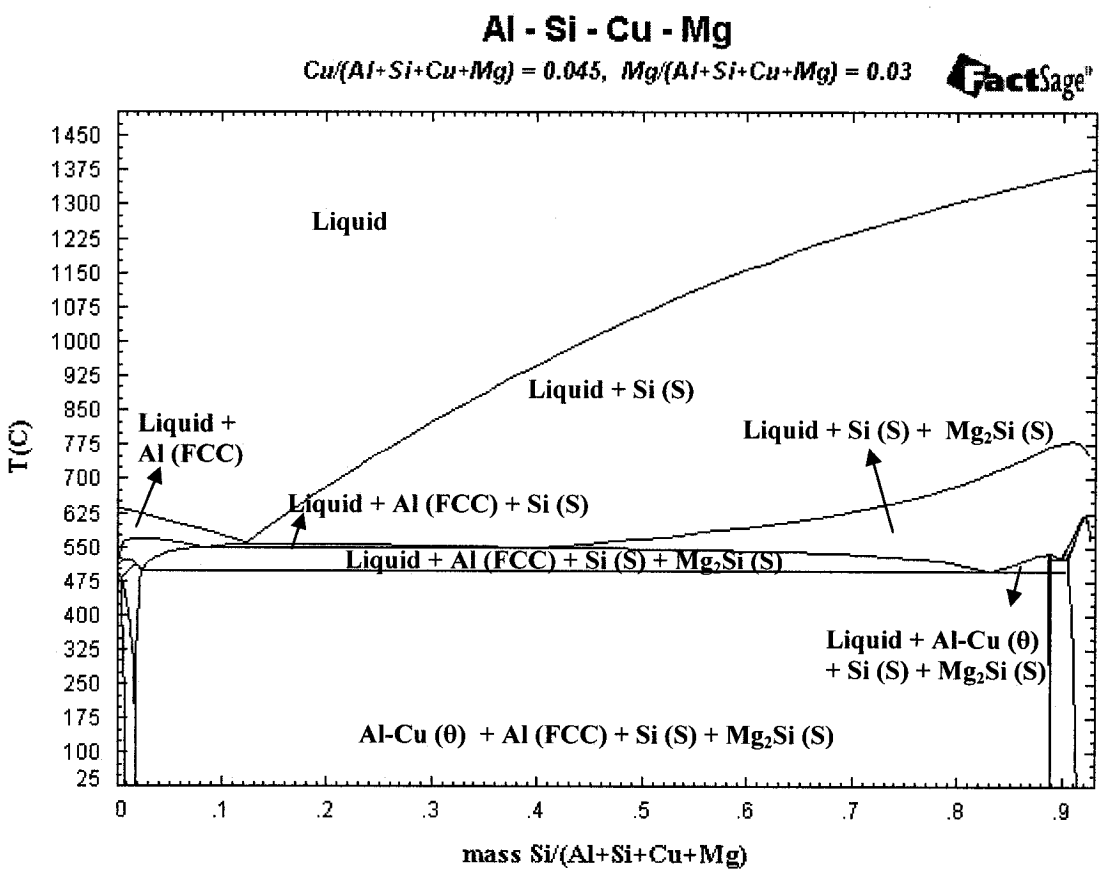

Figure 4.9: A vertical cut of system Al-Si-4.5Cu-3%, Mg

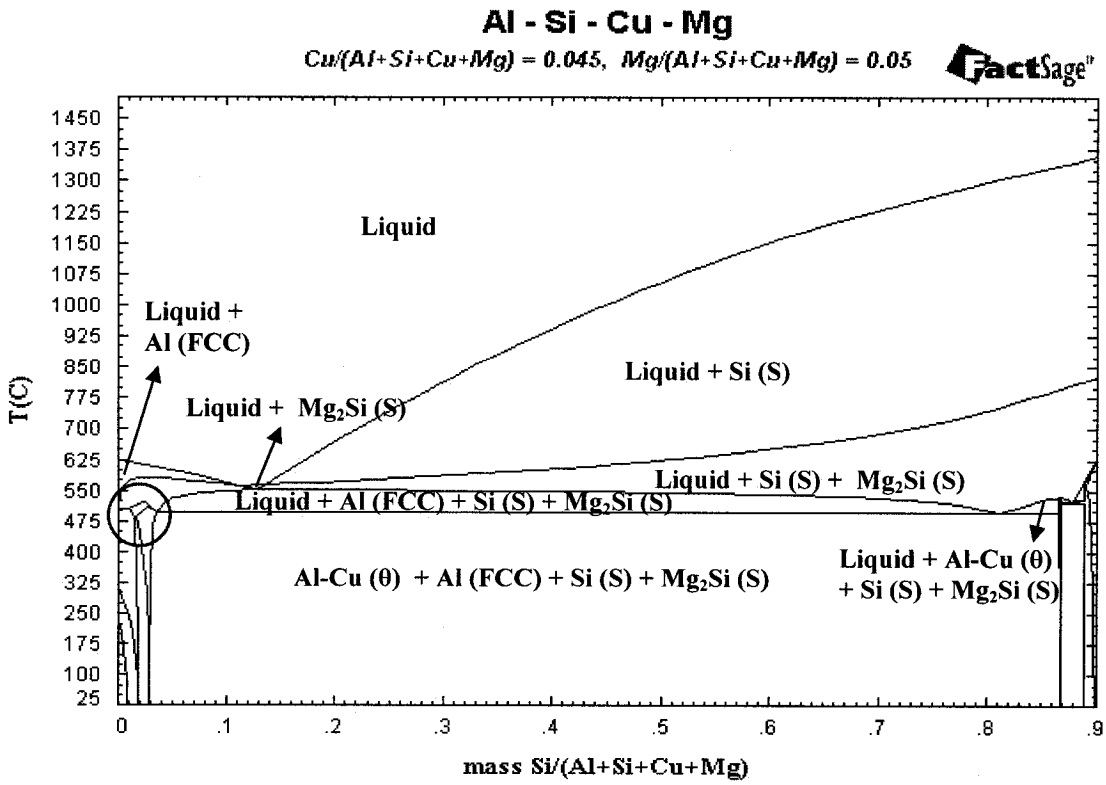

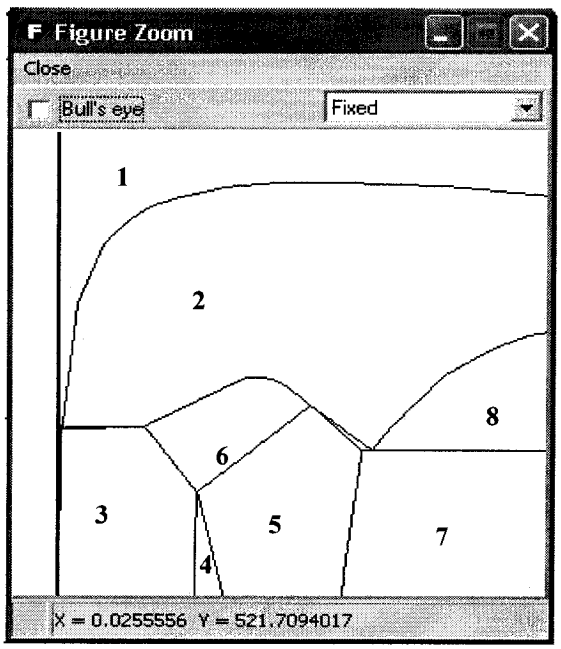

1- Liq. + Al (S)
2- Liq. + Al (S) + Mg_2Si
3- Al (S) + Mg_2Si + Al_2CuMg
4- Al (S) + Mg_2Si + Cu-Al (θ) + Al_2CuMg
5- Al (S) + Mg_2Si + Cu-Al (θ)
6- Al (S) + Mg_2Si
7- Al (S) + Si (S) + Mg_2Si + Cu-Al (θ)
8- Liq. + Al (S) + Si + Mg_2Si

Figure 4.10: A vertical cut of system Al-Si-4.5Cu-5%Mg and circled zone.

At 10%Mg, this new region becomes more pronounced and generates a new solidification path. Comparing the solidification path for this alloy with A390 alloy, the liquidus temperature was calculated to be about 646 ° C as indicated by the dashed line in Fig. 4.11. The solidification starts with the precipitation of Mg_2Si(s) from the liquid (contrary to A390 alloy, where the solidification starts by precipitation of Si at 653 ° C). The solidification then continues with the precipitation of Si at the temperature of 588 ° C. Thereafter, a ternary eutectic reaction occurs at 549 ° C and finally at 496 ° C, a quaternary eutectic reaction takes place where solidification becomes complete as for the case of A390. A microstructural analysis [41] was carried out for the two alloys with 0.5% Mg (Fig. 4.12) and 10% Mg (Fig. 4.13). Primary silicon was observed for both A390 and the case of 10%Mg (Fig. 4.13. a,c). Moreover, the Mg_2Si intermetallic phase only solidifies like Chinese script (Fig. 4.13. c,d) and no other morphology was observed in the microstructure. Therefore, Si starts to solidify as free Si along with the Mg_2Si in the "liquid + Si + Mg_2Si" zone which implies that, for 10% Mg, only Si solidifies in the liquid.

One of the disadvantages of A390 alloy is the formation of large primary silicon particles resulting from the large solidification interval of about 156 ° C and maximum solid fraction of 6.1%. This form of silicon decreases the mechanical and wear behavior of this alloy because the large particles become stress concentrators and result in crack propagation. At 10%Mg, the solidification interval is 92 ° C (from 588 ° C to 496 ° C) with maximum solid fraction of Si 2,6%. This results in fine primary silicon particles. Also,

the presence of Mg_2Si(s) along in the liquid phase at the temperature between 646 ° C to 588 ° C (above the precipitation of Si) plays an important role as a nucleation site for primary silicon and results in finer particles.

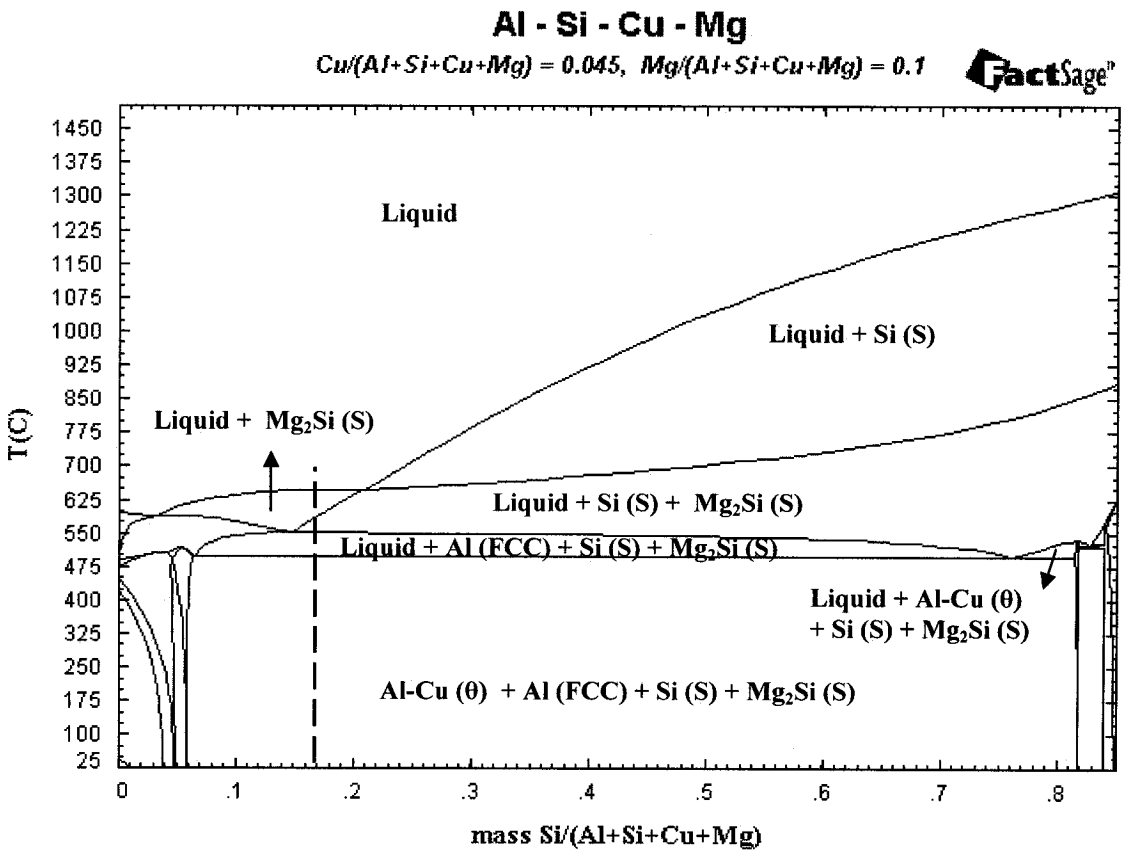

Figure 4.11: A vertical cut of system Al-Si-4.5Cu-10Mg and solidification path at 17%Si

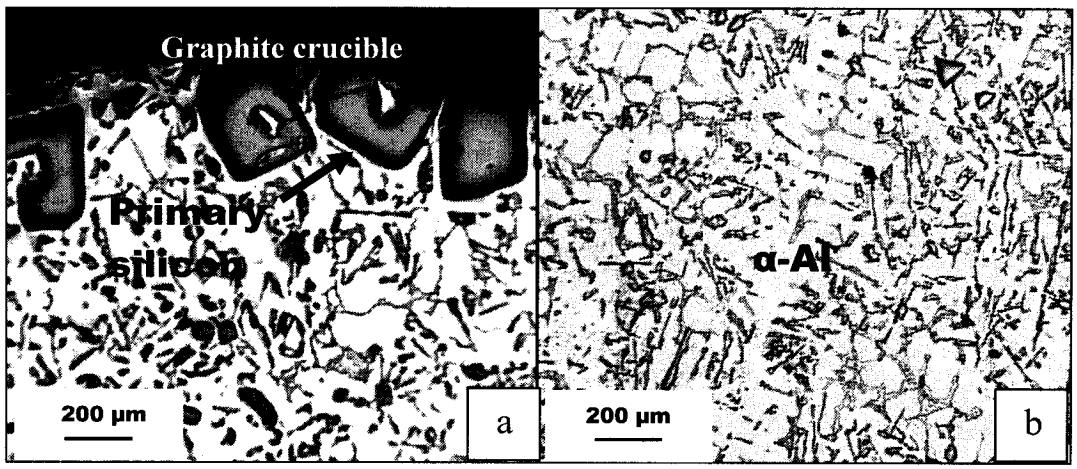

Figure 4.12: Microstructure of A390 (Al-17%Si-4.5%Cu-0.5%Mg) alloy a) in contact with the graphite crucible b) far from the crucible

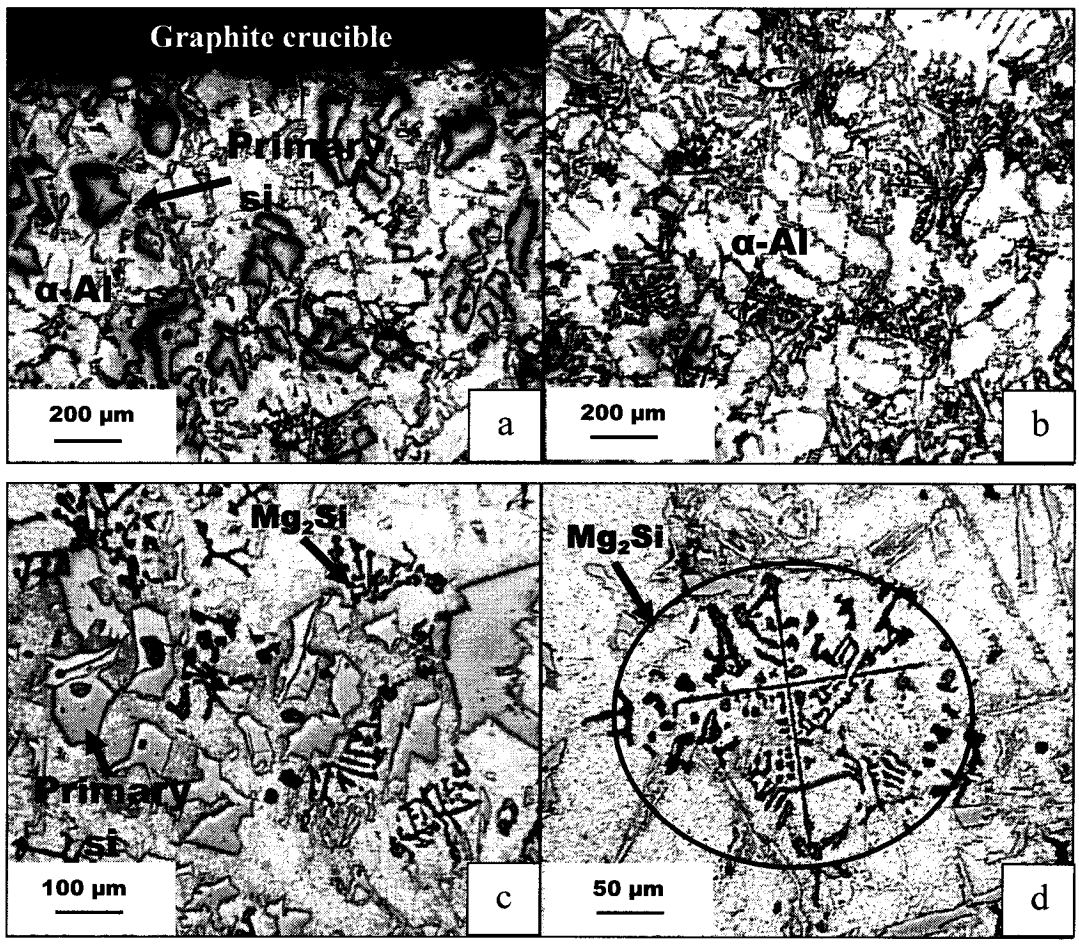

Figure 4.13: Microstructure of Al-17%Si-4.5%Cu-10%Mg a) in contact with the graphite crucible b) far from the crucible without primary silicon c) another region with primary silicon and Mg_2Si (high magnification and d) Chinese script feature of Mg_2Si.

4.2 As cast microstructure of A390

It was observed that the $Cu_2Mg_8Si_6Al_5$ typically nucleates on θ-Al_2Cu in the form of blocky or thin needle-like structures [1]. The θ-Al_2Cu phase precipitates in both a blocky and eutectic (Al+Al_2Cu) forms or as a mixture of both types depending on the cooling rate Fig. 4.14(a,b) [2]. The precipitation of $Cu_2Mg_8Si_6Al_5$ is reported to take place at the end of the Al+Al_2Cu eutectic region [2]. The reaction proposed for the precipitation of $Cu_2Mg_8Si_6Al_5$ is [3]:

$$\text{Liq.} \rightarrow Al+CuAl_2+Cu_2Mg_8Si_6Al_5+\text{Si (solidus reaction)} \qquad (4.4)$$

According to the solidification path of A390 in Fig. 4.5 calculated by Factsage software, the silicon precipitates as primary crystals at 653 ° C, and as a Al-Si binary eutectic at 566 ° C. The silicon that precipitates as the primary phase has a faceted morphology Fig. 4.14(c) and eutectic has coarse plate-like crystals Fig. 4.14(d,e).

The Mg_2Si phase precipitates in the form of large Chinese script particles [1] as shown in Fig. 4.14(f).

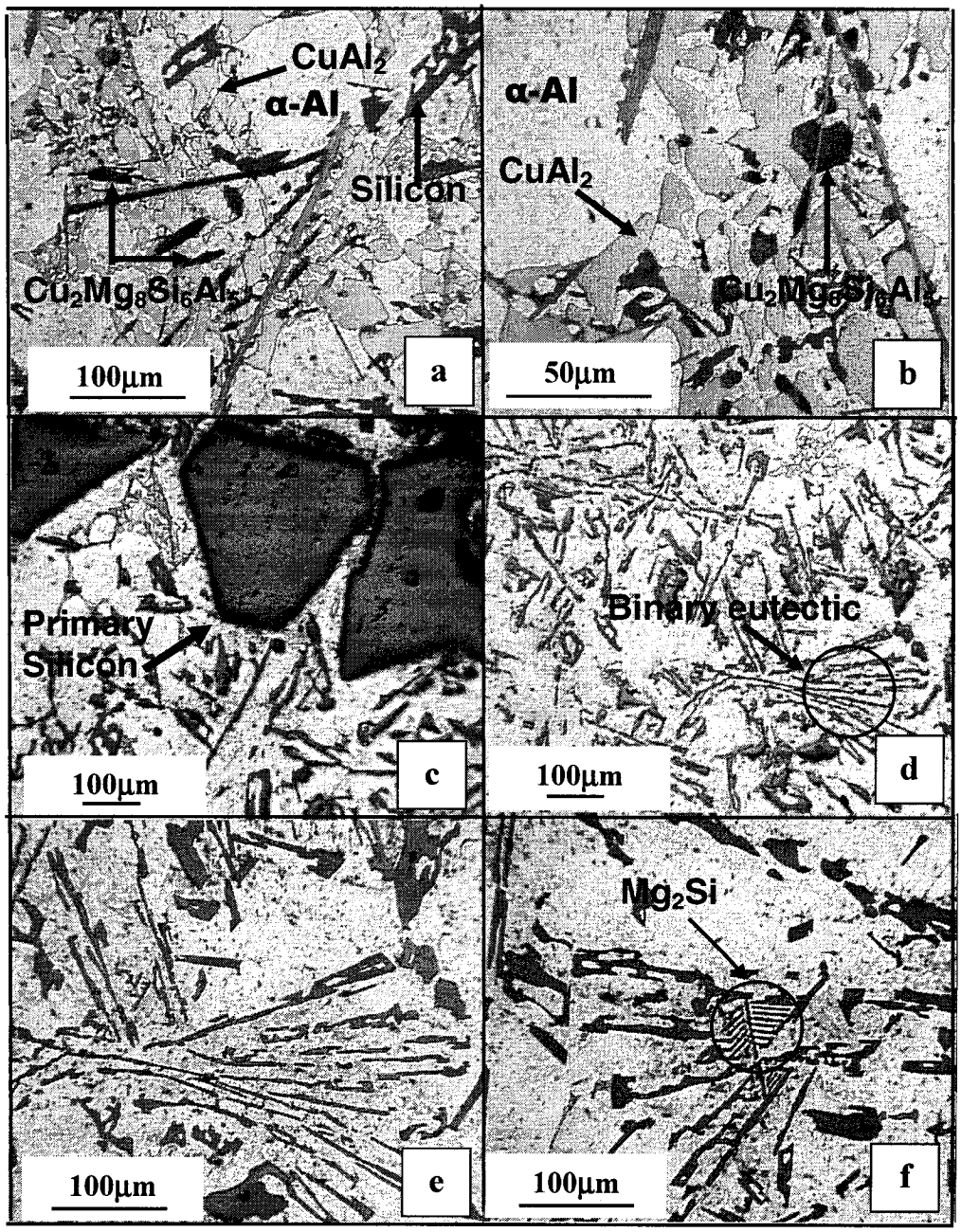

Figure 4.14: Microstructure of as cast A390, (a) precipitation of Al_2Cu and $Cu_2Mg_8Si_6Al_5$ (dark blocky) (b) same region, high magnification (c) primary faceted silicon (d) plate-like crystals of eutectic Si (e) same region, high magnification and (f) Mg_2Si. Etchant R.L.Anderson's AlNQ2.

4.3 The Rheological behaviour of A390

The rheological behaviour was investigated during continuous cooling and isothermal conditions. For the continuous cooling experiments, the alloy is initially heated to the temperature of 700 ° C and then held at a given temperature with maximum rotation velocity (512 rpm) for a 10 minute period in order to achieve a homogeneous semi-solid. After this period the alloy is continuously cooled at a rate of -2 ° C/min and sheared at rates of 15, 59, 123, 250 and 507 s^{-1} in separate tests to the temperature at which the upper limit of the viscometer torque is reached (see Table 3.1). In the isothermal tests, the alloy is also heated to the temperature of 700 ° C and then continually cooled at -2 ° C/min and sheared at 13 s^{-1} until the temperature of 565 ° C was reached, which is within the binary eutectic temperature zone (566 ° C). The alloy was then sheared for 20 minutes under isothermal conditions after which the shear rate was abruptly changed to a new value. In the sequence of "step change" experiments at 565 ° C the shear rates were changed in a sequence of 52-, 104-, 26-, 104- and 13 s^{-1} (see Table 3.1).

4.3.1 Viscosity during continuous cooling

Above the liquidus temperature starting at 700 ° C, the alloy was continuously cooled at a rate of -2 ° C/min and sheared at constant rates of 15, 59, 123, 250 and 507 s^{-1} in separate experiments. The experimental results show that the apparent viscosity of semi-solid slurry of alloy stirred during continuous cooling depends on both the temperature (solid fraction) and shear rate as shown in Fig. 4.15. As the temperature decreases, (increasing the solid fraction) the viscosity starts to increase in a significant manner. This increase is very gradual until the binary eutectic temperature of 566 ° C is reached. Beyond this temperature the viscosity increases rapidly. In all continuous cooling tests the temperature does not reach the quaternary eutectic temperature found to be about 496 ° C because the maximum 4.9 N-cm torque limit of the viscometer is reached before this temperature is attained. At the binary eutectic solidification temperature (566 ° C) the liquid fraction is 93,9% and only a small fraction liquid (3.9%) remains at the quaternary eutectic temperature (496 ° C). The samples were then removed to verify the effect of different shear rates on the continuously cooled microstructure. The apparent viscosity as a function of temperature was plotted and showed a linear and an exponential region. Both regions were analyzed using least squares analysis. The linear region continues up to the binary Al-Si eutectic temperature of 566 ° C where only primary silicon solidifies. The exponential region is initiated by the solidification of the binary Al-Si eutectic which corresponds to the α-Al precipitation.

The corresponding regressions can be represented in the following form:

$$\mu = AT+B \text{ (linear region)} \quad (4.5)$$

$$\mu = C \exp (DT) \text{ (exponential region)} \quad (4.6)$$

Where μ is apparent viscosity (Pa.s), T is temperature ($^\circ$C) and A, B, C, D, are constants values. It is clear that the constant "A" describes slope ($\frac{d\mu}{dT}$) of the linear region and the constant "D" defines the exponent value of apparent viscosity versus temperature diagram in the second region. Table 4.7 shows the constants values for each continuous cooling experiment according to different shear rates.

Table 4.7: The values of the rheological constants for each continuous cooling experiment according to different shear rates.

	Linear region			Exponential region	
Shear rate $\dot{\gamma}$ (s^{-1})	A	B		C	D
15	-0.03	23.15		4E+142	-0.5766
59	-0.02	17.55		2E+71	-0.2898
123	-0.01	7.45		7E+58	-0.2406
250	-0.006	4.07		1E+133	-0.5532
507	-0.007	4.61		4E+148	-0.6223

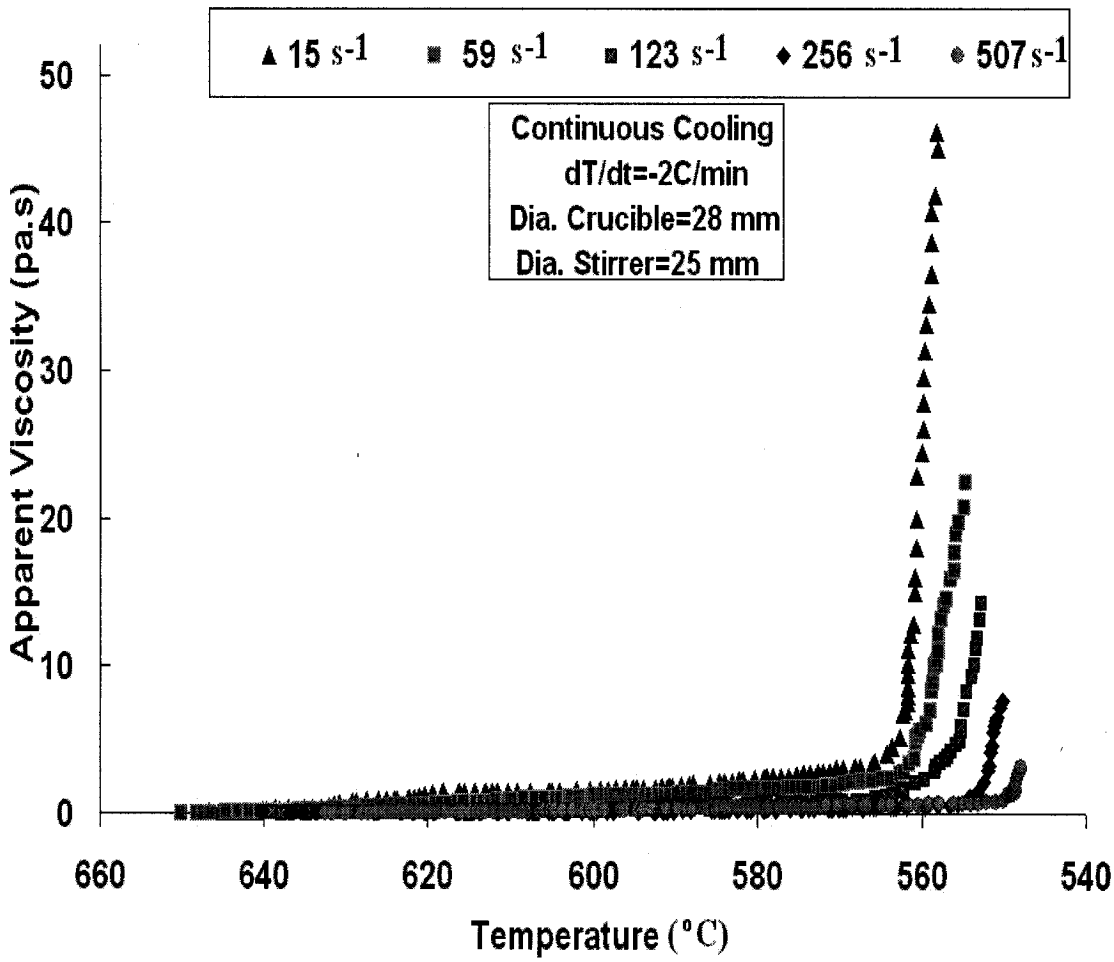

Figure 4.15: Viscosity versus temperature for continuous cooling tests at different shear rate

The linear and exponential region for each shear rate tests is related to the solid fraction versus temperature graph during the solidification period.

Figure 4.16 shows the solid fraction versus temperature graph for the solidification of A390 alloy calculated by Factsage software. As it is expected, the solid faction increases abruptly when binary eutectic reaction starts to occur at 6.1% solid. Before this reaction occurs, the relation is linear due to the low solid fraction which can be interpreted as a dilute suspension of particules.

Figure 4.17 shows the exponential region for the apparent viscosity versus temperature at the shear rate of 15 s^{-1} according to continuous cooling test. A graph of Viscosity vs. Ln(Temperature) indicates that the apparent viscosity as a function of temperature is exponential. The validity of linear region was calculated between 650-566 ° C where the solid fraction starts form 0 to 5.9% according to Figure 4.15. It should be mentioned that the melting point calculated by Factsage indicates the corresponding temperature for quaternary system. However, the commercial A390 ingot produced by Alcan Co. has can also have trace contents of Zn, Mn and Fe which can change the transition reactions to some degree.

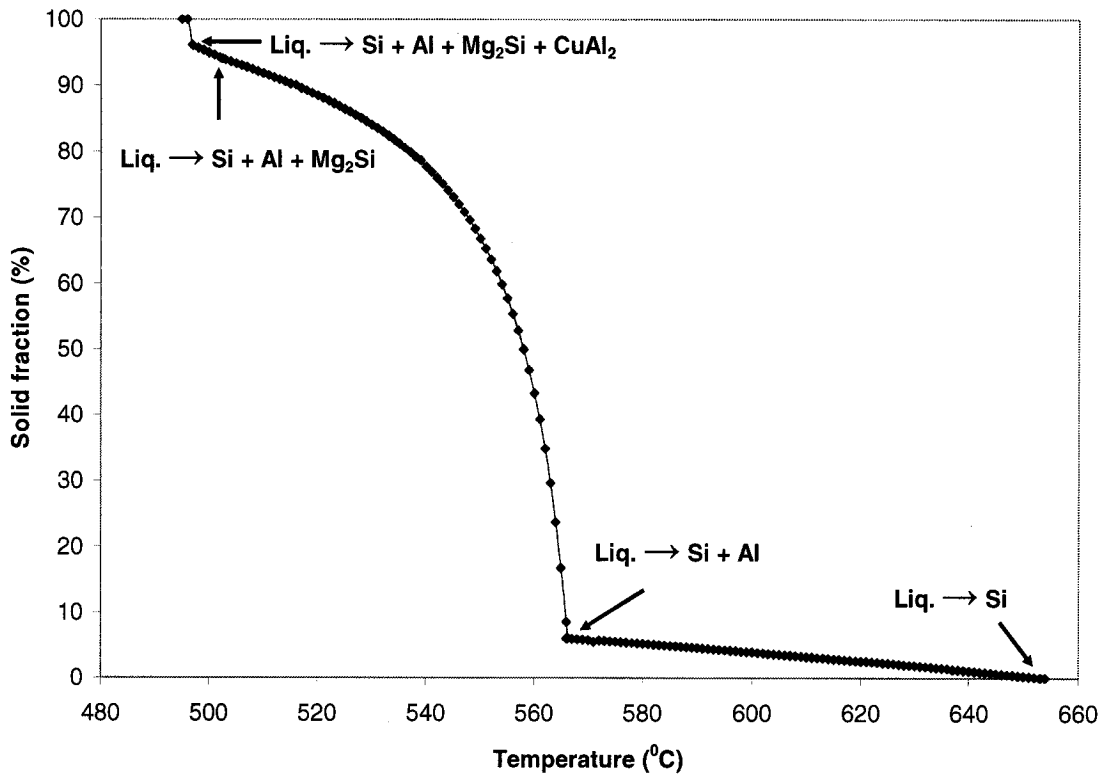

Figure 4.16: The solid fraction versus temperature graph for solidification of A390 alloy calculated by Factsage software

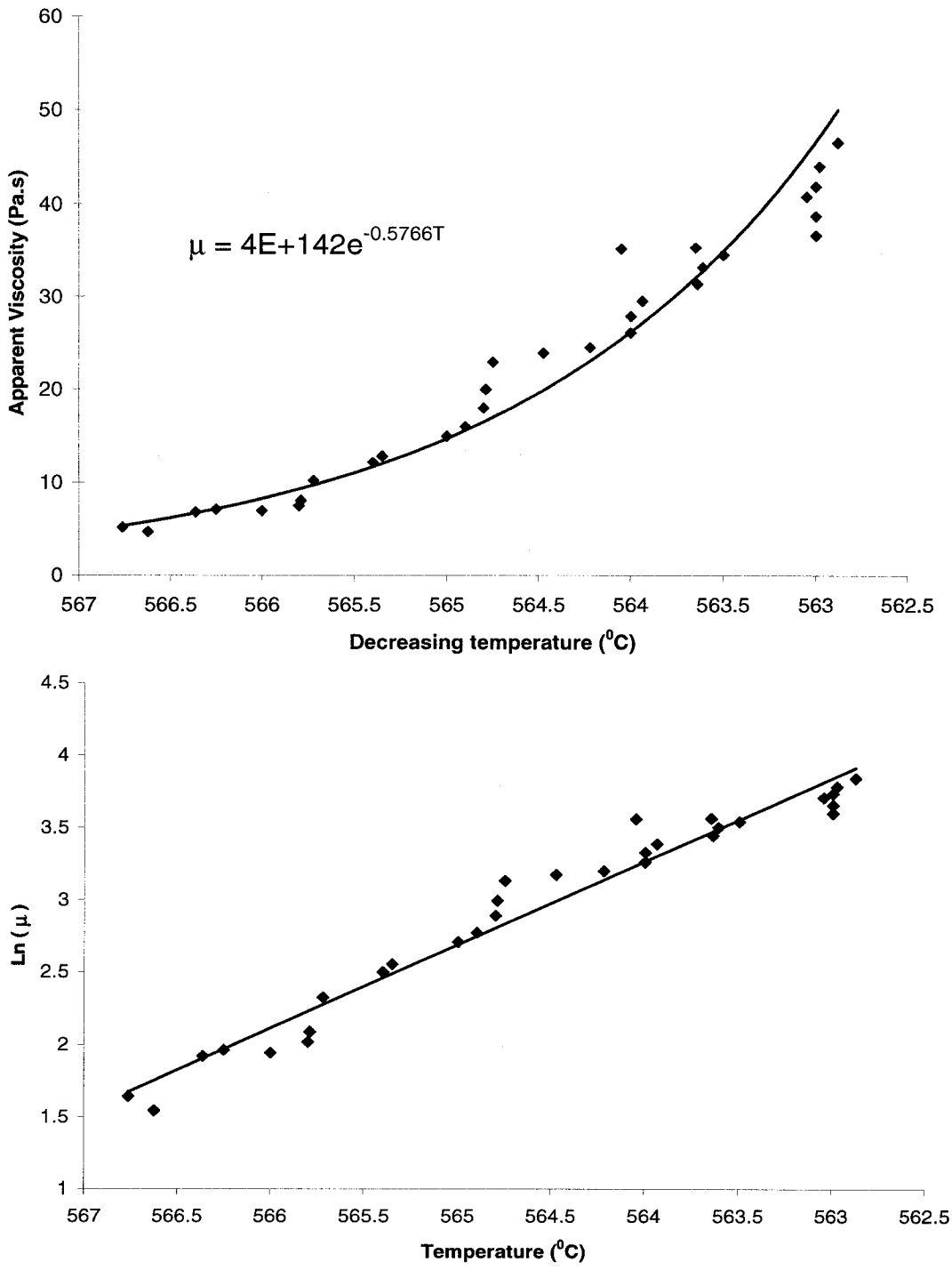

Figure 4.17: Exponential region for the apparent viscosity versus temperature graph at the shear rate 15 s^{-1}

Figures 4.18-4.21 show the exponential region for the apparent viscosity versus temperature graph at the shear rate of 59, 123, 250, and 507s^{-1} determined from the continuous cooling tests. When comparing the linear regions at different shear rates, it was observed that the linear region becomes larger with increasing the shear rate contrary to the exponential region which becomes smaller.

Table 4.8 shows the temperatures of the linear region and the corresponding solid fraction according to different shear rates. At the shear rate of 15 s^{-1}, the linear region continues down to the near binary eutectic temperature (566.7 ^{0}C). With increasing the shear rate, the extent of the linear behaviour with temperature falls into the binary eutectic zone and the solid fraction increases abruptly.

Table 4.8: The linear region of viscosity vs. temperature and corresponding solid fraction according to different shear rates for continuous cooling tests.

Experimental results		Factsage calculation
Shear rate $\dot{\gamma}$ (s^{-1})	Extent of linear range	Corresponding solid fraction (%)
15	566.7	5.9
59	562.1	34.8
123	560.0	43.0
250	554.7	57.4
507	551.0	65.2

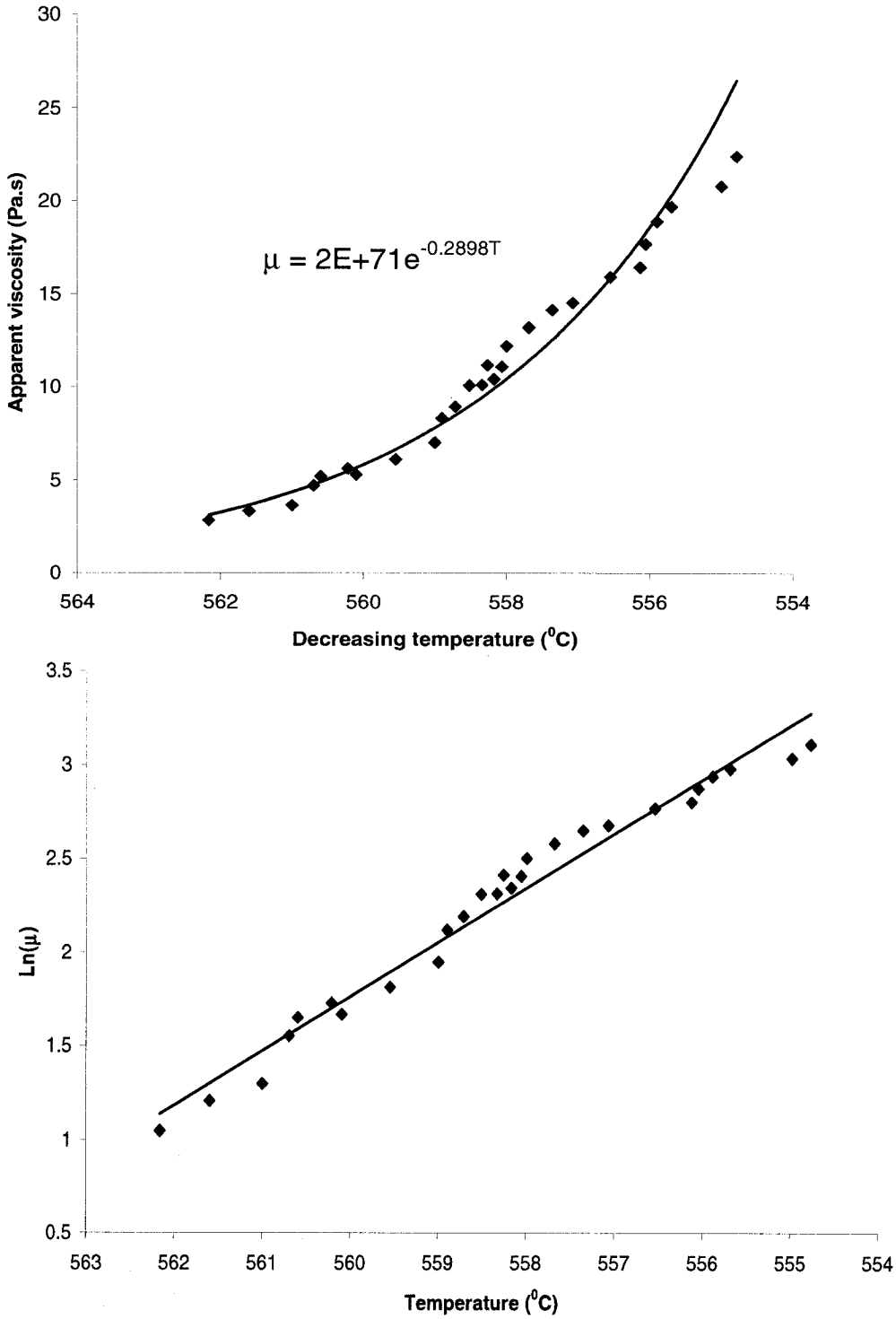

Figure 4.18: Exponential region for the apparent viscosity versus temperature graph at the shear rate 59 s^{-1}

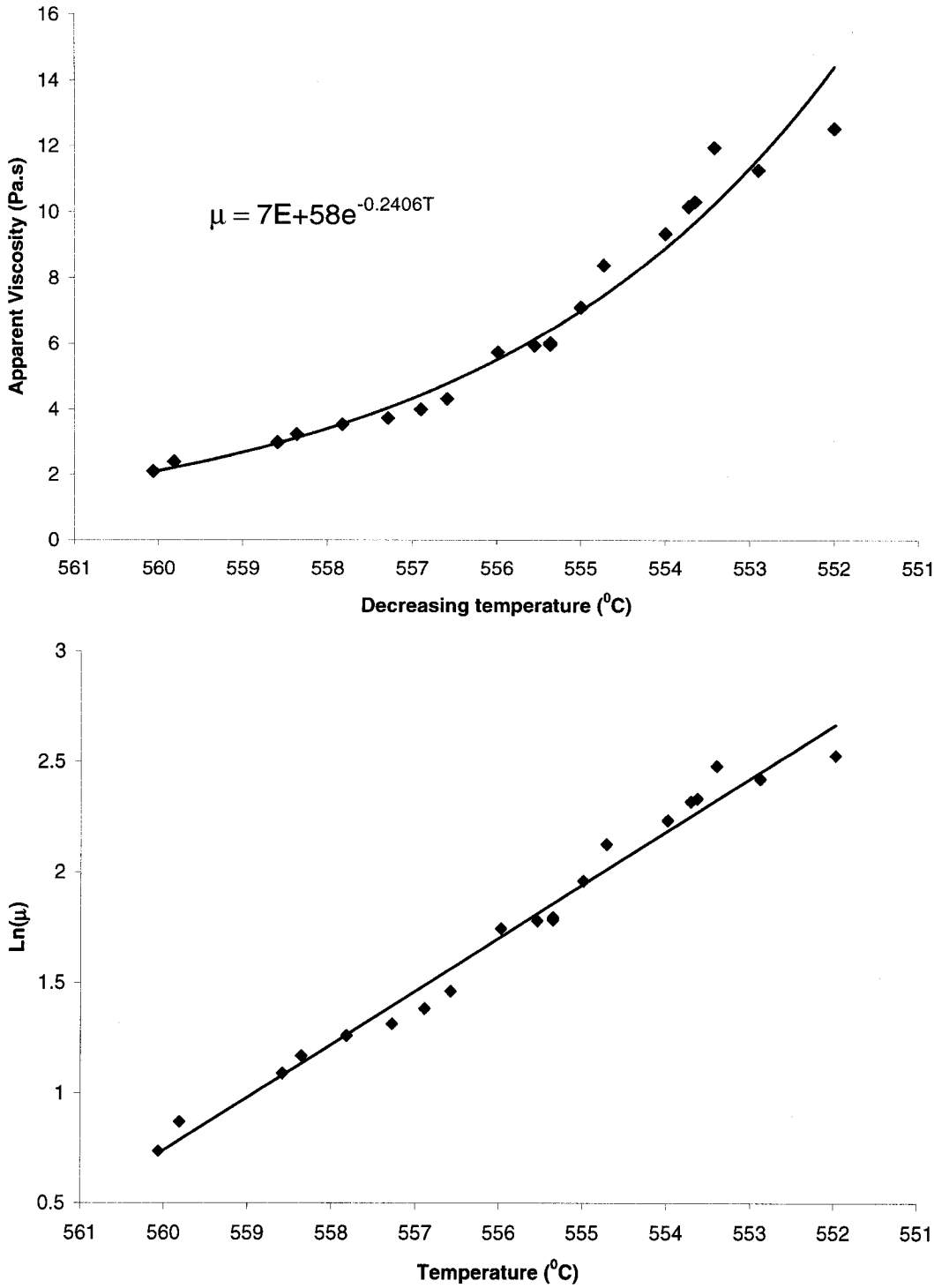

Figure 4.19: Exponential region for the apparent viscosity versus temperature graph at the shear rate 123 s^{-1}

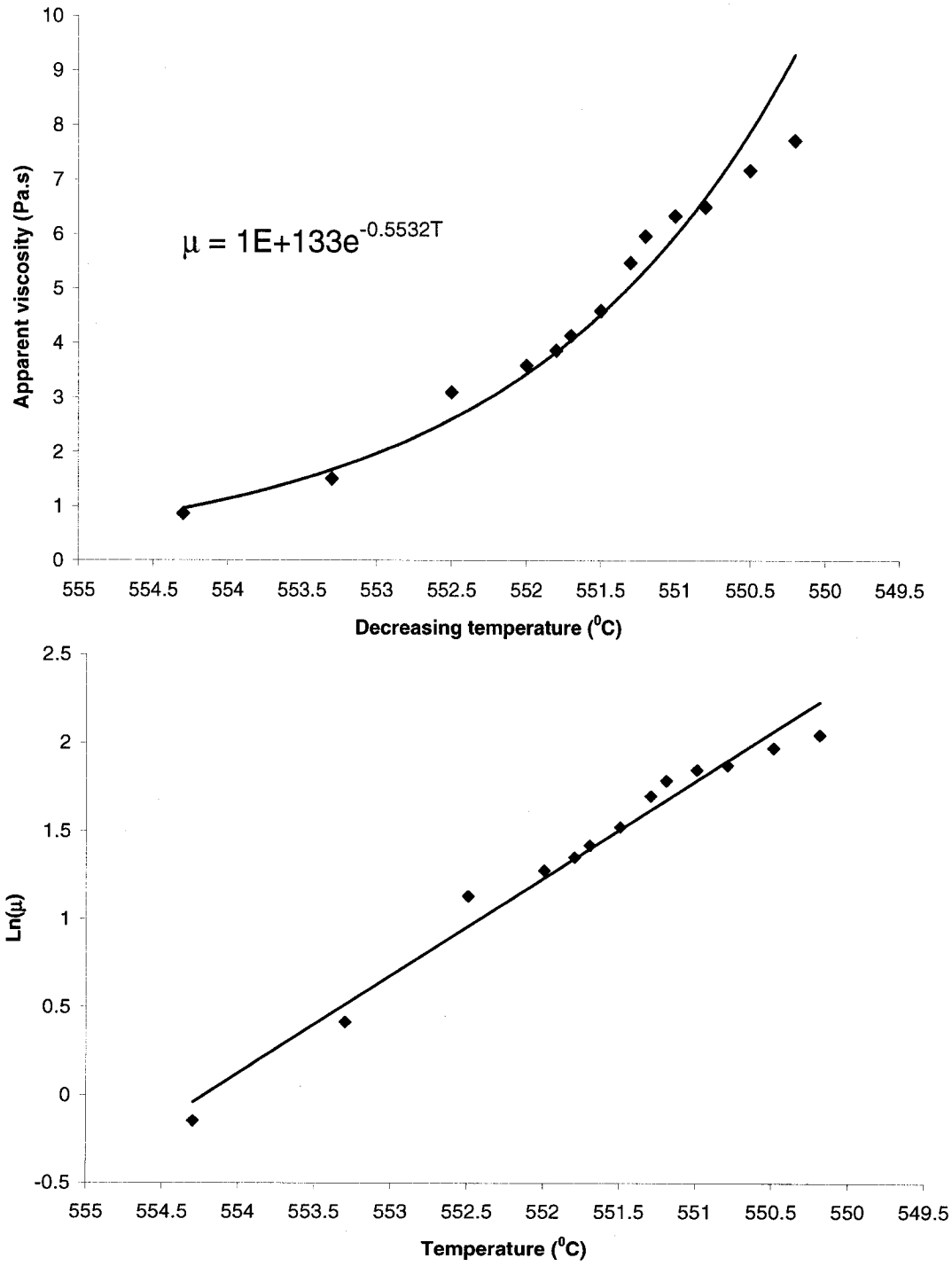

Figure 4.20: Exponential region for the apparent viscosity versus temperature graph at the shear rate 250 s^{-1}

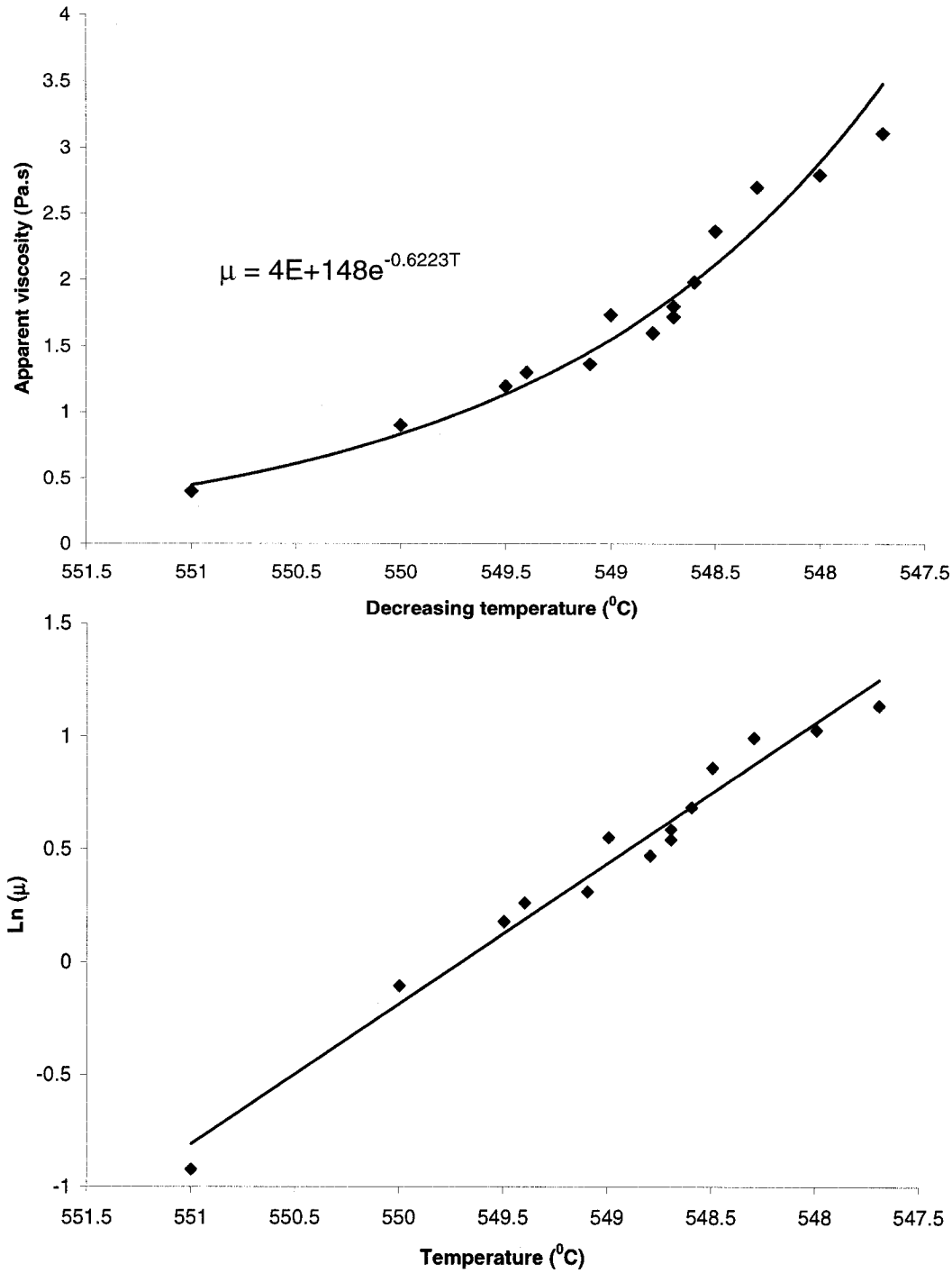

Figure 4.21: Exponential region for the apparent viscosity versus temperature graph at the shear rate 507 s^{-1}

As described at Table 4.8, with increasing shear rate, the absolute values of the constant "A" decreases and demonstrate the effect of fragmentation of the primary Si phase, resulting in a reduced viscosity (Fig. 4.22). However, the values of the constant D, indicate that the variation of the shear rate does not appear to affect the exponential region of the viscosity. The variability of D with shear rate shows considerable dispersion with no specific trend. In the exponential region, the binary eutectic of Al-Si solidifies at 566 ° C which corresponds to the α-Al precipitation. With decreasing temperature a ternary and quaternary eutectic occurs at the temperature of 502 and 496 ° C, respectively. The values of the constant D do not show an order of magnitude change with the variation of shear rate. Even though, 93.9% of the liquid is solidified at this region. It can be concluded that the variation of shear rates (except for 15 s^{-1}, which shows no observed microstructual degradation) changes the morphology of acicular binary eutectic as well as α-Al in the same manner. However, in the linear region, only primary silicon solidifies and with increasing the shear rate, the degree of fragmentation of silicon increases and viscosity decreases, decreasing the value of the slope. It should be noted that the maximum fraction solid of primary silicon at the end of the linear region (566 ° C) is only 6.1%, and the slopes decrease very gradually. It is necessary to note that, as is indicated in the table 4.8, the linear region appears to extend far beyond the onset of the binary reaction which occurs at 566.2 ^{0}C. Due to the mixing at higher shear rates this reaction may be delayed to occur at the lower temperatures (non-equilibrium) since it is not normal to observe the continued linear behaviour for calculation solid fraction.

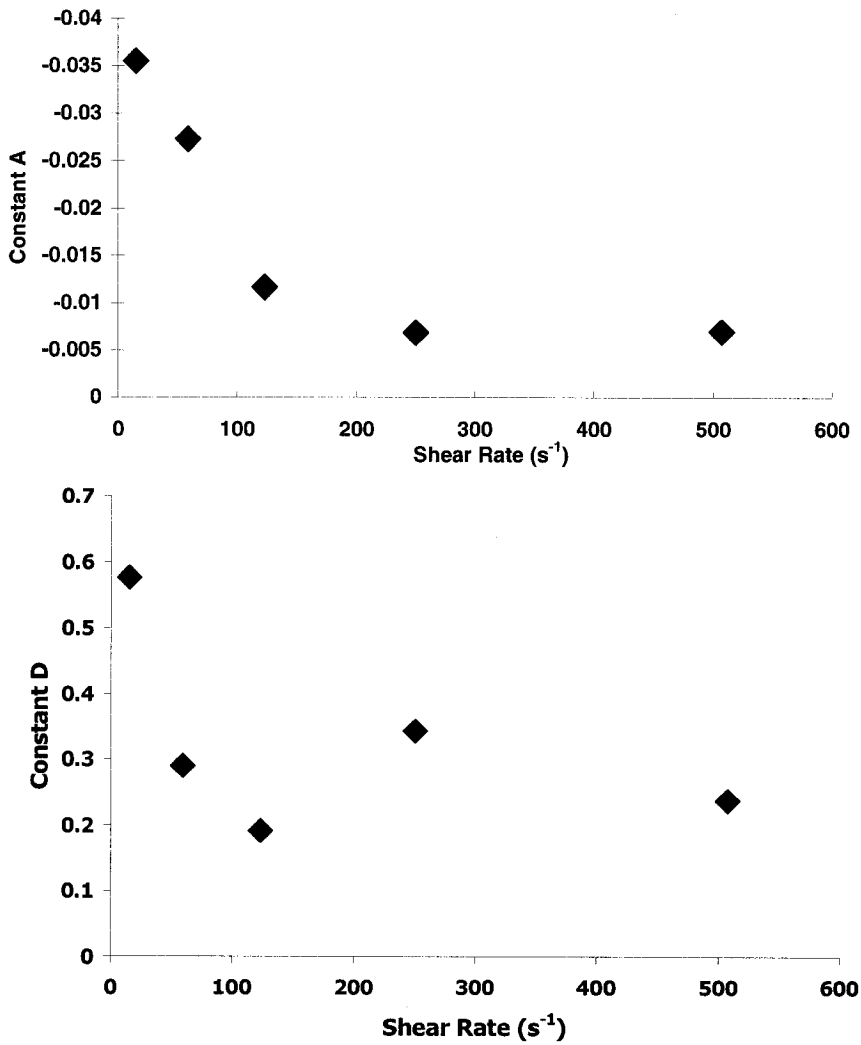

Figure 4.22: Variation of the constants A and D with different shear rates in continuous cooling tests

4.3.1.1 The microstructural evolution during continuous cooling at different shear rates

The microstructural observation shows that the shear rate of 15 s^{-1} is too low to cause a degradation of the structure obtained. For a shear rate of 59 s^{-1} the microstructure is considerably different from the structure at 15 s^{-1}. About 50% of the primary silicon is fragmented where fracture takes place along $\{100\}$and $\{110\}$cleavage planes, as shown in Fig. 4.23(a,b) indicated by the arrows in the figure. However other primary silicon particles can remain faceted without fragmentation. The eutectic silicon can be partially fractured and the acicular silicon also shows a fragmented microstructure. It was observed that θ-Al_2Cu is surrounded by blocky $Cu_2Mg_8Si_6Al_5$ and can be observed in the eutectic region that appears to have nucleated on the large primary silicon as seen in Fig. 4.23(b). It was also observed that this nucleation is more pronounced for large Si particles than for small ones. In addition, an agglomeration of blocky θ-Al_2Cu, eutectic and fragmented eutectic silicon was observed in the matrix as shown in Fig. 4.23(c). Figs. 4.23(c)-4.23(d) also show the globular α-Al presented in several regions.

The experimental results of Lee et al. [9] for binary Al-15.5 %Si show that the fragmentation of the silicon particles does not occur at shear rate below 200 s^{-1}. However, in this work, the fragmentation of the Si crystals in the A390 alloy takes place at a shear rate of 59 s^{-1}. This is attributed to the large solidification interval of A390 (156 ° C) as compared with binary Al-Si (68 ° C), respectively.

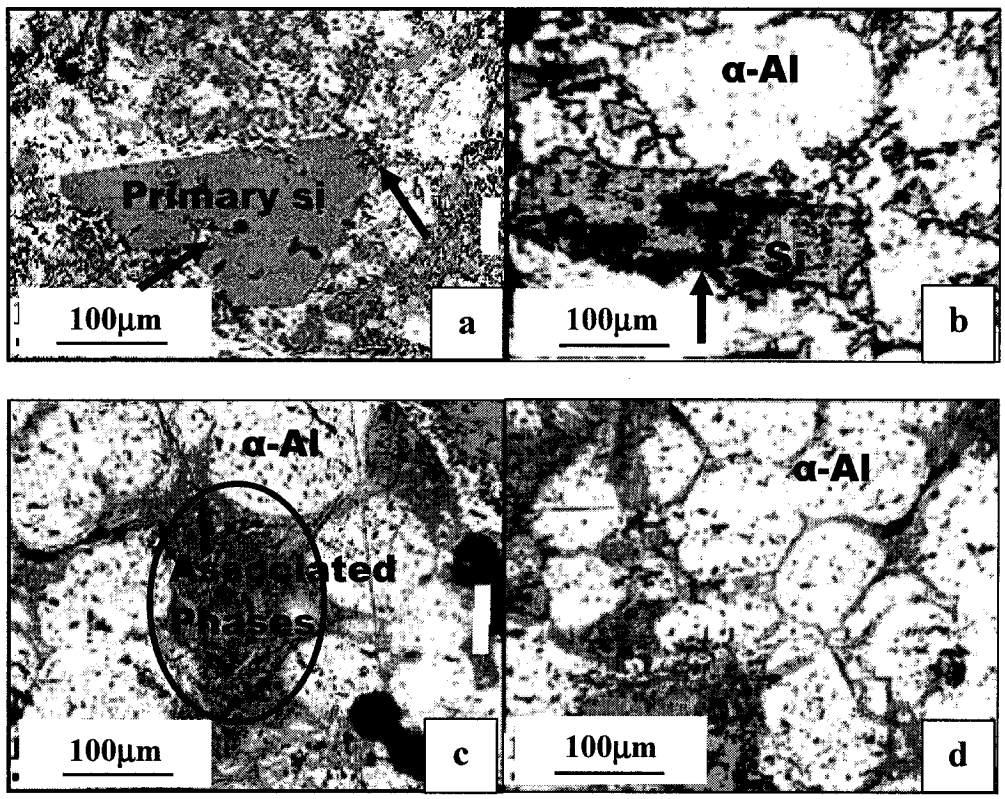

Figure 4.23: Microstructural evolution at shear rate of 59 s^{-1}, (a) fragmentation of large hexagonal Si in the arrows direction, (b) fracture of trapezoidal Si in the arrow direction and eutectic phase associated with Al_2Cu and $Cu_2Mg_8Si_6Al_5$, (c) same phases in matrix not associated with primary silicon and (d) Presence of globular α -Al in microstructure,

The distance between stirrer and crucible wall in this work which is only 1.5 mm (diameters of 25 and 28 mm, respectively). As a result of this narrow gap, the interactions between the silicon particles (mutual collision), the crucible wall and the stirrer are very significant. It has been observed that the effect of gap width in a Couette viscometer influences the particle size of the suspension for equivalent shear rates [45].

At a shear rate of 123 s^{-1} about 80% of faceted morphology of primary silicon becomes fragmented. The fragmented debris was found to be at the periphery of the original particle. However, agglomeration of the fragmented silicon was not observed. Large primary silicon particles are not fragmented and only showed cracks as shown in Fig. 4.24. All of the acicular $Cu_2Mg_8Si_6Al_5$ phase is fragmented and generally found at the periphery of the θ-Al_2Cu particles.

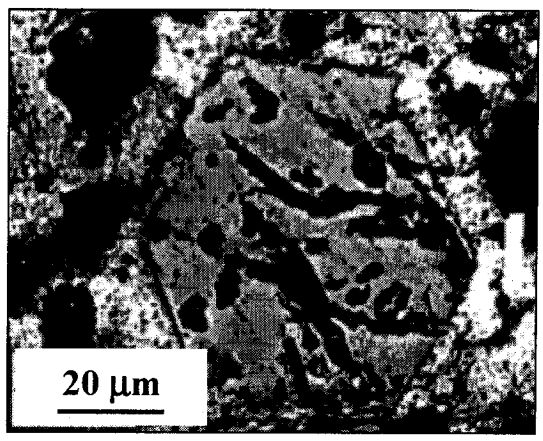

Figure 4.24: A hexagonal Si crystal after shearing at 123 s^{-1} showing cracks within the silicon.

At a shear rate of 250 s^{-1} all of the primary silicon particles become fragmented and the faceted morphology is entirely destroyed due to the break up the primary particles into fragments with different sizes as a result of the shear and collision forces. The fragmented debris of primary Si particles is shown in Fig. 4.25. Generally, the external force to fragment the primary silicon (non-metallic) is much higher when compared to the fragmentation of primary α-Al (metallic). Furthermore, the fragmentation mechanism of primary silicon is significantly different from primary α-Al (which grows dendritically) as previously described by Vogel et al. [9]. On the other hand, careful analysis of microstructure of primary silicon observed by Lee et al. [9] subjected to a large shear force; reveals that the fracture takes place along $\{100\}$ planes and $\{110\}$ cleavage planes (section 2.7, Figure 2.24). This study provides the crucial evidence for distinguishing the fragmentation process that occurs during the shearing of the semi-solid slurry of the hypereutectic as compared to hypoeutectic alloys.

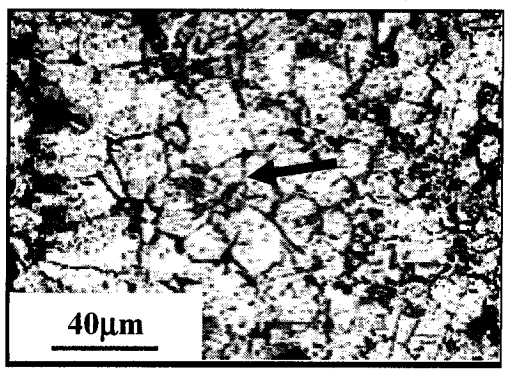

Figure 4.25: Complete fragmentation of Si at shear rate of 250 s^{-1}, Agglomeration of fragmented debris of primary silicon (arrow).

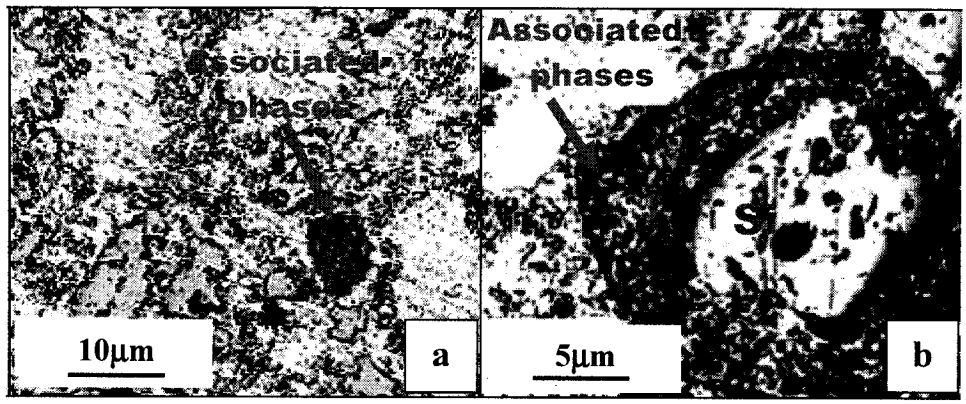

Figure 4.26: Microstructural evolution at shear rate of 507 s^{-1}, (a) region of associated fragments of eutectic silicon , eutectic, θ-Al_2Cu with blocky and fragmented acicular $Cu_2Mg_8Si_6Al_5$ and (b) Same associated phases around a globular Si particle at higher magnification.

At a shear rate of 507 s^{-1} most of the primary silicon changes to a spheroidal shape and disperses in the matrix shown in Fig. 4.26 (a,b). This morphological change reduces the viscosity dramatically (see Figure 4.14, the maximum apparent viscosity reduce from about 44 Pa.s at the shear rate 15 s^{-1} to 5 Pa.s at shear rate at 507 s^{-1}) . The particles in the region consisting of fragmented silicon eutectic, eutectic, θ-Al_2Cu with blocky and broken acicular $Cu_2Mg_8Si_6Al_5$ (associated phases) also become more spheroidal in the matrix (Fig. 4.26(a)) and around the primary silicon as shown in Fig. 4.26(b).

The mean size of primary silicon was decreased from 130 micron in the as-cast condition to about 5 micron at a shear rate of 507 s^{-1}, Fig. 4.26(b).

A summary of microstructural evolution at different shear rate for continuous cooling tests is shown in Table 4.9.

Table 4.9: Summary of microstructural evolution at different shear rate for continuous cooling tests.

$\dot{\gamma}$ (s^{-1})	Amount of Fragmented Si (%)	Si form	Average Si size (μm)
15	0	Faceted	130 ± 10%
59	50	Faceted	98 ± 10%
123	80	Faceted	63 ± 10%
256	100	Faceted	36 ± 10%
507	100	Globular	5 ± 10%

4.3.2 The comparison of the rheological behaviour of A357 and A390 in the continuous cooling condition

The A357 is a hypoeutectic Al-Si alloy (Al-7Si-0.5Mg) with traces of Fe, Zn and Mn. On complete solidification, this alloy has a relatively high eutectic content (about 47%) and the microstructure contains α-Al as primary phase, the eutectic phase as well as a small quantity of intermetallics such as $Al_{15}(Mn,Fe)_3Si_2$, Al_5FeSi, Mg_2Si and $Al_8Mg_3FeSi_6$. Different phases can form during the solidification of 357 as shown in Fig. 4.27 [42]. This figure lists several regions of phase transformation as the alloy solidifies:

1a Nucleation of aluminium dendrites.

1b Development and growth of aluminium dendritic network.

2a Growth of $Al_{15}(Mn,Fe)_3Si_2$, continued growth of aluminum.

2b Growth of Al_5FeSi - (not present in this sample).

3a Nucleation of silicon, continued growth of aluminum.

3b Growth of silicon, continued growth of aluminum.

4 Growth of Mg_2Si, continued growth of aluminum and silicon.

5 Growth of $Al_8Mg_3FeSi_6$, continued growth of previous phases.

The maximum solid fraction of primary phase for A357 (α-Al = 53%) is greater than for A390 (Si = 6.1%) and the solidification temperature interval is therefore smaller as shown in, Table 4.10.

In Fig. 4.28, the apparent viscosity of the two alloys was compared for continuous cooling at a shear rate of 59 s^{-1}. It can be observed that the increase of the solid fraction with decreasing temperature for A357 results in a typical viscosity-temperature i.e. exponantial curve. Generally, the apparent viscosity as a function of temperature for metal semi-solids is exponential. However in the case of A390, as presented in the previous section, two regions were detected. The low solid fraction causes the viscosity to increase very slowly until the binary eutectic temperature of 566 ° C and the precipitation of α-Al is reached (linear region). Beyond this temperature the viscosity increases rapidly to a point near the end of the period of solidification (exponential region). This is primarily due to the rate of formation of the solid fraction in the slurry.

Moreover, the fragmentation of α-Al in A357 is much more significant compared to fragmentation of primary Si in A390 when sheared at 59 s^{-1} because the Si primary phase is very hard and rigid whereas the α-Al is more easily deformed.

Table 4.10: composition, maximum solid fraction and the solidification interval of A390 and A357

Alloy	Composition (wt %)	Max solid fraction of primary phase (%)	Solidification interval (° C)
A390	17Si-4.5Cu-0.5Mg	6.1	156
A357	7Si-0.5Mg-0.2Fe-0.1Zn-0.02Mn	53	48

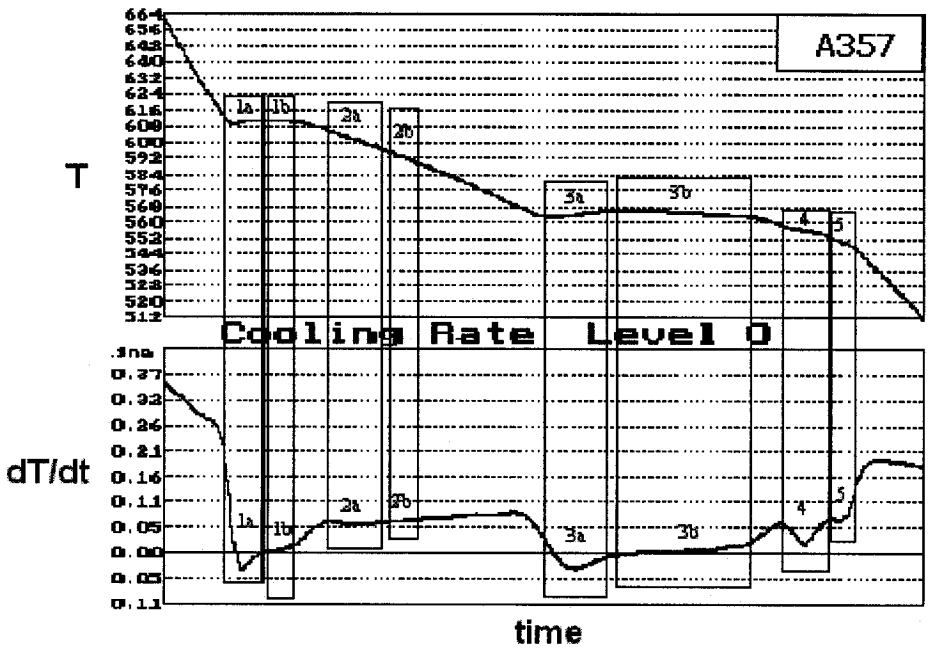

Figure 4.27: Different stages of solidification of 357 Aluminium. [42]

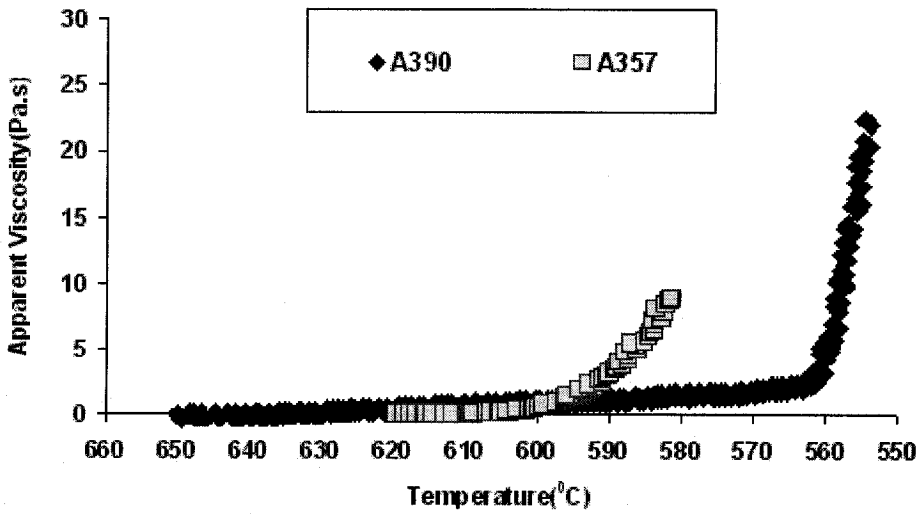

Figure 4.28: The comparison of the rheological behaviour of A357 and A390 in the continuous cooling condition at shear rate 59 s^{-1}.

4.3.3 Viscosity changes at isothermal condition.

The steady state is usually defined as a state where the viscosity of the semi-solid slurry at a fixed temperature or solid fraction (isothermal) does not vary with prolonged shear time at a constant shear rate. For a given alloy system, steady state viscosity is a function of temperature and shear rate [4]. The shear rate dependence of steady state viscosity, or shear thinning behaviour also exhibits pseudoplastic behaviour (section 2.3.1.2.1). It is now generally accepted that the steady state viscosity at a given shear rate depends on the degree of agglomeration between solid particles, which, in turn, is the result of a dynamic equilibrium between agglomeration and de-agglomeration processes [52]. It has been shown that the agglomeration process occurs after a shear rate decrease, whereas the degradation of agglomerates takes place when the shear rate is increased. The time to reach a steady state is a result of the thixotropic behaviour describing the time dependence of the transient state viscosity. This property can also be measured by hysteresis loop or step change experiments (section 2.3.1.3) where the shear rate is increased continuously to a maximum value and then decreased to the initial value. Step change experiments result in information on the rate of structural change (degree of agglomeration-deagglomeration) when the shear rate is changed abruptly for isothermal condition.

In Fig. 4.29, the transient and steady state behaviour of A390 is shown when the shear rate is abruptly changed from 13 $s^{-1}$to 104 s^{-1}, at a temperature near the binary eutectic representing a low solid fraction (about 6,1%). It can be seen that the viscosity decreases

sharply confirming that the degradation kinetics of the agglomerates takes place in only a few seconds. In addition, the very low solid fraction of primary Si allows the new agglomerate structure to be reached very rapidly resulting in the rapid decrease in the viscosity to a new steady state value. At a shear rate of 104 s^{-1} the steady state viscosity is about 0.20 ± 0.05 (Pa.s) as compared to about 11.60 ± 0.40 (Pa.s) at 13 s^{-1}.

In order to examine the microstructure at this stage, the sample was removed 20 minutes after abruptly changing the shear rate to 104 s^{-1} at 565 ° C and rapidly cooling in water. Observation of the microstructure revealed the presence of both dendritic (Fig. 4.30(a)) and globular shape α-Al particles (Fig. 4.30(b)). The fine dendritic structure of α-Al appears due to the fact that the sample could not be solidified instantaneously due to its mass resulting in a dendritic form for the eutectic phase solidification which occurs in a finite time interval starting at 565 ° C. This demonstrates that the range of temperature for the solidification of α-Al starts at 565 ° C (section 2.4). However, the fragmentation of primary silicon did not occur at this shear rate but cracks were observed within the primary silicon particles (Fig. 4.30(c)).

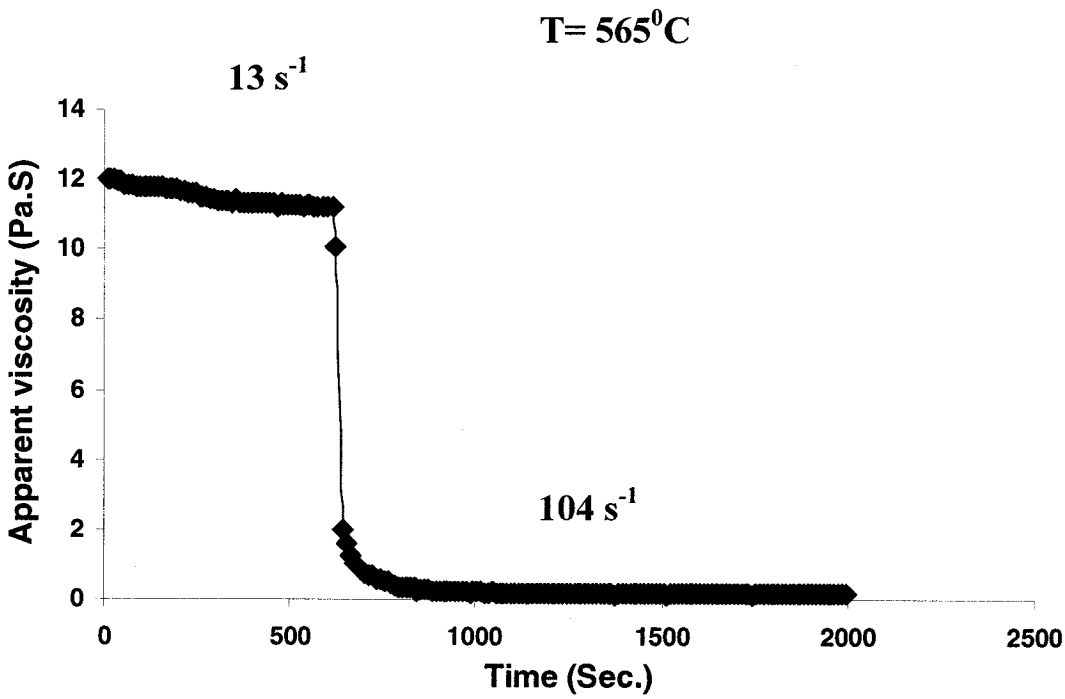

Figure 4.29: Viscosity variation at isothermal condition (565 ° C) with abrupt change in shear rate from 13 s^{-1} to 104 s^{-1}.

Fig. 4.31 shows the thixotropic behaviour of this alloy during step Change experiments. The evolution of the viscosity with shear rate indicates a pseudoplastic behaviour where the apparent viscosity reduces with increasing the shear rate. The results are shown in Fig. 4.32 where the steady state viscosity is plotted against the shear rate. These steady state viscosities are taken from the points on the step Change curve when the viscosity no longer changes with prolonged shear time at a constant shear rate. The straight line in Log (Shear rate)-Log (Apparent viscosity) curve Fig. 4.33 indicates the rheological behaviour at 565 ° C is pseudoplastic which can be described by a power law equation.

The power law parameters at 565 ° C are shown in Table 4.11. Table 4.11 confirms that the crystallization of Si primary phase increases the degree of pseudoplasticity because only primary silicon is solidified but the pseudoplasticity is not significant at this temperature because the solid fraction of primary silicon is very small (only 6.1% near the binary eutectic) and that the crystallization of Si primary phase increases the pseudoplasticity gradually. The results also reveal that the solid fraction of α-Al does not affect the degree of pseudoplasticity because it starts to solidify only at 566 ° C.

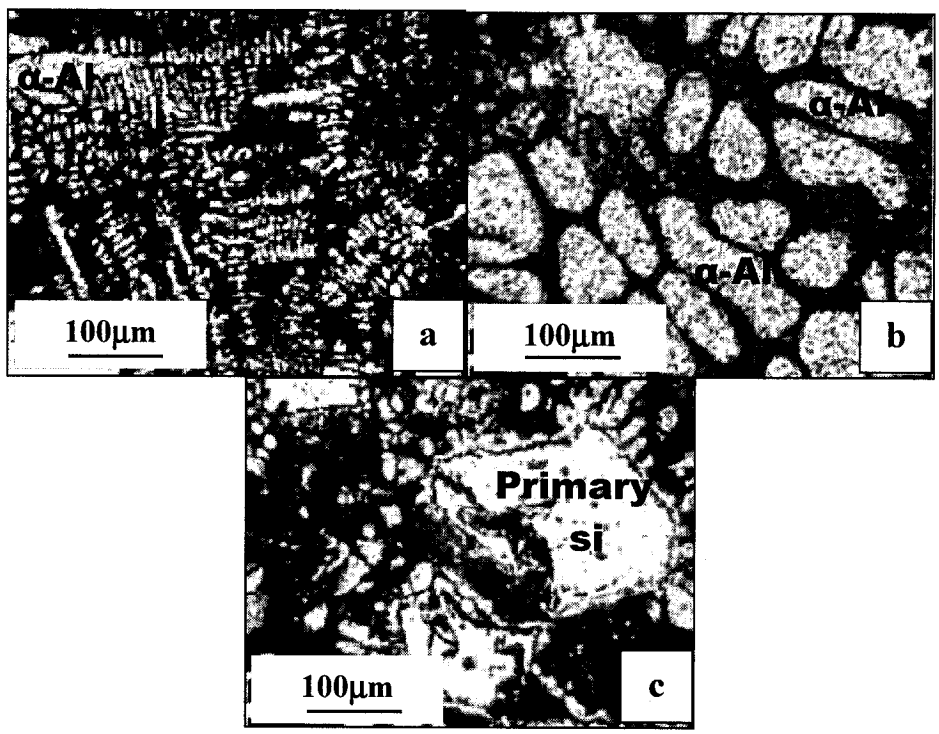

Figure 4.30: Microstructure at isothermal condition (565 ° C) with abrupt change in shear rate from 13 s^{-1} to 104 s^{-1} after 20 min (deep etching), a) dendritic α-Al b) globular α-Al and c) primary silicon.

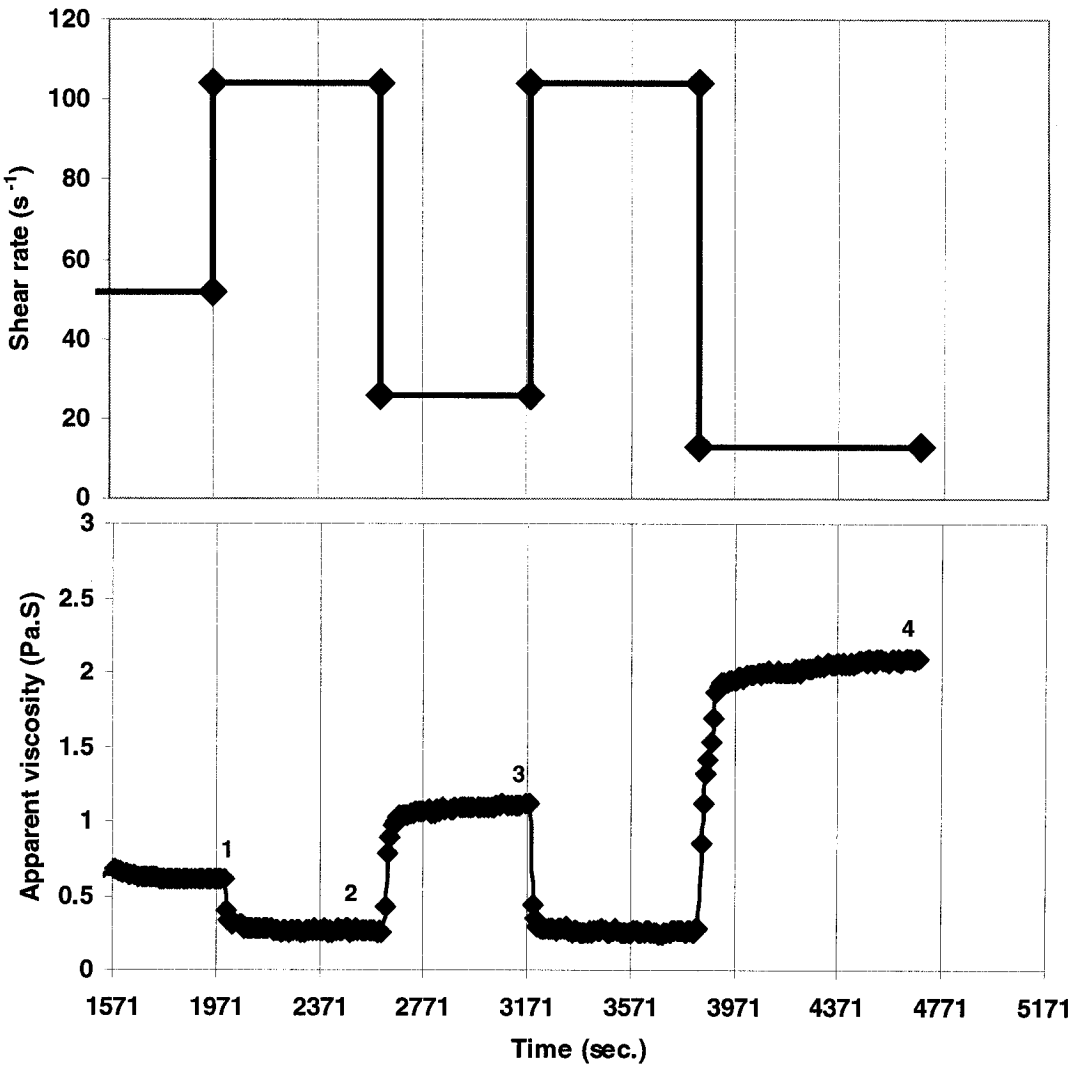

Fig. 4.31: Step changes tests

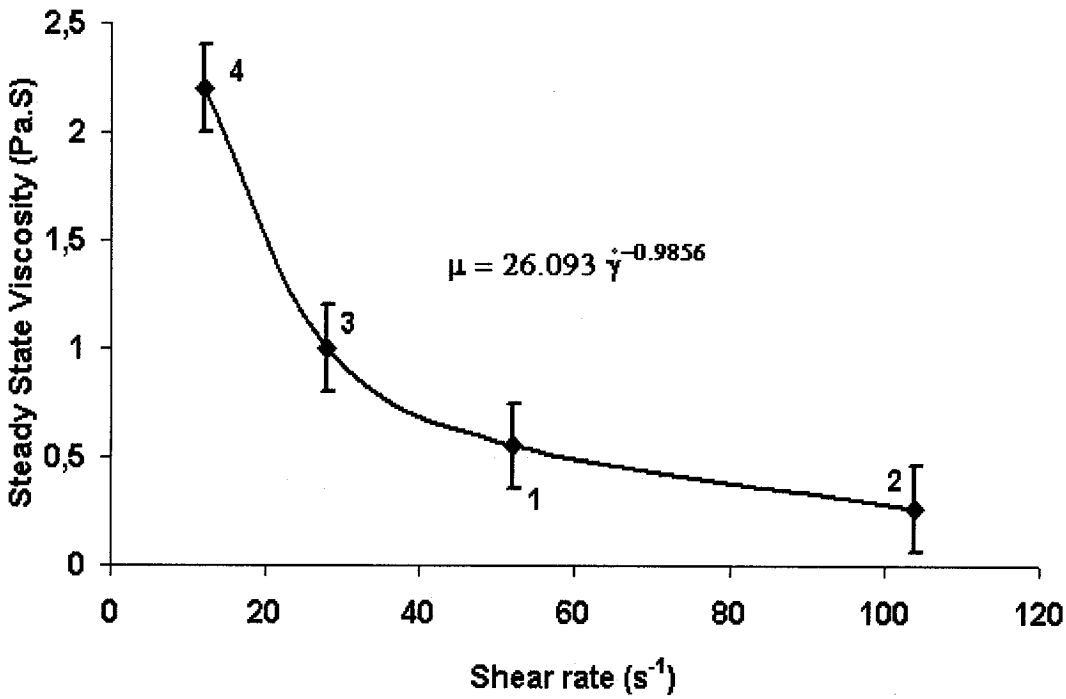

Figure 4.32: Steady state viscosity versus shear rate at 565 ° C

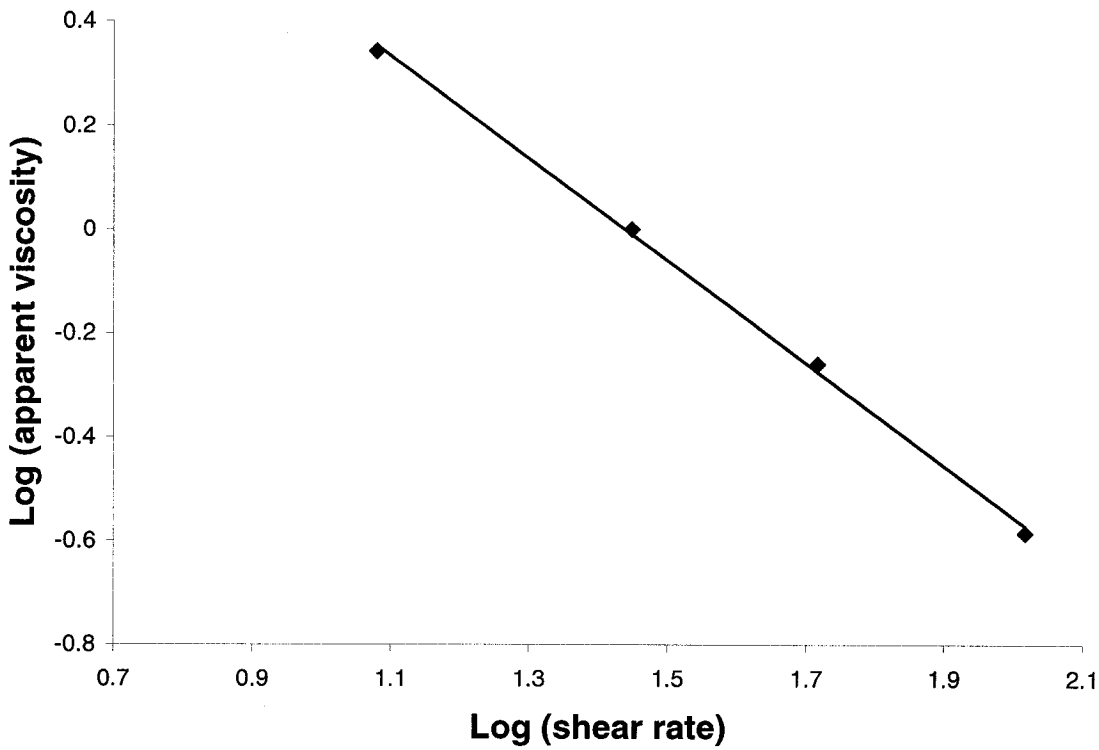

Figure 4.33: The straight line of log-log curve at 565 ° C indicates the pseudoplastic behaviour which is described by power law equation

Table 4.11: Power law parameters in semi-solid case

alloy	Temperature (° C)	n-1	K (Pa.s^n)
A390	565	-0.98	26.09

CHAPTER 5:

CONCLUSIONS AND RECOMMENDATIONS

5.1 Conclusions

1) The quaternary phase diagram for the A390 alloy was calculated using the Factsage software and available thermodynamic data. Differences from the measured experimental values in the literature were observed. One of the reasons for this is the fact that the enthalpies of the quaternary compound such the $Cu_2Mg_8Si_6Al_5$ are not taken into account in the calculated diagram. Hence, the experimental quaternary eutectic reaction takes place at about 507 ° C when the remaining liquid solidifies to Liq. → Al-Cu (θ) + Al (fcc) + Si(s) + $Cu_2Mg_8Si_6Al_5$,

2) When Mg up to 10wt% is added to the A390 alloy composition, the calculation showed that the Mg_2Si intermetallic phase starts to precipitate before primary silicon. Therefore, the Mg_2Si can serve as a nucleation site for silicon and can interact with primary silicon when sheared. However, the solidification interval of primary silicon becomes smaller with increasing Mg content resulting in fine primary silicon and improved rheological behavior.

3) The microstructural observation confirms the presence of α-Al in the eutectic and as individual grains in the matrix. It was shown that, in the region of "Liquid + Si + Al", which correspond to binary eutectic zone, the α-Al solidifies with two morphologies.

This is a characteristic of non-equilibrium solidification and can not be determined by equilibrium phase diagram calculations.

4) Contrary to the results of the viscosity measurement of binary Al-Si alloy during continuous cooling test, where fragmentation of the Si crystals does not occur at shear rate below 200 s^{-1}, the fragmentation of Si crystals in the A390 alloy occurs at a much lower shear rate of 59 S^{-1}. This is attributed to the large solidification interval for the A390 alloy, the very small distance between the stirrer and the crucible wall coupled with the interaction with the other solid phases resulting in reduced viscosity. The mean size of the primary silicon particles was decreased from 130 micron in the as-cast condition to 5 micron at a shear rate of 510 s^{-1}

5) For the continuous cooling experiments, at a shear rate of 15 s^{-1}, the microstructure is the same as the as-cast case. At a shear rate of 59 s^{-1}, 50% of primary silicon becomes fragmented. The morphology of primary silicon is still faceted and there is no agglomeration of fragmented debris. At a shear rate of 123 s^{-1}, 80% of primary silicon becomes fragmented and the morphology of primary silicon is still faceted with no agglomeration of fragmented debris. At the shear rate of 250 s^{-1}, 100% of primary silicon becomes fragmented. The faceted morphology is degraded and the agglomeration of fragmented Si is observed. At shear rate of 507s^{-1}, the most primary silicones become globular resulting in a reduction of viscosity.

6) The apparent viscosity versus temperature graph for different shear rates for the continuous cooling tests revealed two distinct regions. The linear region continues up to the binary Al-Si eutectic temperature of 566 ° C where only primary silicon solidifies. The exponential region is initiated by the solidification of the binary Al-Si eutectic which corresponds to the precipitation of α-Al.

7) For the step change experiments carried out at 565 ° C, the solid fraction of primary Si is only 6.1%. Abrupt changes in the viscosity indicate a very rapid transient period where a new agglomerated state of the solid phases is rapidly established and both particle morphology and particle size are rapidly established for each specific shear rate.

5.2 Recommendations

1- The objective of this work is the refinement of the microstructure by fragmenting of primary silicon. By increasing the Mg content above 4,2wt% for the A390 alloy composition, the Mg_2Si intermetallic phase starts to precipitate as an individual compound before the binary eutectic reaction occurs. At 10wt% Mg, the Mg_2Si solidifies as a primary phase and therefore can serve as a nucleation site for silicon. As a result, the solidification interval of free silicon becomes small with increasing Mg content which generates fine free silicon particles and improved rheological behaviour. The study of the effect of Mg addition on the thermodynamic and microstructural characteristics of A390 alloy would be great interest, together with their effect on the mechanical properties.

2- The distance between the stirrer and the crucible wall is the other important factor to take into account in the fragmenting primary silicon particles when using a Couette rheometer. As was pointed out, the fragmentation mechanism for hypereutectic Al-Si refers to the mutual collision of large irregular shaped Si crystals suspended in the rapidly moving viscous liquid medium. The mutual collision can be carried out between two silicon particles or silicon particles and the crucible wall and the fracture takes place along $\{100\}$ planes and $\{110\}$ cleavage planes. It is clear that the stirrer rotation speed for a large gap and a small gap between crucible and stirrer affects the particle interaction. A study of the effect of spacing between crucible and stirrer on rheological behaviour is recommended.

3- As explored in the literature, the nucleation of Si requires high undercooling based on TPRE (Twin Plan Re-entrant Edge) mechanism, whereas the Si nucleates on reinforcing materials such as SiC or Al_2O_3 with no undercooling kinetic because the contact angle is about 90^0. On the other hand, the growing planes change from the low energy $\{111\}$ plane to other fast growing planes (this is a unique characteristic of Si particles). The future studies should explore this exceptional property to create nucleation sites in order to refine the Si particles and measure the rheological properties of this modified structure alloy.

REFERENCES

[1] L. Backerud, G. Chai and J. Tamminen. (1990). "Solidification Characteristics of Aluminium Alloys", Foundary Alloys, AFS/Skanaluminium , Des Plaines, IL, USA, Vol. 2, page 86.

[2] M.A. Moustafa, F.H. Samuel and H.W. Doty. (2003). "Effect of Solution Heat Traetment and Additives on the Microstructure of Al-Si (A413.1), Automotive Alloys", Journal of Materials Science, 38, 4507-4522.

[3] L.F. Mondolfo.(1978). "Manganese in Aluminum Alloys" , Syracuse University, USA. Publisher: The Centre, ISBN: 2901109012.

[4] Z. Fan. (2002). "Semi-Solid Processing", International Materials Reviews,Vol. 47, No.2, page 4.

[5]H.S. Kang, W.Y. Yoon, K.H. Kim, M.H. Kim and Y.P. Yoon. (2005) "Micros tructure Selections in the Undercooled Hypereutectic Al-Si Alloys", Material Science and Engineering, A, Volume 404, Issues 1-2, Pages 117-123.

[6] S. Spigarelli, E.Evangelista and S.Cucchieri. (2004). "Analysis of the Creep Respon se of an Al-17Si-4Cu-0.55Mg alloy",Material Science and Engineering A 387-389, pages: 702-705.

[7] A.Vogel, R.D. Dohetry and B. Canter. (1979). Proc. Int. Conf. on solidification and casting of metals. Eds., J.Hunt, Sheffield, The Metal Society, page: 581.

[8] R.D. Dohetry, H.I. Lee and E.E. Feest. (1984)."Microstructure of Stir-Cast Metals" Mat. Sci.& Eng. 65(1), pages 181-189.

[9] H.I. Lee, J.I. Lee and M.I. Kim. (1994). Proc. 3rd Int. Conf. on semi-solid processing of alloys and compositions, Eds. M. Kiuchi, Tokyo, page: 281.

[10] D.B. Spencer, R. Mehrabian and M.C. Flemings. (1972). Metal. Trans., Vol. 3, pages: 1925-32.

[11] P.J. Ward, H.V. Atkinson, P.R.G. Anderson, L.G. Elias, B.Garcia, L.Kahlen and J-M. Rodriguez-Ibabe. (1996)."Semisolid Processing of Novel MMCs Based on Hypereutectic Al-Si Alloys", Acta Mater. Vol.44, No.5, pages:1717-1727.

[12] H.Wabusseg. (2003). "Process and Alloy Development for High Quality Aluminium Components for Lightweight Construction – the New Rheocasting Process", Ph.D. thesis ETHZ No. 14512.

[13] W. Kurz and D.J. Fisher. (1986). "Fundamental of Solidification", Trans Tech Publication, Aedermannsdorf, Switzerland.

[14] M.C Flemings. (1974). "Solidification processing", Mc Graw Hill Book Co., New York.

[15] H. Jones. (1984). J. Mater Sci., Vol. 19, pages: 1043-76.

[16] I.M. Lifshitz and V.V. Sloyzov. (1961). "The Kinetic of Precipitation from Supersaturated Solid Solution", Journal of Physic and Chemistry of Solids, 19, (1961), 35, pages: 25-32.

[17] K.P. Young and D.H. Kirkwood. (1975). "The Dendrite Arm spacing of Aluminum-Copper Alloys Solidified under Steady State Condition", Metal Trans., 6A, Page:107.

[18] K.P. Young and C.P. Kyonka, J.A. Courtis. (1984). U.S. Patent 4, 482, 012.

[19] T. Iida and Y. Shiraishi. "Chapter 4 Viscosity" in "Handbook of Physico-chemical Properties at High Temperatures" Edited by Y Kawai and Y Shirashi The Iron and Steel Institute of Japan, 1988

[20] A.R.A. Mclelland, N.G. Henderson, H.V. Atkinson and D.H. Kirkwood. (1997). "Anomalous Rheological Behaviour of Semi-Solid Slurries at Low Shear Rates", Mater. Sci. Eng., 232A, page 110.

[21] T. Hemphill, W. Campos and A. Pilehvari. (1993). "Yield-Power Law Model More Accurately Predicts Mud Rheology," Oil & Gas Journal, no. 34, pages 45-50.

[22] C.L. Carlson and R.M. Slepian. (1975). "Metallography of a Cast Hypereutectic Al-Si Alloy", Microstructural Science, Proceeding of the Seventh Annual Technical Meeting of the International Metallographical Society, P.M. French, R.G. Gary and J.L. Mc call, Eds., American Elsevier Publishing Company, New York, USA, Vol.3, pages: 165-191.

[23] R. Wang, W. Lu and L.M. Hogan. (1999) "Growth Morphology of Primary Silicon in Cast Al-Si Alloys and The Mechanism of Concentric Growth". J. Cryst. Growth, 207, pages: 43-54.

[24] H. V. Atkinson, S. C. Hogg and P. Kapranos. "Silicon Network in Al-High Silicon Alloys and Their Effect on Semi-Solid Processing". Thixoforming conference 2004, pages 241-245.

[25] J. Lipton, W. Kurz and R. Trivedi, Acta Mater. 35 (1987) 957.

[26] K.A. Jackson and J.D. Hunt, Trans. Metall. Soc. AIME 236 (1966) 1129.

[27] X.J. Han, C. Yang, B. Wei, M. Chen and Z.Y. Guo, Mater. Sci. Eng. A307 (2001) 35.

[28] Z. Fan, J. Zhang, Y.Q. Wang and B.L. Zhau. (2001) "Equilibrium Pseudobinary Al-Mg2Si Phase Diagram", Material Science and Technology, Vol.17, Pages 494-496.

[29] J. Zhang, Z. Fan, Y. Q. Wang and B. L. Zhou, "Microstructural development of Al–15wt.%Mg_2Si in situ composite with mischmetal addition", Materials Science and Engineering A, Volume 281, Issues 1-2, 15 April 2000, Pages 104-112.

[30] S.Z. Lu and A.Hellawell. (1985). "Growth Mechanisms of Silicon in Al-Si Alloys", J. Cryst. Growth, 73, page: 316.

[31] C.H. Chiang and Chi.Y.A. Tsao. (2005). "Si Coarsening of Spray-formed High Loading Hypereutectic Al-Si Alloys in the Semisolid State", Journal of Materials Science and Engineering A 396, pages: 263-270.

[32] I.M. Lifshitz and V.V.Slozov.(1961)."The kinetics of Precipitation from Supersaturated Solid Solutions", J. of Phys. Chem. Solid, 19, pages: 35-50.

[33] S.C. Hardy and P.W. Voorhees. (1988). " Ostwald Ripening in a System with a High Volume Fraction of Coarsening Phase", Metal. Trans. 19A, pages: 2713-2721.

[34] F. Ajersch, F. Messaoud and L. Azzi. (2003). "Rheological Characteristics of AZ91E Alloys in Semi-Solid State" , Aluminium 2003, Proceeding, TMS, S.K. Das, Ed., pages: 65-75.

[35] M.Gupta and E.J.Lavernia. (1995). "Effect of the Processing on the Microstructural Variation and Heat-Treatment Response of a Hypereutectic Al-Si Alloy", Journal of Material Processing Technology, 54, pages: 261-270.

[36] H. Phillips. (1959). "Annoted equilibrium diagram of some aluminium alloy system", book, page: 84.

[37] Dr. Sc, Ir.C. and Ir.E. Marc Van Lancker. (1967). "Metallurgy of aluminium alloy", translated [from the French] by E. Bishop, published by London, chapman-hall, pages: 469-476.

[38] P. Kapranos, D. H. Kirkwood, H. V. Atkinson, J. T. Rheinlander, J. J. Bentzen, P. T. Toft, C. P. Debel, G. Laslaz, L. Maenner, S. Blais *et al.* (2003)"Thixoforming of An

Automotive Part in A390 Hypereutectic Al–Si Alloy", journal of Materials Processing Technology, Volume 135, Issues 2-3, Pages 271-277.

[39] Jian Li, M. Elmadagli, V.Y. Gertsman, J. Lo and A.T. Alpas. (2006), "FIB and TEM characterization of subsurfaces of an Al–Si alloy (A390) subjected to sliding wear", Materials Science and Engineering: A, Volume 421, Issues 1-2, Pages 317-327.

[40] C. M. Chen, C. C. Yang and C. G. Chao. (2004), "Thixocasting of hypereutectic Al–25Si–2.5Cu–1Mg–0.5Mn alloys using densified powder compacts", Materials Science and Engineering A, Volume 366, Issue 1, Pages 183-194.

[41] A. R. Hekmat and F. Ajersch, "Effect of Mg on thermodynamical and microstructural characteristics of A390", to be published.

[42] H. Charbonnier. (1984). "Microprocessor Assisted Thermal Analysis Testing of Aluminum Alloy Structure", Transactions of the AFS, Vol. 92, page: 907.

[43] M. Mada and F. Ajersch, Mater. Sci. Eng., 1996, A212, 171-177.

[44] Christopher W. Bale and Arthur D. Pelton, FACTSAGE 5.4.1, C.R.C.T (Centre of Research for Computational Thermochemistry), École Polytechnique de Montréal.

[45] A.R. Hekmat and F. Ajersch, (2006) "Morphological Evolution of Solid Phase Particles of Hypo- and Hyper Etectic Al-Si Alloys Sheared in the Semi-Solid State" MET. SOC. (COM 2006) Conference.

Appendixes

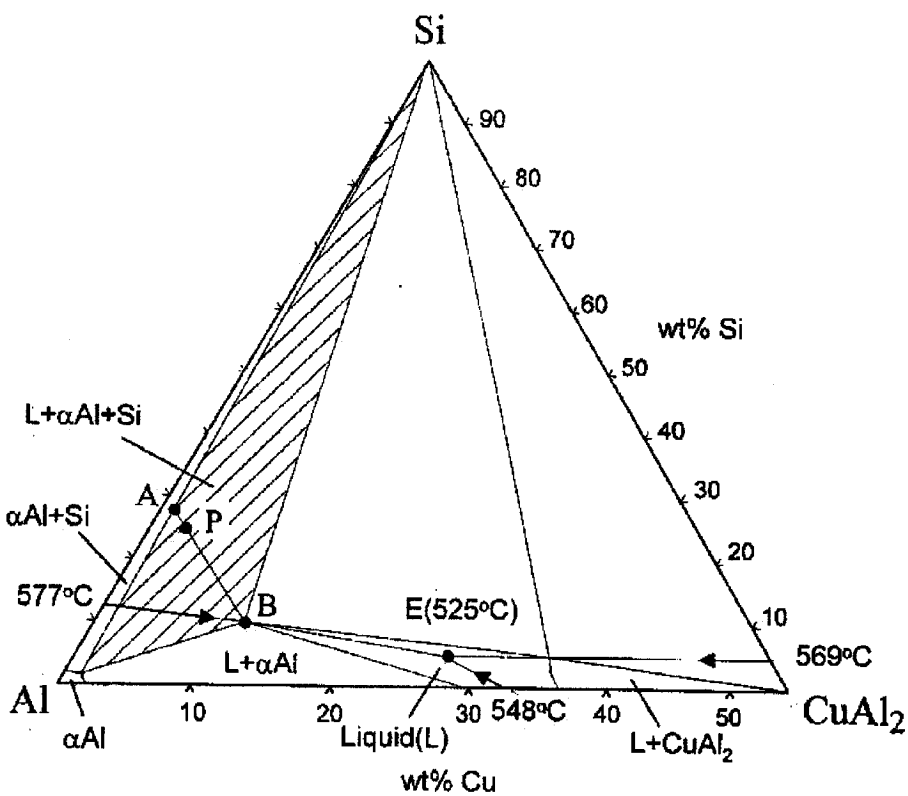

The Al-Si-Cu isothermal phase diagram at 560 ^{0}C. Hatched zone show three phase region, i.e. α-Al, Si and liquid.

Schematic of unit cell in Al, Al–Si and Si crystal

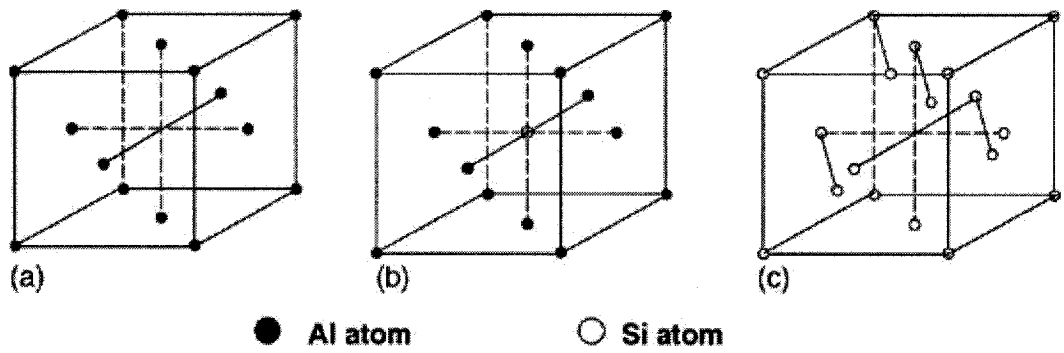

(a) Al unit cell; (b) Al–Si unit cell; (c) Si unit cell.

Al has *Fm*3*m* type structure with lattice constant a = 4.0496 A° , symmetry centre is located at (*m*3*m*), and the equivalent atom positions are (0,0,0), (0,1/2,1/2) (1/2,1/2,0), (1/2,0,1/2), respectively. Because the solubility of Si in liquid Al is very large, the symmetry center of the Al–Si unit cell is located at(*m*3*m*), i.e., one Si atom is located at (1/2,1/2,1/2) , one Al atom, Al*c*, is located at (0,0,0), three other Al atoms, Al*f*, are located at (0,1/2,1/2) (1/2,1/2,0), (1/2,0,1/2), respectively. Si has *Fd*3*m* type structure with lattice constant a = 5.4307 A° , zero position is located at $\bar{4}3m$, and the symmetry center ($\bar{3}m$) is located at ($\bar{1}/3,\bar{1}/3,\bar{1}/3$), and the equivalent atom positions are (0,0,0; 0,1/2,1/2; 1/2,0,1/2; 1/2,1/2,0) + (0,0,0; 1/4,1/4,1/4), respectively.